







## Article

# The First Inventory of Rock Glaciers in the Zhetysu Alatau: The Aksu and Lepsy River Basins

Azamat Kaldybayev <sup>1,2,\*</sup>, Nurmakhambet Sydyk <sup>1,2</sup>, Alena Yelisseyeva <sup>1</sup>, Aibek Merekeyev <sup>1</sup>,  
Serik Nurakynov <sup>1</sup>, Kanat Zulpykharov <sup>1,2</sup>, Gulnura Issanova <sup>3</sup> and Yanning Chen <sup>4</sup>

<sup>1</sup> Institute of Ionosphere, 050020 Almaty, Kazakhstan

<sup>2</sup> Department of Geography and Environmental Sciences, Al-Farabi Kazakh National University, 050040 Almaty, Kazakhstan

<sup>3</sup> Research Centre for Ecology and Environment of Central Asia (Almaty), 050060 Almaty, Kazakhstan

<sup>4</sup> State Key Laboratory of Desert and Oasis Ecology, Xinjiang Institute of Ecology and Geography, Chinese Academy of Sciences, Urumqi 830011, China

\* Correspondence: azamat.kaldybayev@gmail.com

**Abstract:** While rock glaciers (RGs) are widespread in the Zhetysu Alatau mountain range of Tien Shan (Kazakhstan), they have not yet been systematically investigated. In this study, we present the first rock glacier inventory of this region containing 256 rock glaciers with quantitative information about their locations, geomorphic parameters, and downslope velocities, as established using a method that combines SAR interferometry and optical images from Google Earth. Our inventory shows that most of the RGs are talus-derived (61%). The maximum downslope velocity of the active rock glaciers (ARGs) was 252 mm yr<sup>-1</sup>. The average lower height of rock glaciers in this part of the Zhetysu Alatau was 3036 m above sea level (ASL). The largest area of rock glaciers was located between 2800 and 3400 m ASL and covered almost 86% of the total area. Most rock glaciers had a northern (northern, northeastern, and northwestern) orientation, which indicated the important role of solar insolation in their formation and preservation.

**Keywords:** rock glacier; inventory; Tien Shan; InSAR; Zhetysu (Dzhungar) Alatau; permafrost



**Citation:** Kaldybayev, A.; Sydyk, N.; Yelisseyeva, A.; Merekeyev, A.; Nurakynov, S.; Zulpykharov, K.; Issanova, G.; Chen, Y. The First Inventory of Rock Glaciers in the Zhetysu Alatau: The Aksu and Lepsy River Basins. *Remote Sens.* **2023**, *15*, 197. <https://doi.org/10.3390/rs15010197>

Academic Editors: Ulrich Kamp, Dmitry Ganyushkin and Bijeeesh K. Veettil

Received: 11 November 2022

Revised: 24 December 2022

Accepted: 27 December 2022

Published: 30 December 2022



**Copyright:** © 2022 by the authors. Licensee MDPI, Basel, Switzerland. This article is an open access article distributed under the terms and conditions of the Creative Commons Attribution (CC BY) license (<https://creativecommons.org/licenses/by/4.0/>).

## 1. Introduction

### 1.1. Importance of Inventorying Rock Glaciers

There are many options for defining rock glaciers; therefore, different researchers interpret this term differently. Several scientists [1–4] have defined a rock glacier as an accumulated mixture of debris and ice located on a mountain slope that has been deformed under gravity and has formed vicious striking tongue formations that flow up to a kilometer wide and up to several kilometers long. According to Berthling [5], rock glaciers can be determined as “a visible manifestation of cumulative deformation resulting from long-term creep of mixtures of ice and debris in permafrost conditions.” The same definition was used by [6] in their work. It has been reported [7–10] that rock glaciers are reed or lobed landforms on high mountain slopes, usually consisting of a mixture of loose rock fragments and ice.

In this paper, we used the definition presented in the documents of the International Permafrost Association (IPA) [11,12], which define rock glaciers as detrital landforms formed as a result of former or current creep of frozen ground (permafrost), found in a landscape with the following morphology: front (mandatory criterion), lateral margins (mandatory criterion), and possibly a ridged and furrowed surface (optional criterion) (Figure 1). That is, rock glaciers are (or were) landforms that carry debris from an uplift (original zone or root zone) to their front.

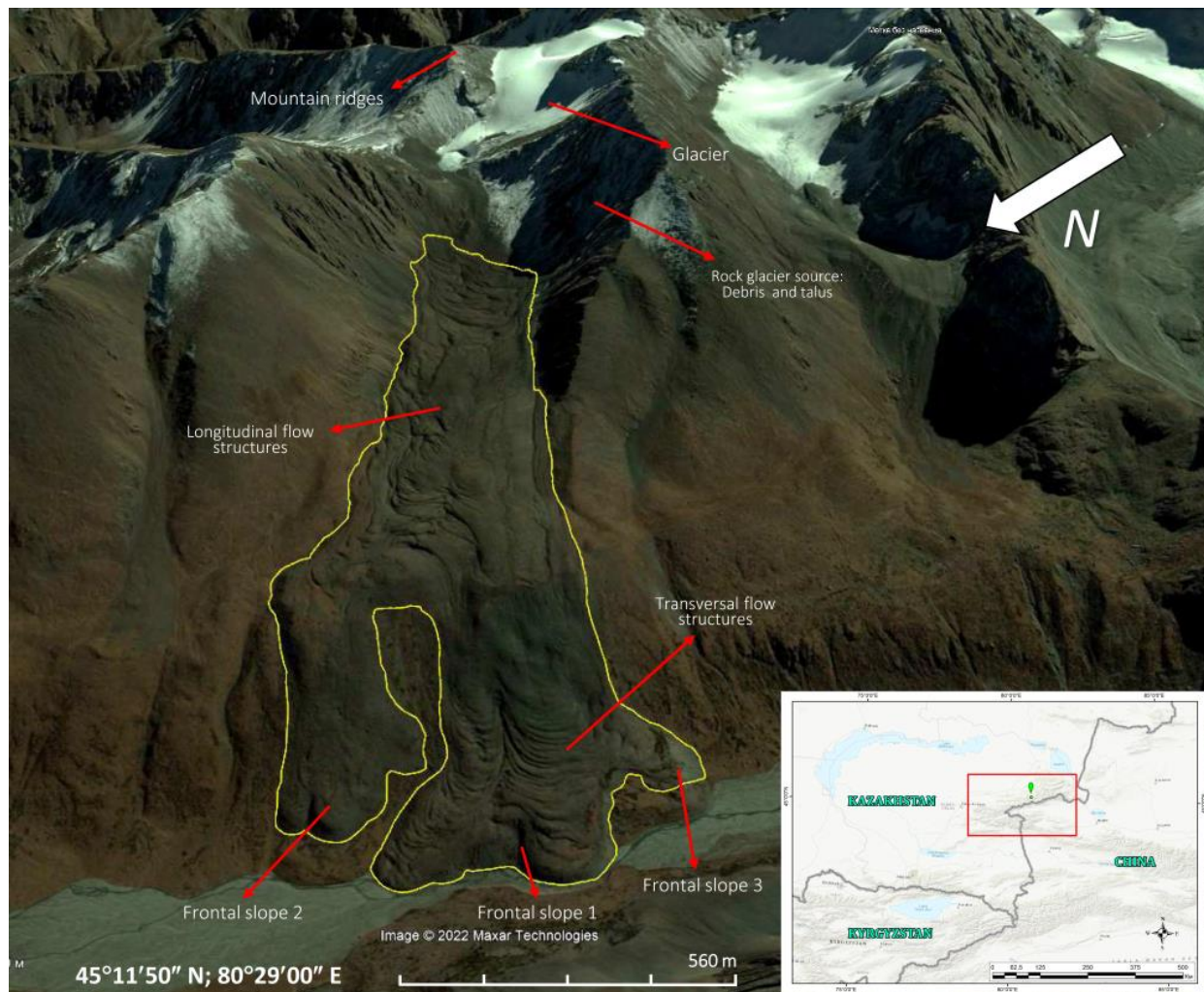


**Figure 1.** Geomorphology of the rock glacier (RG Nizkomorennny, Lepsi river basin).

Rock glaciers play an important role in the water balance of high mountain regions [13]. Mountain rock glaciers contain globally significant water stores. Their ability to store fresh water in winter makes them important sources of fresh water in summer for semi-arid and arid regions such as the central Andes and the Sierra Nevada [14–18]. Recent studies have highlighted the importance of rock glaciers as temperature- and climate-tolerant water stores, as well as buffers for hydrological seasonality due to the insulating effect of debris [13,19,20]. Their importance in mountain hydrology is likely to increase in the coming decades due to global glacier retreat [21].

Rock glaciers have geomorphological, climatic, and hydrological significance in alpine periglacial conditions. Rock glaciers can take several thousand years to form and are visible indicators of permafrost that contribute significantly to the mass transport of alpine landforms [22,23]. As such, knowledge of their distribution can provide reliable information on past occurrences of permafrost and associated climatological conditions [24–27]. However, there are cases where subsurface ice can still be found in favorable conditions at much lower altitudes.

### 1.2. Classification of Rock Glaciers by Their Activity

An active rock glacier is a landform that transports sediment from the root zone to its front. It is characterized by a steep front (steeper than the angle of repose) and possibly by flanks with fresh exposed material at the top [11]. The displacement rate can vary from tens of centimeters to several meters per year [28]. Transitional (intermediate) rock

glaciers have ice in their composition and move at a speed of less than one decimeter per year. Depending on the topographic and/or climatic context, transitional rock glaciers can evolve either into a relict or an active state. A relict rock glacier is a landform that no longer transports sediments from the root zone to its front due to permafrost depletion. In other words, they do not move and do not have ice in their composition. Relic rock glaciers are usually formed at lower elevations than active rock glaciers.

Speed is affected by changes in ground temperature, as well as the presence of moisture, which can speed up or slow down a rock glacier on a ten-year scale [29–32]. Rock glaciers also show strong seasonal fluctuations in surface movement in many cases, with higher velocities in summer and autumn compared to winter and spring [27,33,34].

The IPA Rock Glacier Inventory (RoGI) and Kinematics Action Group, established in 2018 [35], intends to support the development of generally accepted basic concepts and standard guidelines for the inventory of rock glaciers in mountainous permafrost regions [11]. One of the most important elements in standardized RoGI catalogs is kinematic information. Since indirect kinematic information is often inaccurate as it relates to operator interpretations, the result of visual observations of morphological (e.g., fore angle) indicators associated with vegetation [36,37] can be highly unsatisfactory. Recently, more accurate approaches based on remote sensing data (e.g., Sentinel-1 image satellite interferometry) [38] have been developed to characterize rock glacier kinematics on a large scale [16,34,39–41].

In this context, as part of the European Space Agency (ESA) Permafrost Climate Change Initiative (Permafrost\_CCI), the so-called CCN2 project (<https://climate.esa.int/en/projects/permafrost/>; last accessed: 10 October 2021)—in line with the basic concepts proposed by the IPA Action Group [11,42]—specific guidance has been developed [28] for the systematic integration of kinematic information into RoGI using InSAR data. Under this framework, workflow is reduced to outlining moving areas and assigning a speed class based on the results of interferometric analyses; attribute information is filled in according to IPA standards.

Rock glaciers are common in Northern Tien Shan, and their descriptions can be found in studies from the beginning of 20th century; moreover, in 1923, researchers took measurements of the rock glacier front [43–46].

It was initially believed that these rock glaciers were mainly of a periglacial origin, but they may also contain sedimentary ice [47,48]. One of the latest studies of rock glaciers in the Zhetysu Alatau region Gorbunov [49] identified about 850 active rock glaciers based on aerial photography at a scale of 1:10,000; the photographs are dated 1969, 1979, and 1984, and they do not specify information about geographical coordinates and topographic parameters. However, descriptions and detailed ground-based geodetic measurements were performed for only one of them—the rock glacier Nizkomorenniy [50]. The altitudinal boundaries of the active rock glaciers are 200–300 m lower in this region than in the relatively well-studied Ile Alatau Range of the Tien Shan mountain system [49].

Other research results are absent for the Zhetysu Alatau region. Our inventory work was started from scratch, and has so far been completed for the Aksu and Lepsy River Basins of the Zhetysu Alatau. Therefore, the main task of our work was to compile an initial digital catalog according to international standards [11,12,28] and evaluate the kinematic performance of rock glaciers in the region.

## 2. Territory of Interest

The Zhetysu Alatau (or Dzhungar Alatau) is a mountain system stretching from west-southwest to east-northeast along the state border between the Republic of Kazakhstan and the People's Republic of China. The total area of the Zhetysu mountain system, including the basin of the river Borotala in China, is about 40,000 km<sup>2</sup> [51]. The Zhetysu mountain system is located mostly in Kazakhstan.

The Ile River is the southern border of this mountain system, while the northern border is the Balkhash Plain and the Alakol Lake and Dzhungar Gates are the northeastern border.



The longitudinal river valleys—Koksu in the west and Borotala in the east—divide the Zhetysu Alatau into two large ridges parallel to each other: the North Central and the South Central.

The length of the North Central Range is about 400 km, and that of the South Range 300 km. The Northern Zhetysu Alatau includes the longest and highest ridge of this mountainous country. Sub-latitudinally, the ridge stretches for 260 km, reaching the highest elevation of 4622 m ASL (Besbakan). The largest spurs of the ridge are Kungei and Tastau.

The Southern Zhetysu Alatau includes the Toksanbay and Bedzhintau ridges, both of which have many spurs. The Muztau mountain range houses the highest peak of the Southern Zhetysu Alatau, which reaches 4370 m ASL. The Southern Zhetysu Alatau also includes the Tyshkantau ridge, as well as the isolated, relatively low Koyandytau, Suat, and Altynnemel ridges with low-mountain spurs [52].

The Zhetysu Alatau is influenced by arctic, polar, and tropical air masses, which undergo significant transformations on their way to the ridges. Arctic air masses come from the north and northwest, from the regions of the Barents and Kara Seas. More often, they come during the early winter period, and their invasions are accompanied by a sharp drop in air temperature.

In the Zhetysu Alatau, the average annual rainfall is 600–800 mm; in the southeast of the ridge, average annual rainfall is 400 mm. In western Dzungaria, the largest annual precipitation in the entire range of altitudes falls in river basins. Chizha Range has the highest precipitation rate (1400–1600 mm) and thus propels moisture-carrying air masses.

The average long-term air temperatures in the lower parts of the glacial zone (at altitudes of 3200–3600 m ASL) during the accumulation period are  $-8$ – $-10$  °C; in the upper parts (above 4000 m ASL), temperatures drop by up to  $-14$ – $-16$  °C. The coldest month is January, with temperatures of  $-17$ – $-19$  °C. The maximum temperatures associated with the intrusions of thermal air from the surrounding deserts reach  $13$ – $15$  °C, and the observed absolute maximum is  $25$  °C. Thus, the great differences in the absolute heights of the mountain relief of the Zhetysu Alatau and its complex morphology are the cause of a wide variety of climatic conditions. The altitudinal boundary of the permafrost belt in the Dzungarian Alatau coincides approximately with the isohypse of 2500 m ASL; these are 200 m lower than in the Northern Tien Shan [53]. However, unfortunately, the data for this book were collected mainly during 1988.

The average height of the Zhetysu Alatau glaciers is about 3578 m in 2016 and the average maximum and minimum heights are 4545 m and 2869 m, respectively [54–58]. The relative average height of the glaciation zones is lower than in other regions of the Tien Shan. For example, in the central Tien Shan, the average height of the glacier is about 4316 m, respectively, the average maximum and minimum heights are 5112 m and 3707 m [59]. Additionally, in the northern part of the Tien Shan, according to research by Narama and others [60], the average height of glaciers is 3909 m (Ili-Kungöy), the average maximum and minimum heights are 4939 m and 3306 m., respectively.

The Zhetysu Alatau glaciers, as the main source of moraine-derived rock glaciers, have been studied by number of authors. Severskiy and others [61] conducted detailed studies of the ice-cover dynamics for the entire Zhetysu Alatau Range over the period from 1956 to 2011, and they showed that the annual glacier reduction rate was 0.7% in the Aksu–Bien and Lepsy–Baskan river basins. At the same time, they noted that the most intensive reduction rate of the glaciers was observed mainly in the basins of the Southern Zhetysu Alatau, while it was at its lowest in orographic closed basins. In this paper, we considered areas of the Aksu and Lepsi river basins of the Zhetysu Alatau Range (Figure 2).



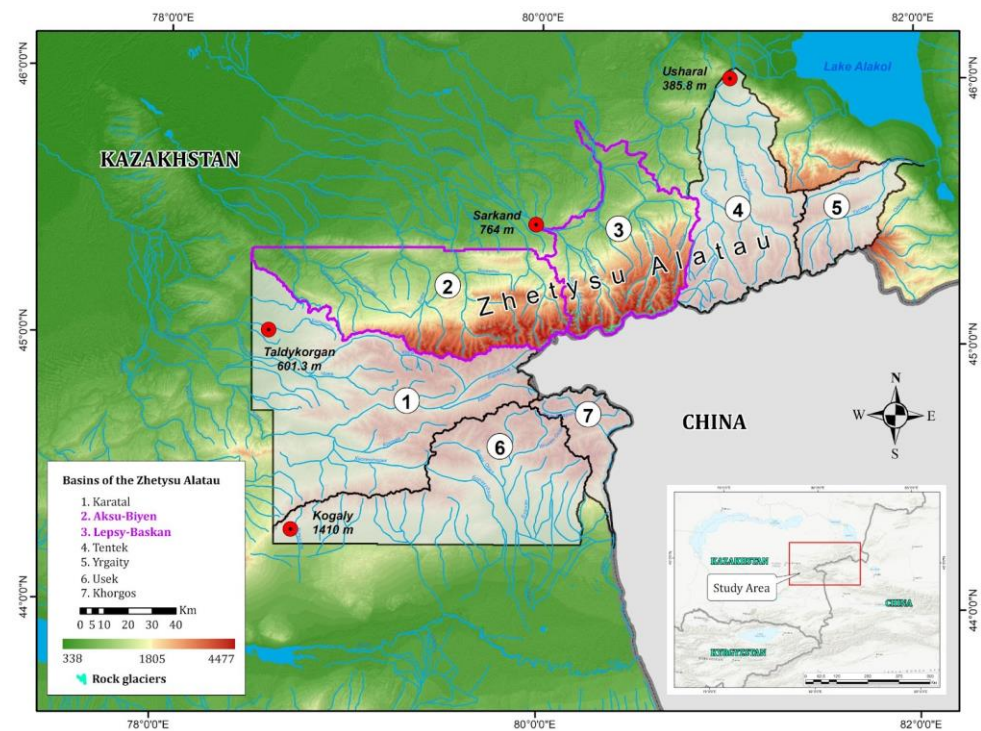


**Figure 2.** The Zhetysay Alatau basins, including Aksu and Lepsi rivers (purple boundary).

### 3. Materials and Methods

We used two basic approaches as the main methodology: geomorphologic and kinematic. In this regard, the general workflow for creating an inventory of rock glaciers consists of the following steps: the manual interpretation of the rock glacier contours were based on optical satellite images in the Google Earth environment by visual interpretation of their geomorphological features; then, generate the line-of-sight direction (LOS) surface velocity estimated from Sentinel-1 InSAR data [6,40,62,63], which are described in the IPA and International Centre for Integrated Mountain Development (ICIMOD) manuals. According to the guidelines of the IPA [11,12,42], the systematic inventory procedure for rock glaciers consists of three stages, which are described below and illustrated in Figure 3. This diagram [64] was adapted to the conditions and availability of initial data for the study region.

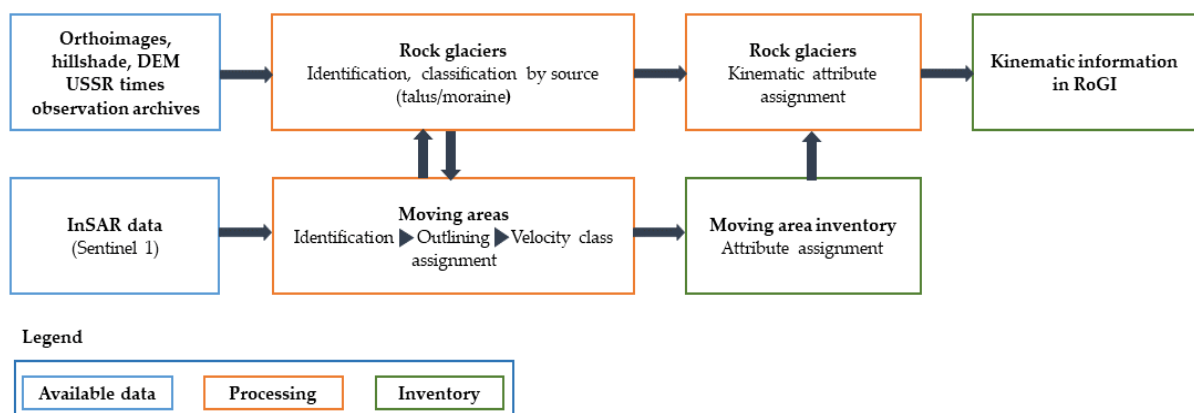


**Figure 3.** Conceptual diagram of a standardized method for creating a moving area inventory and RoGI, including kinematic information. The analysis is performed in the GIS environment.

### 3.1. Delineation of Rock Glaciers by Geomorphologic Approach

The geomorphological approach represents visual detection using high-resolution images and DEM-based products. Surface texture and morphometric analyses can also be used for this purpose. This is a classic approach that is complemented by field visits. This makes it possible to produce an exhaustive list of assumed moving and stationary landforms, the distinction of which (activity classes) is primarily based on geomorphological characteristics. Photogrammetry and LiDAR DEM imaging, when available, facilitates the identification of rock glaciers in forested areas.

We inventoried rock glaciers by geomorphological characteristics using high-resolution remote sensing data available on the Google Earth platform according to the methods explained in [65,66] according to the descriptions given in the IPA instructions. Rock glaciers frequently have transverse ridges and furrows, lateral margins, and talus-like fronts due to the deformation of internal ice (see Figure 1). They rarely have the following indicators: crevasses with exposed ice, abundant thermokarst, abundant supraglacial lakes, ice cliffs, supraglacial streams/channels, and a high (over 1 m/yr) subsidence rate. Due to the constant supply of talus or debris, the surface textures of rock glaciers are usually different from the surrounding slopes, and their surface slopes usually have little or no vegetation [40]. Based on these criteria, we visually mapped the landforms in the images correspond to the moving targets in the interferograms and identified the rock glacier. To distinguish the rock glaciers from permafrost and bare ground surface velocity obtained from InSAR was used.

Google Earth data have been applied to a number of research areas [67–73]. Google Earth uses SPOT images or Digital Globe products (e.g., Ikonos and QuickBird) at a resolution that is close to aerial photographs. The images were georeferenced with a DEM based on the Shuttle Radar Topography Mission SRTM data, which have a resolution of 90 m in the study area. In addition, Google Earth supports user-friendly GIS tools that help in building custom databases and exporting data as KML files and converting them to shapefiles for further analysis in the GIS environment [13,74]. Google Earth has previously been used as a platform for rock glacier mapping in British Columbia, the Bolivian Andes, the Hindu Kush Himalaya region, and the Himalayas of Nepal [13,22,74–76]. In the absence of any spectral and spatial information about the images used, quantifying uncertainty into the inventory was difficult. However, in a similar location [74], image fidelity was found to be sufficient for this purpose. Rock glaciers are classified as transitional or active based on their surface velocity. Rock glaciers with unclear surface velocity only fired if the InSAR sensitivity in that area was low, in which case they fired with indeterminate activity. Debris-covered glaciers and rock glaciers are two ends of a continuum [19,77]. Debris-covered glaciers with visible bodies of ice upslope, abundant thermokarst, abundant supraglacial lakes and other visible indicative features listed in IPA guidelines [12] were not included in the rock glacier inventory.

### 3.2. Identifying Surface Velocity Using SAR Interferometry

**Kinematic approach:** The differential interferometry method detects the movements of the Earth's surface using the phase differences between two radar images taken at different times [78]. Since the phases of the differential interferogram were wrapped between  $-\pi$  and  $\pi$ , one phase cycle corresponded to half a wavelength (e.g., 2.8 cm for C-band [16]) of surface displacements along the direction of the radar sighting beam [78].

In our paper, images from the Sentinel-1 satellites of the SLC level were used; these are a freely available Alaska Satellite Facility (<https://asf.alaska.edu/> (accessed on 26 April 2022)) resource, and they make it possible to select a stack of images for multi-pass processing. The IW mode has a resolution of 20 m in azimuth and 5 m in range. The selection of radar images was based on the following criteria: The survey period was 5 years from 8 August 2017 to 28 September 2021 with a seasonal restriction (only 2 months of August and September were selected); the total number of images was 25 for ascending and 26 for descending orbits. To achieve high interferometric coherence, a maximum time base

of 48 days was chosen. According to the specified criteria, 49 interferometric pairs were built for images in the upward survey geometry and 52 pairs for the downward survey. Basic survey parameters: ascending orbit—path 158, frame 142; descending orbit—path 136, frame 441; IW survey mode.

We chose only two months of observations because of minimal snow cover occurring only during August and September. This is a serious limitation in achieving sufficient coherence between surveys [79]. The image series was processed using the intermitted SBAS method [80] or discrete SBAS, where the timeline was set as hard and the whole stack started with broken links (because only a few months were included in the processing). The discrete SBAS method interpolates the time periods when pixel coherence falls below the selected coherence threshold on some interferograms, and also results in a significant improvement in spatial coverage compared to the original SBAS algorithm for partially vegetated study areas [81,82].

Interferometric processing was performed using ENVI software with an additional Sarscape multimodule (©Sarmap SA, 2001–2020). Stack processing was performed in the standard settings of the Sentinel TOPSAR mode and according to the pipeline (processing steps) in the SBAS module.

Then, the values of displacement velocities from LOS units were converted into values of vertical velocities in millimeters. The resulting raster surfaces of vertical velocities were cut from a vector file with geomorphological contours of rock glaciers; from the stripped values, the maximum and minimum speed indicators were extracted into the attribute information. Raster surfaces, prior to cutting geomorphological contours, also underwent an additional procedure for evaluating all selected moving areas in order to validate and cut-off moving areas whose kinematic nature was associated with slope processes and other phenomena. When re-comparing the geomorphological contours of rock glaciers and the raster of motion velocities, several objects were refined and supplemented. To move into the kinematic categories, seven classes were created (<1, 1, 1–10, 10, 10–100, 100, and >100 cm/yr). The choice of kinematic classes was made according to the proposals of the international working group [42].

Where the calculated speed was close to the upper limit of the speed class, the ARG was assigned to that faster class because the one-dimensional line-of-sight measurement provided by radar interferometry represents only one motion component, and thus typically underestimates the actual three-dimensional surface motion [6]. The same was enacted with the natural temporal variations in surface displacement rates; i.e., if two or more classes were present during the observation time interval, the highest displacement speed was used to determine the speed class.

Finally, we derived the topographic/geometric parameters using Spatial Analyst tools in the GIS environment. Height information was determined from the SRTM DEM. Our inventory lists the geographical locations (including longitude, latitude, and altitude), the geomorphic attributes (including area, length, aspect and PISR), and the surface velocity of each rock glacier. Then, we compiled a spreadsheet to summarize the characteristics and calculate the total statistics.

#### 4. Results

For the first time since the 1990s, rock glacier identification and inventorization work was carried out in the Lepsy and Aksu River basins of the Zhetysy Alatau, and their detailed digital catalog was compiled in accordance with international standards [11,83].

A total of 256 rock glaciers were identified, with a total area of more than 28.5 km<sup>2</sup> and an average lowest boundary at 3036 m ASL; the rock glaciers were 0.11 km<sup>2</sup> by average size. The largest rock glacier was 1.53 km<sup>2</sup> by size, while the smallest rock glacier had an area of about 0.004 km<sup>2</sup>. According to the kinematic categorization for speed assessment, we found that active rock glaciers counted for 204 units; 47 of their total number were included in the transitional category and 5 were relics.



#### 4.1. Type of Rock Glaciers Origin

Talus-derived types of rock glaciers were more numerous than those of moraine origin. About 61%, or 156 rock glaciers, were formed from talus in the Lepsy and Aksu River basins, while the remaining 39% (100 glaciers) were formed from moraines (Figure 4). Several rock glaciers were also found in the study area with several episodes of activity, where newer lobes dominated older ones. Complex rock glaciers with more than one root zone are most common in the study area. Figure 5 shows examples of rock glacier origin types in two basins of the Zhetysu Alatau Range.

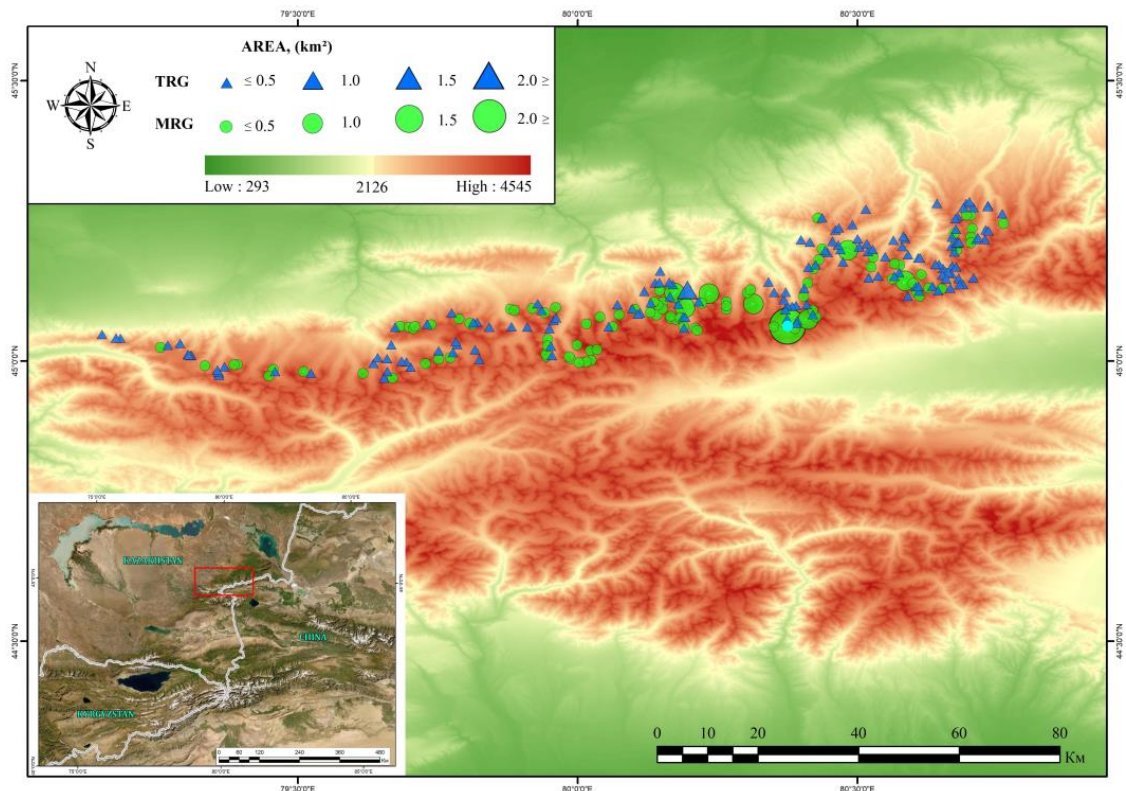


**Figure 4.** Topographic map of the Zhetysu Alatau. Green circles and blue triangles represent Moraine rock glaciers (MRG) and Talus rock glaciers (TRG), respectively. The size of the circle and triangle represents the size of the rock glacier.

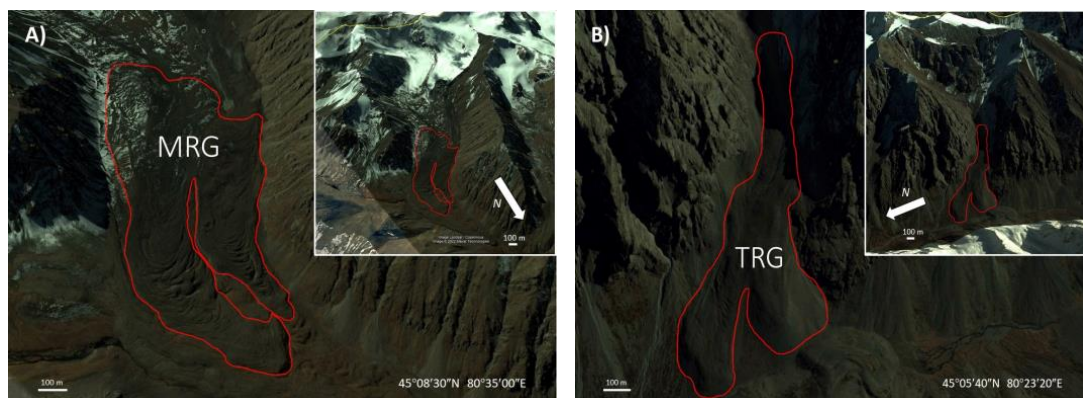


**Figure 5.** Google Earth images of (A) typical moraine rock glacier (MRG) and (B) talus rock glacier (TRG). The insets show the topographic and morphological features surrounding the same rock glaciers.

According to the results of the analysis of the topographic/geometric parameters, the north-facing slopes, which have lower solar radiation, are more favorable for the formation of rock glaciers than the south-facing slopes. The number of inventoried rock glaciers in this study can be considered a conservative estimation due to limitations in remote sensing data and human factors. As such, more rock glaciers in this area cannot be ruled out. Table 1 lists the main characteristics of the rock glaciers obtained in our analysis.

**Table 1.** Main characteristics of rock glaciers located in the Aksu and Lepsy River basins.

	Area (km <sup>2</sup> )	Slope (°)	Altitude (m)	Pot. Radiation (W/m <sup>2</sup> )	Minimum Altitude at the Front (m)	Maximum Altitude of Rock Glaciers (m)
Mean	0.11	16.9	3101	1,025,519	3036	3165
Std deviation	0.16	5.0	205	76,791	212	199
Minimum	0.004	7.7	2384	836,379	2384	2614
Maximum	1.53	42.0	3723	1,234,567	3640	3723

#### 4.2. Surface Velocity Evaluation

Quantitative analysis of the distribution of identified rock glaciers showed the following distribution over the combined watersheds of the Aksu and Lepsy Rivers. Thus, 102 RGs were allocated for the Aksu basin and 154 RGs for the Lepsy basin. Depending on topographic factors (topography, slope, size, and amount of ice in the composition), rock glaciers move differently, even if they are located close to each other. According to the manuals [64,83] and research [6], when calculating the velocity, in the case of different speed indicators on the body of one rock glacier, we took the maximum value. In Figures 6 and 7, one circle represents one individual rock glacier with its maximum velocity.

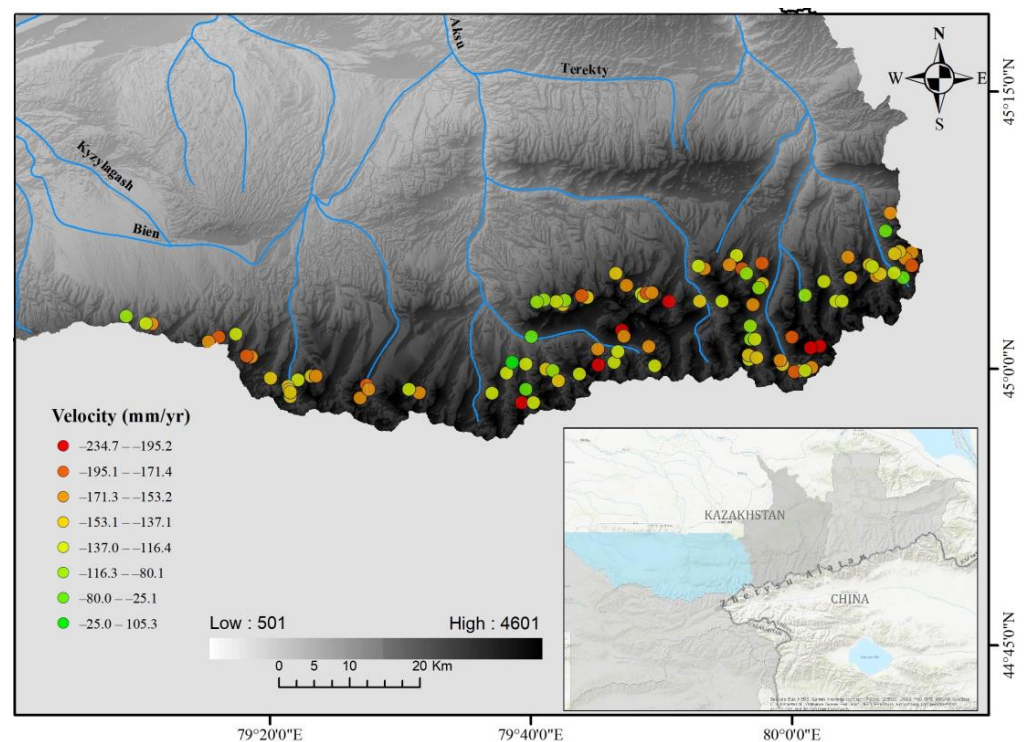


**Figure 6.** Displacement rates of rock glaciers in the integrated Aksu catchment area.

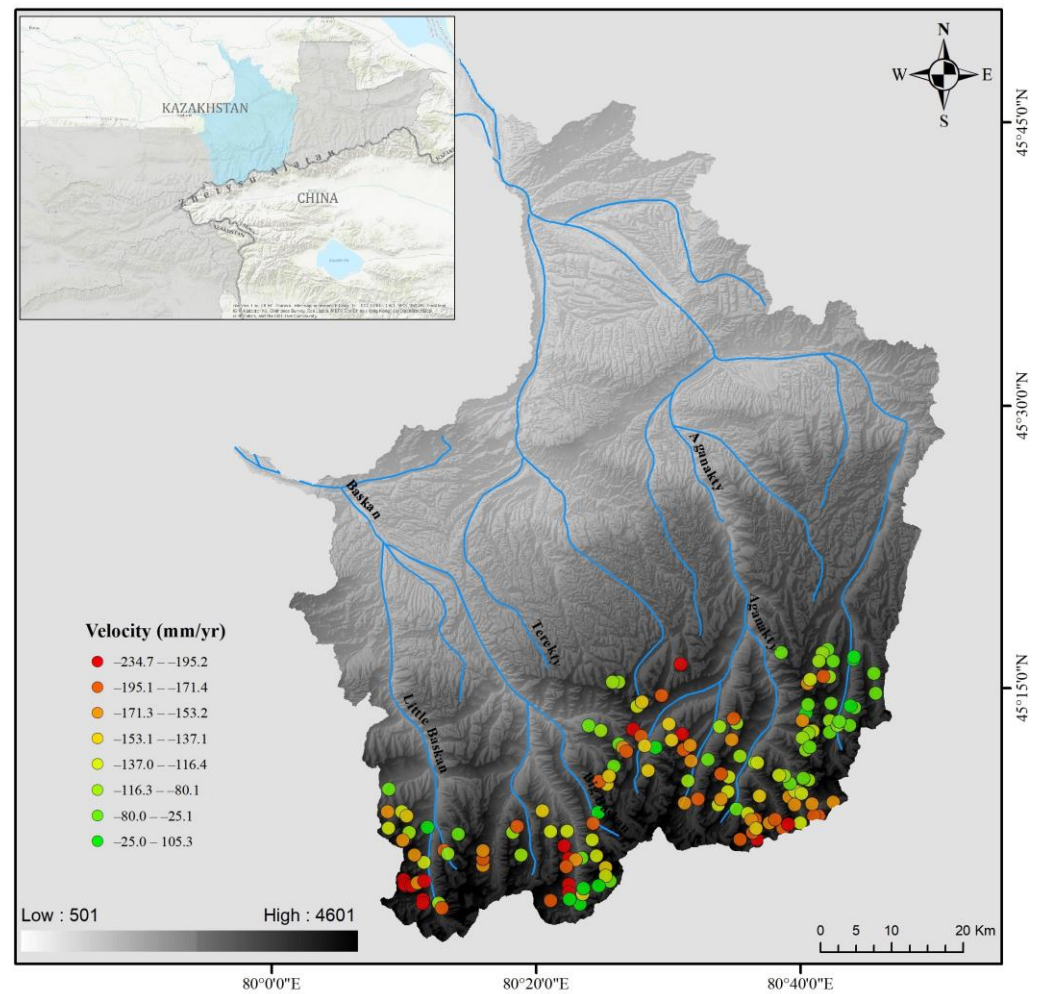


**Figure 7.** Rock glaciers inventory results for the integrated Lepsy catchment area.

#### 4.2.1. Aksu River Basin

In the Aksu River basin, 93 active rock glaciers were identified, with a displacement rate of up to  $240 \text{ mm yr}^{-1}$  (Figure 6); eight units fell into the transitional category and one was classified as a relic. The lower elevation mark at which active rock glaciers are located in the basin is 3100 m ASL and the maximum value is 3700 m ASL.

#### 4.2.2. Lepsy River Basin

In the Lepsy River basin, 154 rock glaciers were identified, of which 111 units were active: 39 in the transitional category and 4 in the relict category. The displacement rate in the analyzed basin was also  $-252 \text{ mm yr}^{-1}$  (Figure 7). The lower and upper heights of the location of active rock glaciers ranged from 2600 m ASL to 3720 m ASL.

Velocity field distribution analysis made it possible to identify several groups of rock glaciers with a similar pattern of velocity distribution over the glacier body (Figure 8):

- The first type—the main distribution of moving areas in the middle of the rock glacier body;
- The second type—the location of the moving areas closer to the forehead of the rock glacier;
- The third type is a complex distribution of moving sections in several areas in same glacier body.



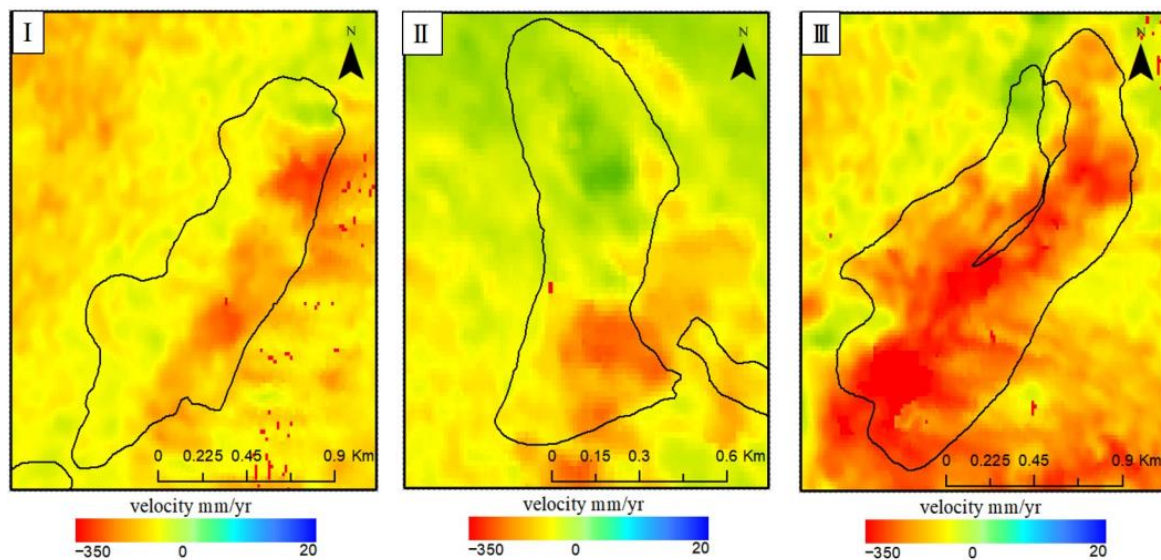


**Figure 8.** Examples of displacement fields by types of velocity distribution (type I—moving area in the middle, type II—forehead moving area, type III—several moving areas).

A more detailed analysis of velocity distribution types will be carried out in the next part of the work with a scaling of the study area (the entire Zhetysu Alatau).

#### 4.3. Additional Geomorphological Features

##### 4.3.1. Aspect

About 54% of the total area (or 15.4 km<sup>2</sup>) of rock glaciers was located on slopes with northern exposure: 17% in the northern, more than 20% in the northeastern, and almost 17% in the northwestern exposures. On slopes with western and eastern exposures, 13% and 17% of the total area of rock glaciers were formed, respectively. Only 16% of rock glaciers, covering 4.5 km<sup>2</sup> of the area, were formed on slopes with southern exposure, including on the slopes of southeastern exposure (SE), where 7% of rock glaciers were observed; in the southwestern exposure (SW), 5% were formed, while only 4% were formed in the southern (S) exposure (Figure 9a,b).

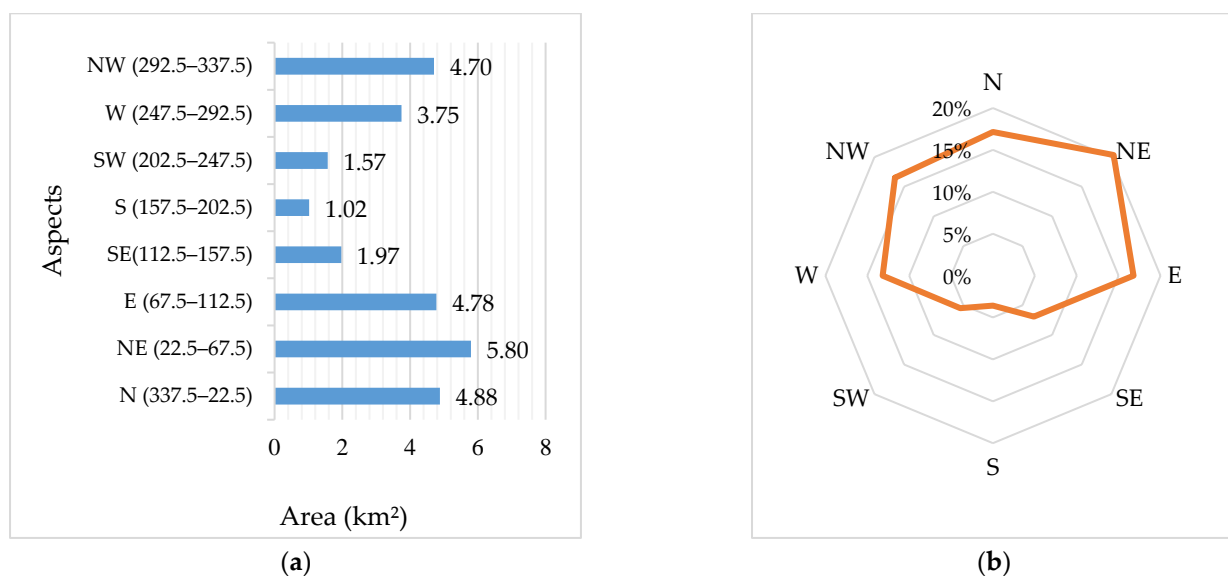


**Figure 9.** Distribution of rock glaciers by aspect: (a) area ratio (km<sup>2</sup>) per aspect; (b) percentage of area per aspect.

The overall analysis showed that the rock glaciers developed at lower elevations in the slopes of northern aspects and at higher elevations in southern aspects. Significant variability was observed in the aspect distribution of the rock glacier area. The northeast (NE) slopes have a large area of rock glacier, followed by the north (N) and east (E) slopes. In total, more than 5.8 km<sup>2</sup> of the rock glacier area is located on the northeastern slopes (Figure 9a).

#### 4.3.2. Height Distribution

The largest area of rock glaciers was 24.5 km<sup>2</sup> and was located between 2800 and 3400 m ASL. This is almost 86% of the total area of the inventoried rock glaciers (Figure 10a,b). Of these, 11.83 km<sup>2</sup>, or 41.5%, of the total area lies within altitudes of 3000–3200 m ASL. The smallest concentration is located between 2200 and 2400 m ASL and 3600 and 3800 m ASL, where glacier amounts are less than 1% in total.

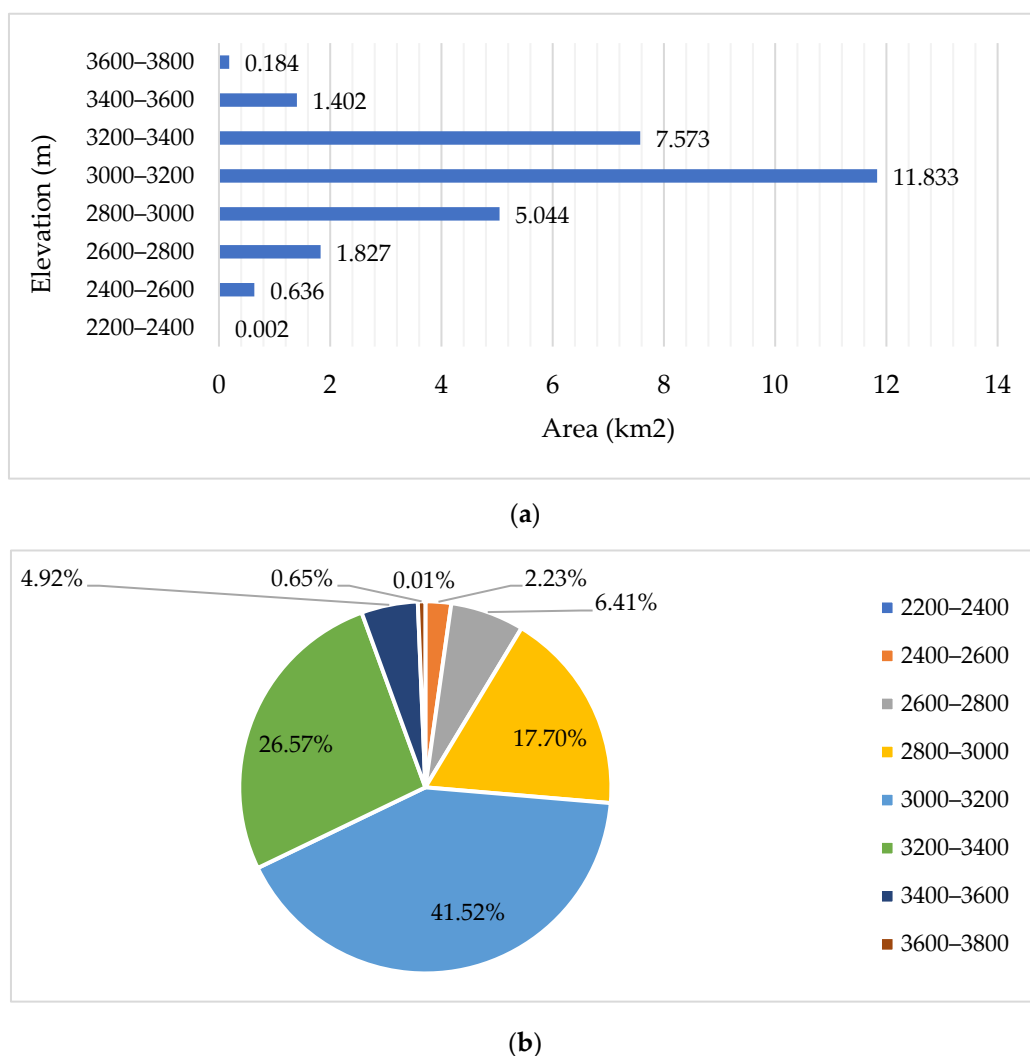


**Figure 10.** Distribution of rock glaciers by height: (a) ratio of area (km<sup>2</sup>) to height; (b) percentage of area per height.

#### 4.3.3. Accuracy of Evaluation

Accuracy was assessed by two operators by isolating the boundaries of three active rock glaciers once each day over three days (Figure 11). All three rock glaciers were of moraine origin.

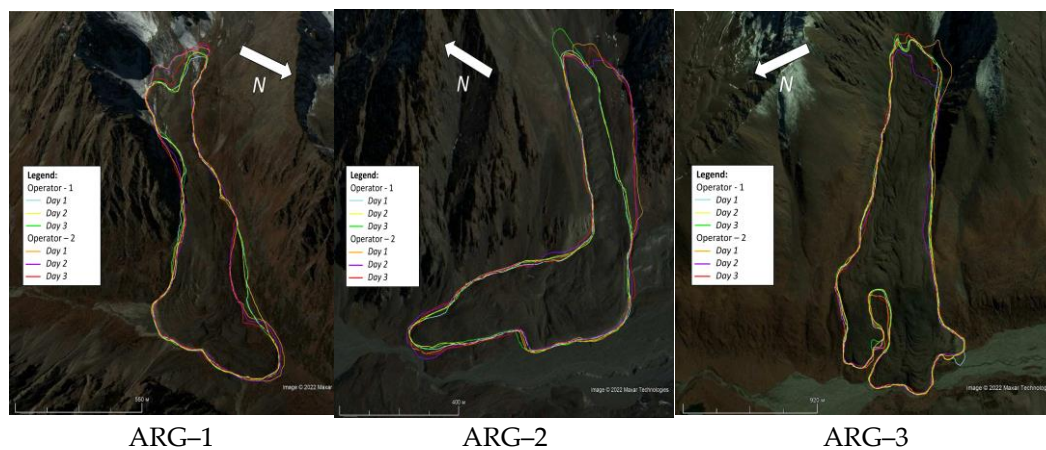


**Figure 11.** Polygonal outlines of rock glaciers.

During mapping, the fronts of the main tongues were plotted on the map with small differences, and the minimum height of each ARG remained almost unchanged. Rooting zones demonstrated higher variability, which significantly affected maximum height variability (differences in the height of the root zone between two operators: 1-ARG—14 m, 2-ARG—35 m, and 3-ARG—8 m). The sides of the third ARG remained identical for both operators during all three days, while opinions were divided regarding the first and second ARGs. One operator singled out, in the main, the most obvious creeping beats. The other also included scree cones. For ARG-3, the average area for the first operator was 0.58 km<sup>2</sup>, for the second—0.598 km<sup>2</sup>, and for ARG-2—0.198 km<sup>2</sup> and 0.24 km<sup>2</sup>, respectively (Table 2).

**Table 2.** The results of the evaluation of accuracy by two operators.

Operator 1				Mean Area (km <sup>2</sup> )	Standard Deviation
	Day-1 (km <sup>2</sup> )	Day-2 (km <sup>2</sup> )	Day-3 (km <sup>2</sup> )		
Rock glacier-1	0.572916	0.586109	0.582255	0.580426	0.005539008
Rock glacier-2	0.194221	0.198028	0.202213	0.198154	0.003263937
Rock glacier-3	0.906863	0.911821	0.913899	0.910861	0.002951556
Operator 2				Mean Area (km <sup>2</sup> )	Standard Deviation
	Day-1 (km <sup>2</sup> )	Day-2 (km <sup>2</sup> )	Day-3 (km <sup>2</sup> )		
Rock glacier-1	0.615497	0.601093	0.577631	0.598073667	0.015605464
Rock glacier-2	0.240758	0.239961	0.239547	0.240088667	0.000502563
Rock glacier-3	0.963554	0.888456	0.917465	0.923158333	0.030921815

## 5. Discussion

In our inventory, 256 rock glaciers were identified in the Aksu and Lepsy River basins (northern Zhetysu Alatau). This inventory of the selected basins made it possible to create a novel digital database on the available rock glaciers in the region, develop cataloging methods according to international standards, and study the features of the region. Based on the experience we gained, even more work is underway to scale the inventory to the entire Zhetysu Alatau region.

Of the main features of rock glacier formation conditions, it is worth noting that northern slopes receiving a lower PISR may represent the most favorable conditions for rock glacier formation, even at lower elevations.

Additionally, glaciers, as the main source of rock glaciers of moraine origin, are rapidly decreasing in size. According to the authors [61], the rate of annual glacier reduction in



the Aksu–Bien and Lepsy–Baskan River basins for the period from 1956 to 2011 is 0.7%. According to Kaldybayev et al. [84], for the period of 2001–2016, Aksu–Bien and Lepsy–Baskan shrank in glacier area by  $1.2\% \text{ a}^{-1}$  and  $1\% \text{ a}^{-1}$ , respectively. In the future, this accelerated shrinkage rate may lead to the appearance of more rock glaciers of moraine origin in the region. It is widely accepted, and many scientists believe, that glaciers with less favorable climatic conditions turn into rock glaciers [19].

The glacier area of the region was obtained from Kaldybayev et al. [84]. The ratio between the area of rock glaciers and the area of glaciers (Figure 12) was significantly higher for the Lepsy basin than for the Aksu basin. This ratio can be considered an indicator of the predominance of glacial and periglacial activity in the region. It can be concluded that periglacial activity in the Lepsy basin prevailed over glacial activity. However, this analysis was simply an attempt to understand the relationship and should be treated with caution due to the lack of comprehensive field observations and validations.

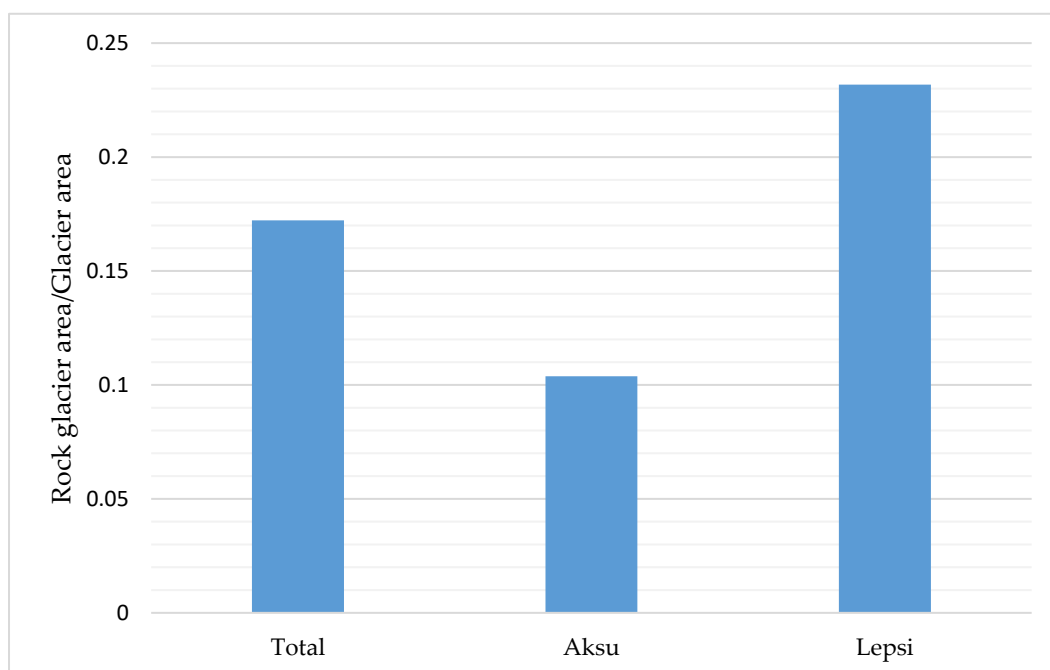


**Figure 12.** Distribution of the ratio between the area of the rock glacier and total glacier area.

### 5.1. InSAR Technology Ambiguities

In terms of kinematic-information-collection methods, InSAR time series analysis has great potential for monitoring low-amplitude movement velocities, but this method is not without significant limitations.

The main limitations that arise when calculating displacements using radar interferometry methods are the following: (a) The lack of calculation of displacements measured on moving sections, and the slope displacement projection calculation provides information on displacements in 3D projection; it is worth noting that the magnitudes of the displacements of moving segments on the northern and southern sides are calculated less accurately, even when processing data from the ascending and descending orbits of the satellite; and (b) estimating low-speed moving sections (displacement rates less than 3 cm per year) is insufficient since interferograms with a long timeline contain too much noise, while slow-current displacements are better distinguished by pairs with a large time interval.

The problem of InSAR sensitivity is well known and it causes many issues, especially for landforms with a very low offset. Projecting the LOS offset onto the intended direction of travel (i.e., along the steepest slope) does indeed provide more representative results [85], but the rates are probably still somewhat underestimated. Rock glaciers in areas with poor

InSAR sensitivity are included in the inventory even if their line-of-sight velocity is  $<1$  cm/yr for this reason. Their activity is classified as “undefined”.

### 5.2. Comparison with Previous Studies of Tien Shan Rock Glaciers

Previous studies of rock glaciers in the Eastern Tien Shan are limited. According to Gorbunov and Titkov [48] active rock glaciers in the Zhetysu Alatau are confined to the zone between 2300 and 3500 m, whereas relict rock glaciers occur down to 2100 m. The bulk of the active near-glacier (moraine-derived) rock glaciers are concentrated within the elevational range of 3000–3200 m, whereas the bulk of the active near-slope (talus derived) rock glaciers are found between 2900 and 3100 m a.s.l. The belt of rock glaciers is 200–300 m lower than in the Northern Tien Shan mountains corresponding to its more northerly latitude [49]. These findings are generally consistent with our inventory. For the sections of the two basins analyzed in our work, the following altitude ranges were identified from 2600 m ASL to 3720 m ASL, which means an increase in the lower limits of the placement of rock glaciers by 300 m higher and an increase in the upper limits by 220 m. The highest surface velocity was found at altitudes of 3000–3400 m ASL (Figure 13). Most likely, this is due to the fact that 68% of the total area of the inventoried rock glaciers is located in this interval.

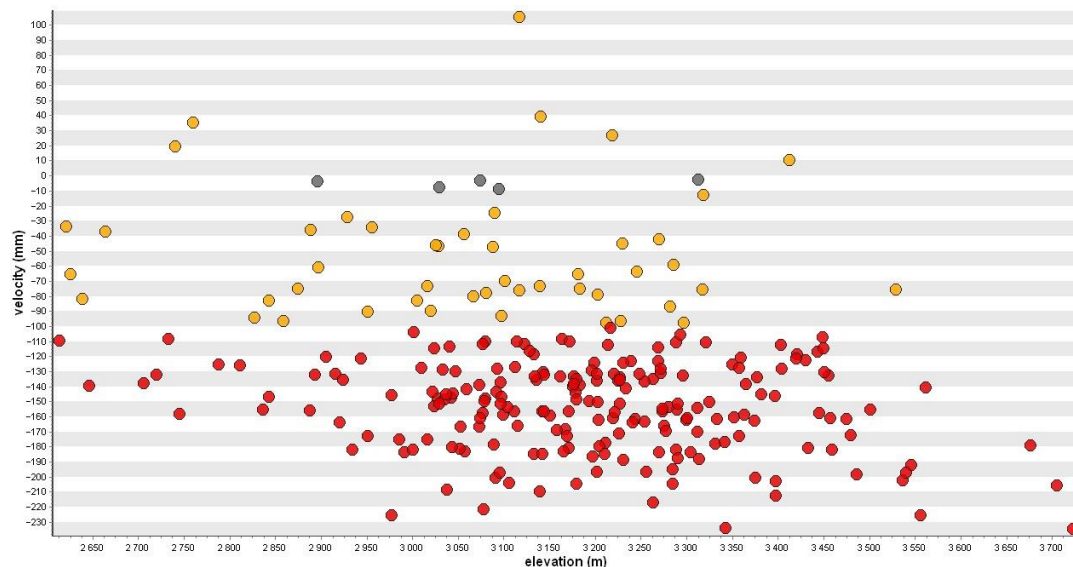


**Figure 13.** The distribution of the kinematic activity of rock glaciers by height.

The mean size of rock glacier in the Northern Tien Shan is  $0.27 \text{ km}^2$  [6]. The highest rooting zone of a rock glacier is situated above 4000 m and the mean elevation is 3480 m. Wang [40] compiled an inventory of active rock glaciers for the Boro-Khoro area (Eastern Tien Shan). Despite the more northern location of the Zhetysu Alatau than the Boro-Khoro ridge, the average PISR value for the slopes of the northern and southern exposures is higher by  $1.04 \times 10^5 \text{ W m}^{-2}$  and  $1.14 \times 10^5 \text{ W m}^{-2}$ , respectively. For both ranges, north-facing slopes are more favorable for rock glacier formation than south-facing slopes. The detected displacement rate in the study region reaches  $240 \text{ mm yr}^{-1}$ , which is several times less than in Boro-Khoro where, according to researchers, the rates reach  $114 \text{ cm yr}^{-1}$ . The average area of a rock glacier in the basins of the Aksu and Lepsy Rivers was  $0.11 \text{ km}^2$ , while it was  $0.35 \text{ km}^2$  on the Boro-Khoro ridge [40]. Additionally, the ratio of types of rock glaciers of talus and moraine origins is 61% and 39%, respectively, while in Boro-Khoro, the ratios are 31% and 69%, respectively.

### 5.3. Building a Digital Data Catalog That Meets International Standards

For the entire period of observations of rock glaciers in the Zhetysu Alatau, no practical catalog was developed; there were only oral reports from researchers and some field observations of individual rock glaciers. In [53], the author claims that there are at least 850 active rock glaciers in the entire Zhetysu Alatau, while no specific works, inventories, or catalogs have been found in the archives. In our work, for the first time, we have digitalized rock glaciers in the combined watersheds of the Aksu and Lepsy Rivers of the Zhetysu Alatau and compiled a catalog.

However, at the same time, the most studied rock glacier of Central Asia is located in Zhetysu Alatau, which is Nizkomorenniy (Figures 1 and 14). The first cycles of observations on it were started in 1948 by Palgov N.N. [50] and continued until the 1990s. The formation of the rock glacier is associated with the glacier located above, from which the moraine broke off and began to move down the slope with a steepness of 15 degrees, acquiring the form of a rock glacier. The steepness of the frontal ledge is 40–45°. For 34 years (observation periods 1949–1953–1959–1964–1970–1982), the module of the surface velocity of the rock glacier was 0.17 m/year, the maximum was 0.35 m/year, and the total value of its movement was 8.91 m [86].

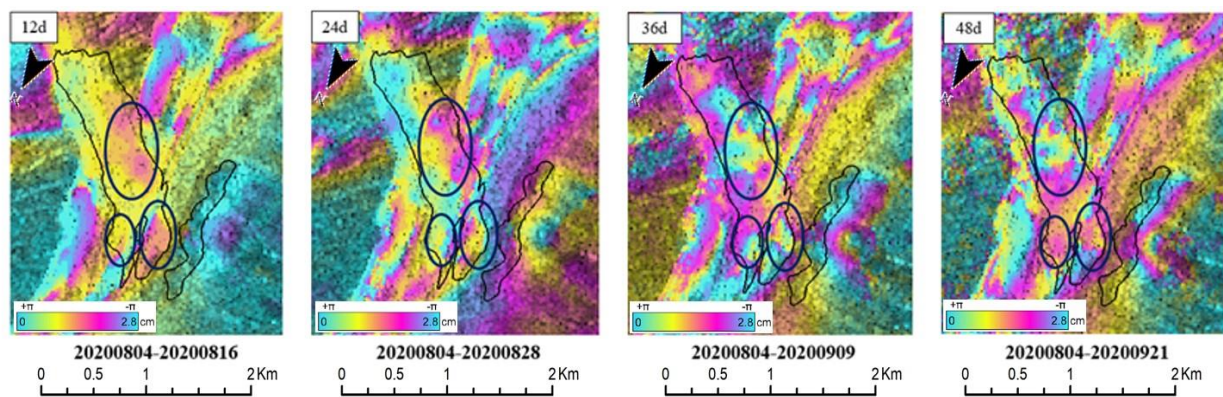


**Figure 14.** An example of differential interferogram series for the rock glacier—Nizkomorenniy.

In the above series of differential interferograms (Figure 14) for the Nizkomorenniy rock glacier, three areas of movement are clearly distinguished: in the central part of the rock glacier, significant changes in the movement field are noted over 48 days; motion zones are also noted on two frontal slopes of the rock glacier. It should be noted that the two main frontal slopes move with different signs of movement: the first actively gives off mass, while the second one accumulates mass. It bears emphasis, that the described rock glacier has a history of observations of about 70 years and still retains its activity. This glacier has an annual surface velocity rate of  $-45--250 \text{ mm yr}^{-1}$  (these values are taken from the surface velocity map by the SBAS method for the 2017–2021 period).

## 6. Conclusions

This study provided the first comprehensive up-to-date documentation on the characteristics of rock glaciers in the Aksu and Lepsy River basins of the Zhetysu Alatau.

A total of 256 active rock glaciers covering an estimated area of 28.5 km<sup>2</sup> were inventoried and mapped by combining the use of SAR interferometry and optical imagery from Google Earth.

The average lower height of rock glaciers in this part of the Zhetysu Alatau was 3036 m ASL. About 39% of rock glaciers were of moraine origin, and 61% of them were talus-related. The largest area of rock glaciers was located between 2800 and 3400 m ASL and covered 24.5 km<sup>2</sup>; this was almost 86% of the total area of the inventoried rock glaciers.

Most rock glaciers had a northern (northern, northeastern, or northwestern) orientation, which indicated the important role of solar insolation in their formation and



preservation. Slopes with lower PISR favored the development of rock glaciers. The height of rock glaciers generally increased from east to west and decreased from south to north, indicating the effect of latitude and longitude on rock glacier location by height.

We also conducted a detailed study of differential interferograms with different time bases to map the surface flow of the Nizkomorennny rock glacier. We found two fast-moving branches in the lower part (frontal slope) of the rock glacier, and a flow zone in the central part of the rock glacier was also relatively active. More importantly, we saw active areas of multidirectional movement throughout the body of the rock glacier.

This inventory has provided a baseline dataset for further studies of rock glaciers as a reservoir, as well as for studying permafrost for slope instability, water resources, and greenhouse gas emissions. The successful application of the proposed method in the Zhetyu Alatau demonstrates that this approach can be applied to other high mountain regions of the world, thereby helping to fill gaps in our knowledge of mountain glaciers on a global scale. This new knowledge will be useful in inferring the distribution of alpine permafrost in high mountains.

**Author Contributions:** Conceptualization, A.K. and Y.C.; methodology, A.K., N.S. and A.Y.; software, A.Y., N.S. and A.M.; validation, S.N.; investigation, A.K. and N.S.; data curation, A.K. and K.Z.; writing—original draft preparation, N.S. and A.Y.; writing—review and editing, A.K., N.S., A.Y. and G.I.; visualization K.Z.; supervision, A.K. and Y.C.; project administration, A.K.; funding acquisition, A.K. and S.N. All authors have read and agreed to the published version of the manuscript.

**Funding:** This research has been funded by the Science Committee of the Ministry of Education and Science of the Republic of Kazakhstan within the framework of the projects: AP08856470, AP14872134, AP09058619 and supported by the Postdoctoral Fellowship provided by Al-Farabi Kazakh National University. The APC was funded by the project budget.

**Data Availability Statement:** Sentinel-1 Single Look Complex images used in this study can be downloaded from the Alaska Satellite Facility at <https://asf.alaska.edu> (accessed on 26 April 2022). Shuttle Radar Topography Mission (SRTM) 90m DEM used in this study can be downloaded from CGIARCSI consortium for spatial information at <https://cgiarcsi.community/> (accessed on 24 April 2022). High-resolution optical images with 3D representation used in this study are available in the program Google Earth.

**Acknowledgments:** We are grateful to the providers of free data for this study: European Space Agency (ESA)/European Commission (EC) Copernicus, Alaska Satellite Facility (ASF), United States Geological Survey (USGS) and others.

**Conflicts of Interest:** The authors declare no conflict of interest.

## References

1. Capps, S.R. Rock Glaciers in Alaska. *J. Geol.* **1910**, *18*, 359–375. [[CrossRef](#)]
2. Haeberli, W. Creep of Mountain Permafrost: Internal Structure and Flow of Alpine Rock Glaciers. *Mitteilungen der Versuchsanstalt für Wasserbau, Hydrologie und Glaziologie an der Eidgenössischen Technischen Hochschule Zürich*, (77). 1985. Available online: <https://ethz.ch/content/dam/ethz/special-interest/baug/vaw/vaw-dam/documents/das-institut/mitteilungen/1980-1989/077.pdf> (accessed on 29 December 2022).
3. Martin, H.E.; Whalley, W.B. Rock Glaciers: Part 1: Rock Glacier Morphology: Classification and Distribution. *Prog. Phys. Geogr.* **1987**, *11*, 260–282. [[CrossRef](#)]
4. Barsch, D. Rockglaciers: Indicators for the Present and Former Geocology in High Mountain Environments. *Geogr. J.* **1996**, *164*, 218. [[CrossRef](#)]
5. Berthling, I. Beyond Confusion: Rock Glaciers as Cryo-Conditioned Landforms. *Geomorphology* **2011**, *131*, 98–106. [[CrossRef](#)]
6. Kääb, A.; Strozzi, T.; Bolch, T.; Caduff, R.; Kon Trefall, H.; Stoffel, M.; Kokarev, A. Inventory and Changes of Rock Glacier Creep Speeds in Ile Alatau and Kungöy Ala-Too, Northern Tien Shan, since the 1950s. *Cryosphere* **2021**, *15*, 927–949. [[CrossRef](#)]
7. Barsch, D. Nature and importance of mass-wasting by rock glaciers in alpine permafrost environments. *Earth Surf. Process.* **1977**, *2*, 231–245. [[CrossRef](#)]
8. Humlum, O. The Geomorphic Significance of Rock Glaciers: Estimates of Rock Glacier Debris Volumes and Headwall Recession Rates in West Greenland. *Geomorphology* **2000**, *35*, 41–67. [[CrossRef](#)]
9. Brenning, A. Geomorphological, Hydrological and Climatic Significance of Rock Glaciers in the Andes of Central Chile (33–35°S). *Permafrost. Periglac. Process.* **2005**, *16*, 231–240. [[CrossRef](#)]

10. Degenhardt, J.J. Development of Tongue-Shaped and Multilobate Rock Glaciers in Alpine Environments—Interpretations from Ground Penetrating Radar Surveys. *Geomorphology* **2009**, *109*, 94–107. [CrossRef]
11. *Towards Standard Guidelines for Inventorying Rock Glaciers: Baseline Concepts (Version 4.2.2)*; IPA Action Group Rock Glacier Inventories and Kinematics, 2022; pp. 1–13. Available online: [https://bigweb.unifr.ch/Science/Geosciences/Gemorphology/Pub/Website/IPA/Guidelines/V4/220331\\_Baseline\\_Concepts\\_Inventorying\\_Rock\\_Glaciers\\_V4.2.2.pdf](https://bigweb.unifr.ch/Science/Geosciences/Gemorphology/Pub/Website/IPA/Guidelines/V4/220331_Baseline_Concepts_Inventorying_Rock_Glaciers_V4.2.2.pdf) (accessed on 29 December 2022).
12. *Towards Standard Guidelines for Inventorying Rock Glaciers: Practical Concepts (Version 2.0)*; IPA Action Group Rock Glacier Inventories and Kinematics, 2022; pp. 1–10. Available online: [https://bigweb.unifr.ch/Science/Geosciences/Gemorphology/Pub/Website/IPA/Guidelines/RGI\\_PC/V2/220411\\_Practical\\_Concepts\\_Inventorying\\_Rock\\_Glaciers\\_V2.0.pdf](https://bigweb.unifr.ch/Science/Geosciences/Gemorphology/Pub/Website/IPA/Guidelines/RGI_PC/V2/220411_Practical_Concepts_Inventorying_Rock_Glaciers_V2.0.pdf) (accessed on 29 December 2022).
13. Jones, D.B.; Harrison, S.; Anderson, K.; Betts, R.A. Mountain Rock Glaciers Contain Globally Significant Water Stores. *Sci. Rep.* **2018**, *8*, 2834. [CrossRef]
14. Azócar, G.F.; Brenning, A. Hydrological and Geomorphological Significance of Rock Glaciers in the Dry Andes, Chile (27–33°s). *Permafr. Periglac. Process.* **2010**, *21*, 42–53. [CrossRef]
15. Rangecroft, S.; Harrison, S.; Anderson, K. Rock Glaciers as Water Stores in the Bolivian Andes: An Assessment of Their Hydrological Importance. *Arct. Antarct. Alp. Res.* **2015**, *47*, 89–98. [CrossRef]
16. Villarroel, C.D.; Beliveau, G.T.; Forte, A.P.; Monserrat, O.; Morvillo, M. DInSAR for a Regional Inventory of Active Rock Glaciers in the Dry Andes Mountains of Argentina and Chile with Sentinel-1 Data. *Remote Sens.* **2018**, *10*, 1588. [CrossRef]
17. Halla, C.; Henrik Blöthe, J.; Tapia Baldis, C.; Trombotto Liaudat, D.; Hilbich, C.; Hauck, C.; Schrott, L. Ice Content and Interannual Water Storage Changes of an Active Rock Glacier in the Dry Andes of Argentina. *Cryosphere* **2021**, *15*, 1187–1213. [CrossRef]
18. Millar, C.I.; Westfall, R.D.; Delany, D.L. Thermal and Hydrologic Attributes of Rock Glaciers and Periglacial Talus Landforms: Sierra Nevada, California, USA. *Quat. Int.* **2013**, *310*, 169–180. [CrossRef]
19. Anderson, R.S.; Anderson, L.S.; Armstrong, W.H.; Rossi, M.W.; Crump, S.E. Glaciation of Alpine Valleys: The Glacier—Debris-Covered Glacier—Rock Glacier Continuum. *Geomorphology* **2018**, *311*, 127–142. [CrossRef]
20. Brighenti, S.; Tolotti, M.; Bruno, M.C.; Wharton, G.; Pusch, M.T.; Bertoldi, W. Ecosystem Shifts in Alpine Streams under Glacier Retreat and Rock Glacier Thaw: A Review. *Sci. Total Environ.* **2019**, *675*, 542–559. [CrossRef] [PubMed]
21. Jones, D.B.; Harrison, S.; Anderson, K.; Whalley, W.B. Rock Glaciers and Mountain Hydrology: A Review. *Earth-Sci. Rev.* **2019**, *193*, 66–90. [CrossRef]
22. Ran, Z.; Liu, G. Rock Glaciers in Daxue Shan, South-Eastern Tibetan Plateau: An Inventory, Their Distribution, and Their Environmental Controls. *Cryosphere* **2018**, *12*, 2327–2340. [CrossRef]
23. Scotti, R.; Brardinoni, F.; Alberti, S.; Frattini, P.; Crosta, G.B. A Regional Inventory of Rock Glaciers and Protalus Ramparts in the Central Italian Alps. *Geomorphology* **2013**, *186*, 136–149. [CrossRef]
24. Humlum, O. The Climatic Significance of Rock Glaciers. *Permafr. Periglac. Process.* **1998**, *9*, 375–395. [CrossRef]
25. Konrad, S.K.; Humphrey, N.F.; Steig, E.J.; Clark, D.H.; Potter, N.; Pfeffer, W.T. Rock Glacier Dynamics and Paleoclimatic Implications. *Geology* **1999**, *27*, 1131–1134. [CrossRef]
26. Millar, C.I.; Westfall, R.D.; Evenden, A.; Holmquist, J.G.; Schmidt-Gengenbach, J.; Franklin, R.S.; Nachlinger, J.; Delany, D.L. Potential Climatic Refugia in Semi-Arid, Temperate Mountains: Plant and Arthropod Assemblages Associated with Rock Glaciers, Talus Slopes, and Their Forefield Wetlands, Sierra Nevada, California, USA. *Quat. Int.* **2015**, *387*, 106–121. [CrossRef]
27. Sorg, A.; Kääb, A.; Roesch, A.; Bigler, C.; Stoffel, M. Contrasting Responses of Central Asian Rock Glaciers to Global Warming. *Sci. Rep.* **2015**, *5*, 8228. [CrossRef]
28. Rock Glacier Velocity as an associated parameter of ECV Permafrost (Version 3.1). IPA Action Group Rock glacier inventories and kinematics, 2022; 12p. Available online: [https://bigweb.unifr.ch/Science/Geosciences/Gemorphology/Pub/Website/IPA/RGV/RockGlacierVelocity\\_V3.1.pdf](https://bigweb.unifr.ch/Science/Geosciences/Gemorphology/Pub/Website/IPA/RGV/RockGlacierVelocity_V3.1.pdf) (accessed on 29 December 2022).
29. Kääb, A.; Frauenfelder, R.; Roer, I. On the Response of Rockglacier Creep to Surface Temperature Increase. *Glob. Planet. Chang.* **2007**, *56*, 172–187. [CrossRef]
30. Kellerer-Pirklbauer, A.; Kaufmann, V. About the Relationship between Rock Glacier Velocity and Climate Parameters in Central Austria. *Austrian J. Earth Sci.* **2012**, *105*, 94–112.
31. Kenner, R.; Pruessner, L.; Beutel, J.; Limpach, P.; Phillips, M. How Rock Glacier Hydrology, Deformation Velocities and Ground Temperatures Interact: Examples from the Swiss Alps. *Permafr. Periglac. Process.* **2020**, *31*, 3–14. [CrossRef]
32. Cicoira, A.; Beutel, J.; Faillietaz, J.; Vieli, A. Water Controls the Seasonal Rhythm of Rock Glacier Flow. *Earth Planet. Sci. Lett.* **2019**, *528*, 115844. [CrossRef]
33. Wirz, V.; Gruber, S.; Purves, R.S.; Beutel, J.; Gärtner-Roer, I.; Gubler, S.; Vieli, A. Short-Term Velocity Variations at Three Rock Glaciers and Their Relationship with Meteorological Conditions. *Earth Surf. Dyn.* **2016**, *4*, 103–123. [CrossRef]
34. Strozzi, T.; Caduff, R.; Jones, N.; Barboux, C.; Delaloye, R.; Bodin, X.; Kääb, A.; Mätzler, E.; Schrott, L. Monitoring Rock Glacier Kinematics with Satellite Synthetic Aperture Radar. *Remote Sens.* **2020**, *12*, 559. [CrossRef]
35. Delaloye, R.; Barboux, C.; Bodin, X.; Brenning, A.; Hartl, L.; Hu, Y.; Ikeda, A.; Kaufmann, V.; Kellerer-Pirklbauer, A.; Lambiel, C.; et al. Rock Glacier Inventories and Kinematics: A New IPA Action Group. In Proceedings of the 5th European Conference on Permafrost, Chamonix-Mont Blanc, France, 23 June–1 July 2018; p. 18.
36. Barsch, D. Permafrost Creep and Rockglaciers. *Permafr. Periglac. Process.* **1992**, *3*, 175–188. [CrossRef]

37. Brardinoni, F.; Scotti, R.; Sailer, R.; Mair, V. Evaluating Sources of Uncertainty and Variability in Rock Glacier Inventories. *Earth Surf. Process. Landf.* **2019**, *44*, 2450–2466. [\[CrossRef\]](#)
38. Yague-Martinez, N.; Prats-Iraola, P.; Gonzalez, F.R.; Brcic, R.; Shau, R.; Geudtner, D.; Eineder, M.; Bamler, R. Interferometric Processing of Sentinel-1 TOPS Data. *IEEE Trans. Geosci. Remote Sens.* **2016**, *54*, 2220–2234. [\[CrossRef\]](#)
39. Necsoiu, M.; Onaca, A.; Wigginton, S.; Urdea, P. Rock Glacier Dynamics in Southern Carpathian Mountains from High-Resolution Optical and Multi-Temporal SAR Satellite Imagery. *Remote Sens. Environ.* **2016**, *177*, 21–36. [\[CrossRef\]](#)
40. Wang, X.; Liu, L.; Zhao, L.; Wu, T.; Li, Z.; Liu, G. Mapping and Inventorying Active Rock Glaciers in the Northern Tien Shan of China Using Satellite SAR Interferometry. *Cryosphere* **2017**, *11*, 997–1014. [\[CrossRef\]](#)
41. Brencher, G.; Handwerger, A.L.; Munroe, J.S. InSAR-Based Characterization of Rock Glacier Movement in the Uinta Mountains, Utah, USA. *Cryosphere* **2021**, *15*, 4823–4844. [\[CrossRef\]](#)
42. *Optional Kinematic Attribute in Standardized Rock Glacier Inventories (Version 3.0.1)*; IPA Action Group Rock Glacier Inventories and Kinematics, 2022. Available online: [https://bigweb.unifr.ch/Science/Geosciences/Geomorphology/Pub/Website/IPA/CurrentVersion/Current\\_KinematicalAttribute.pdf](https://bigweb.unifr.ch/Science/Geosciences/Geomorphology/Pub/Website/IPA/CurrentVersion/Current_KinematicalAttribute.pdf) (accessed on 29 December 2022).
43. Palgov, N. Glaciers of Bolshaja Almatinka in Zailiyskij Alatau. *News of the MGO*, 1 January 1932; 322–326. (In Russian)
44. Goloskokov, V. *Old Glaciers of Zailiyskij Alatau*; Academy of Sciences of the Kazakh SSR: Almaty, Kazakhstan, 1949; pp. 80–82. (In Russian)
45. Iveronova, M. *Rock Glaciers in Northern Tien Shan*; Institute of Geography of the Academy of Sciences of the USSR: Moscow, Russia, 1950; pp. 69–88. (In Russian)
46. Gorbunov, A. *Permafrost in Tien Shan*; Publishing house Ilim: Bishkek, Kyrgyzstan, 1967; pp. 1–164. (In Russian)
47. Gorbunov, A. *Rock Glaciers of Zailiyskij Alatau*; USSR Academy of Sciences: Moscow, Russia, 1979; pp. 5–34. (In Russian)
48. Gorbunov, A.; Titkov, S. *Rock Glaciers of the Central Asian Mountains*; USSR Academy of Sciences: Moscow, Russia, 1989; pp. 1–164. (In Russian)
49. Gorbunov, A.; Titkov, S.; Polyakov, V. Dynamics of Rock Glaciers of the Northern Tien Shan and the Djungar Ala Tau, Kazakhstan. *Permafrost. Periglac. Process.* **1992**, *3*, 29–39. [\[CrossRef\]](#)
50. Palgov, N. Movement Observations of a Rock Glacier in the Dzhungar Alatau. *Quest. Geogr. Kazakhstan* **1957**, *2*, 195–207. (In Russian)
51. Vilesov, E.; Morozova, V.; Seversky, I. *Glaciation of the Dzungarian (Zhetysu) Alatau: Past, Present, Future*; KazNU: Almaty, Kazakhstan, 2013. (In Russian)
52. Yudichev, M. *Dzungarian Alatau. Materials on Geology and Minerals of Kazakhstan*; KazFAN USSR: Leningrad, Russia, 1940; Volume 14. (In Russian)
53. Gorbunov, A.; Gorbunova, I. *Geography of Rock Glaciers of the World*; KMK Scientific Press Ltd.: Moscow, Russia, 2010. (In Russian)
54. Kaldybayev, A.; Chen, Y.; Vilesov, E. Glacier Change in the Karatal River Basin, Zhetysu (Dzhungar) Alatau, Kazakhstan. *Ann. Glaciol.* **2016**, *57*, 11–19. [\[CrossRef\]](#)
55. Cherkasov, P. *Glacier Inventory of the USSR. Lake Balkhash Basin, Part 4*; Hydrometeorological Publishing House: Leningrad, Russia, 1975; Volume 13. (In Russian)
56. Cherkasov, P. *Glacier Inventory of the USSR. Lake Balkhash Basin, Part 5*; Hydrometeorological Publishing House: Leningrad, Russia, 1980; Volume 13. (In Russian)
57. Cherkasov, P. *Glacier Inventory of the USSR. Lake Balkhash Basin, Part 6*; Hydrometeorological Publishing House: Leningrad, Russia, 1970; Volume 13. (In Russian)
58. Cherkasov, P.; Erasov, V. *Glacier Inventory of the USSR. Lake Balkhash Basin, Part 7*; Hydrometeorological Publishing House: Leningrad, Russia, 1969; Volume 13. (In Russian)
59. Pieczonka, T.; Bolch, T. Region-Wide Glacier Mass Budgets and Area Changes for the Central Tien Shan between ~1975 and 1999 Using Hexagon KH-9 Imagery. *Glob. Planet. Chang.* **2015**, *128*, 1–13. [\[CrossRef\]](#)
60. Narama, C.; Käab, A.; Duishonakunov, M.; Abdrakhmatov, K. Spatial Variability of Recent Glacier Area Changes in the Tien Shan Mountains, Central Asia, Using Corona (~1970), Landsat (~2000), and ALOS (~2007) Satellite Data. *Glob. Planet. Chang.* **2010**, *71*, 42–54. [\[CrossRef\]](#)
61. Severskiy, I.; Vilesov, E.; Armstrong, R.; Kokarev, A.; Kogutenko, L.; Usmanova, Z.; Morozova, V.; Raup, B. Changes in Glaciation of the Balkhash-Alakol Basin, Central Asia, over Recent Decades. *Ann. Glaciol.* **2016**, *57*, 382–394. [\[CrossRef\]](#)
62. Reinosch, E.; Gerke, M.; Riedel, B.; Schwalb, A.; Ye, Q.; Buckel, J. Rock Glacier Inventory of the Western Nyainqentanglha Range, Tibetan Plateau, Supported by InSAR Time Series and Automated Classification. *Permafrost. Periglac. Process.* **2021**, *32*, 657–672. [\[CrossRef\]](#)
63. Liu, L.; Millar, C.I.; Westfall, R.D.; Zebker, H.A. Surface Motion of Active Rock Glaciers in the Sierra Nevada, California, USA: Inventory and a Case Study Using InSAR. *Cryosphere* **2013**, *7*, 1109–1119. [\[CrossRef\]](#)
64. Bertone, A.; Barboux, C.; Bodin, X.; Bolch, T.; Brardinoni, F.; Caduff, R.; Christiansen, H.H.; Darrow, M.M.; Delaloye, R.; Etzelmüller, B.; et al. Incorporating InSAR Kinematics into Rock Glacier Inventories: Insights from 11 Regions Worldwide. *Cryosphere* **2022**, *16*, 2769–2792. [\[CrossRef\]](#)
65. Stumm, D.; Schmid, M.-O.; Gruber, S.; Baral, P.; Shahi, S.; Shrestha, T.; Wester, P. *Manual for Mapping Rock Glaciers in Google Earth*; International Centre For Integrated Mountain Development (ICIMOD): Kathmandu, Nepal, 2015.

66. Pandey, P. Inventory of Rock Glaciers in Himachal Himalaya, India Using High-Resolution Google Earth Imagery. *Geomorphology* **2019**, *340*, 103–115. [CrossRef]
67. Butler, D. The Web-Wide World. *Nature* **2006**, *439*, 776–778. [CrossRef]
68. Nourbakhsh, I.; Sargent, R.; Wright, A.; Cramer, K.; McClendon, B.; Jones, M. Mapping Disaster Zones. *Nature* **2006**, *439*, 787–788. [CrossRef]
69. Ballagh, L.M.; Parsons, M.A.; Swick, R. Visualising Cryospheric Images in a Virtual Environment: Present Challenges and Future Implications. *Polar Rec.* **2007**, *43*, 305–310. [CrossRef]
70. Ballagh, L.M.; Raup, B.H.; Duerr, R.E.; Khalsa, S.J.S.; Helm, C.; Fowler, D.; Gupte, A. Representing Scientific Data Sets in KML: Methods and Challenges. *Comput. Geosci.* **2011**, *37*, 57–64. [CrossRef]
71. Chang, A.Y.; Parrales, M.E.; Jimenez, J.; Sobieszczyk, M.E.; Hammer, S.M.; Copenhaver, D.J.; Kulkarni, R.P. Combining Google Earth and GIS Mapping Technologies in a Dengue Surveillance System for Developing Countries. *Int. J. Health Geogr.* **2009**, *8*, 49. [CrossRef] [PubMed]
72. Sheppard, S.R.J.; Cizek, P. The Ethics of Google Earth: Crossing Thresholds from Spatial Data to Landscape Visualisation. *J. Environ. Manag.* **2009**, *90*, 2102–2117. [CrossRef]
73. Yu, L.; Gong, P. Google Earth as a Virtual Globe Tool for Earth Science Applications at the Global Scale: Progress and Perspectives. *Int. J. Remote Sens.* **2012**, *33*, 3966–3986. [CrossRef]
74. Schmid, M.O.; Baral, P.; Gruber, S.; Shahi, S.; Shrestha, T.; Stumm, D.; Wester, P. Assessment of Permafrost Distribution Maps in the Hindu Kush Himalayan Region Using Rock Glaciers Mapped in Google Earth. *Cryosphere* **2015**, *9*, 2089–2099. [CrossRef]
75. Charbonneau, A.A.; Smith, D.J. An Inventory of Rock Glaciers in the Central British Columbia Coast Mountains, Canada, from High Resolution Google Earth Imagery. *Arct. Antarct. Alp. Res.* **2018**, *50*, e1489026. [CrossRef]
76. Rangecroft, S.; Harrison, S.; Anderson, K.; Magrath, J.; Castel, A.P.; Pacheco, P. A First Rock Glacier Inventory for the Bolivian Andes. *Permafr. Periglac. Process.* **2014**, *25*, 333–343. [CrossRef]
77. Haeberli, W.; Hallet, B.; Arenson, L.; Elcinon, R.; Humlum, O.; Kääb, A.; Kaufmann, V.; Ladanyi, B.; Matsuoka, N.; Springman, S.; et al. Permafrost Creep and Rock Glacier Dynamics. *Permafr. Periglac. Process.* **2006**, *17*, 189–214. [CrossRef]
78. Rosen, P.A. Synthetic Aperture Radar Interferometry. *Proc. IEEE* **2000**, *88*, 333–380. [CrossRef]
79. Klees, R.; Massonnet, D. Deformation Measurements Using SAR Interferometry: Potential and Limitations. *Geol. En Mijnb. /Neth. J. Geosci.* **1998**, *77*, 161–176. [CrossRef]
80. Berardino, P.; Fornaro, G.; Lanari, R.; Sansosti, E. A New Algorithm for Surface Deformation Monitoring Based on Small Baseline Differential SAR Interferograms. *IEEE Trans. Geosci. Remote Sens.* **2002**, *40*, 2375–2383. [CrossRef]
81. Sowter, A.; Bateson, L.; Strange, P.; Ambrose, K.; Fifiksyafudin, M. Dinsar Estimation of Land Motion Using Intermittent Coherence with Application to the South Derbyshire and Leicestershire Coalfields. *Remote Sens. Lett.* **2013**, *4*, 979–987. [CrossRef]
82. Bateson, L.; Cigna, F.; Boon, D.; Sowter, A. The Application of the Intermittent SBAS (ISBAS) InSAR Method to the South Wales Coalfield, UK. *Int. J. Appl. Earth Obs. Geoinf.* **2015**, *34*, 249–257. [CrossRef]
83. *Rock Glacier Inventory Using InSAR (Kinematic Approach), Practical Guidelines (Version 3.0.2)*; IPA Action Group Rock Glacier Inventories and Kinematics, 2020. Available online: [https://bigweb.unifr.ch/Science/Geosciences/Gemorphology/Pub/Website/CCI/CurrentVersion/Current\\_InSAR-based\\_Guidelines.pdf](https://bigweb.unifr.ch/Science/Geosciences/Gemorphology/Pub/Website/CCI/CurrentVersion/Current_InSAR-based_Guidelines.pdf) (accessed on 29 December 2022).
84. Kaldybayev, A.; Yaning, C. Assessment of changes in the area of glaciers in the northern part of the zhetysu alatau based on remote sensing data. *J. Geogr. Environ. Manag.* **2022**, *2022*, 4–16. [CrossRef]
85. Notti, D.; Herrera, G.; Bianchini, S.; Meisina, C.; García-Davalillo, J.C.; Zucca, F. A Methodology for Improving Landslide PSI Data Analysis. *Int. J. Remote Sens.* **2014**, *35*, 2186–2214. [CrossRef]
86. Cherkasov, P. Dynamics of a Low-Littered Rock Glacier in the Dzungarian Alatau for 35 Years. In *Glaciers, Snow Cover and Avalanches in the Mountains of Kazakhstan*; Publishing house Nauka: Alma-Ata, Kazakhstan, 1989; pp. 180–216. (In Russian)

**Disclaimer/Publisher’s Note:** The statements, opinions and data contained in all publications are solely those of the individual author(s) and contributor(s) and not of MDPI and/or the editor(s). MDPI and/or the editor(s) disclaim responsibility for any injury to people or property resulting from any ideas, methods, instructions or products referred to in the content.



## Article

# Accelerated Glacier Area Loss in the Zhetysu (Dzhungar) Alatau Range (Tien Shan) for the Period of 1956–2016

Serik Nurakynov <sup>1,2</sup>, Azamat Kaldybayev <sup>1,3,4,\*</sup>, Kanat Zulpykharov <sup>1,3</sup> , Nurmakhambet Sydyk <sup>1,3</sup>, Aibek Merekeyev <sup>1</sup> , Daniker Chepashev <sup>1</sup>, Aiman Nyssanbayeva <sup>3</sup> , Gulnura Issanova <sup>5</sup> and Gonghuan Fang <sup>4</sup> 

<sup>1</sup> Institute of Ionosphere, Almaty 050000, Kazakhstan

<sup>2</sup> Department of Surveying and Geodesy, Satbayev University, Almaty 050000, Kazakhstan

<sup>3</sup> Faculty of Geography and Environmental Sciences, Al-Farabi Kazakh National University, Almaty 050000, Kazakhstan

<sup>4</sup> State Key Laboratory of Desert and Oasis Ecology, Xinjiang Institute of Ecology and Geography, Chinese Academy of Sciences, Urumqi 830011, China

<sup>5</sup> Research Centre for Ecology and Environment of Central Asia, Almaty 050060, Kazakhstan

\* Correspondence: azamat.kaldybayev@gmail.com

**Abstract:** An updated glacier inventory is important for understanding the current glacier dynamics in the conditions of actual accelerating glacier retreat observed around the world. Here, we present a detailed analysis of the glaciation areas of the Zhetysu Alatau Range (Tien Shan) for 1956–2016 using well-established semiautomatic methods based on the band ratios. The total glacier area decreased by  $49 \pm 2.8\%$  or by  $399 \pm 11.2 \text{ km}^2$  from  $813.6 \pm 22.8 \text{ km}^2$  to  $414.6 \pm 11.6 \text{ km}^2$  during 1956–2016, while the number of glaciers increased from 985 to 813. Similar rates of area change characterized the periods 1956–2001, 2001–2012, 2012–2016, and 2001–2016:  $-296.2 \pm 8.3$  ( $-0.8\% \text{ a}^{-1}$ ),  $-63.7 \pm 1.8$  ( $-1.1\% \text{ a}^{-1}$ ),  $-39.1 \pm 1.1$  ( $-2.2\% \text{ a}^{-1}$ ) and  $-102.8 \pm 2.9$  ( $-1.3\% \text{ a}^{-1}$ )  $\text{km}^2$ , respectively. The mean glacier size decreased from  $0.57 \text{ km}^2$  in 2001 to  $0.51 \text{ km}^2$  in 2016. Most glaciation areas of the Zhetysu Alatau faced north (north, northwest, and northeast), covered  $390.35 \pm 11 \text{ km}^2$ , and were located in altitudes between 3000 and 4000 m.a.s.l. With shrinkage rates of about  $-0.8\%$  and  $-1.3\% \text{ a}^{-1}$  for the periods of 1956–2001 and 2001–2016, our results show that study area has the highest shrinkage rate compared to other glacierized areas of Central Asian mountains, including Altai, Pamir, and even the inner ranges of Tien Shan. It was found that a significant increase in temperature ( $0.12 \text{ }^\circ\text{C}/10 \text{ years}$ ) plays a main role in the state of glaciers.

**Keywords:** inventory; glacier shrinkage; climate change; Eastern Tien Shan; the Zhetysu (Dzhungar) Alatau



**Citation:** Nurakynov, S.; Kaldybayev, A.; Zulpykharov, K.; Sydyk, N.; Merekeyev, A.; Chepashev, D.; Nyssanbayeva, A.; Issanova, G.; Fang, G. Accelerated Glacier Area Loss in the Zhetysu (Dzhungar) Alatau Range (Tien Shan) for the Period of 1956–2016. *Remote Sens.* **2023**, *15*, 2133. <https://doi.org/10.3390/rs15082133>

Academic Editors: Ulrich Kamp, Shridhar Jawak and Dariusz Ignatiuk

Received: 2 March 2023

Revised: 5 April 2023

Accepted: 14 April 2023

Published: 18 April 2023



**Copyright:** © 2023 by the authors. Licensee MDPI, Basel, Switzerland. This article is an open access article distributed under the terms and conditions of the Creative Commons Attribution (CC BY) license (<https://creativecommons.org/licenses/by/4.0/>).

## 1. Introduction

In arid and semiarid regions with a low amount of precipitation during the summer, glaciers play a vital role in forming river flow, as melt water is released from the ice when other sources, such as melting snow and the end of the wet season, are exhausted [1,2]. The function of glaciers as a “Water Tower” is of great importance, especially in arid regions, where there is often a shortage of water in the form of rain and snow [3,4]. This case is clearly visible in the Tien Shan, one of the largest mountain systems in the world, located in the Central Asian region. Here, in the summer, glaciers make a significant contribution to the provision of fresh water reserves in the densely populated arid lowlands of Kyrgyzstan, Kazakhstan, Uzbekistan, Turkmenistan, and Xinjiang (China) [5–7].

The semiarid and arid climate typical of most regions of Central Asia is characterized by unique water-dependent ecosystems, and for millennia, human communities have developed in close interaction with limited natural water resources such as rivers, lakes, and areas of shallow groundwater [8]. It has been demonstrated that even a basin with a <5% glacier surface fraction can provide significant amounts of meltwater, contributing to

river runoff during summer, when water is needed most for irrigation [7,9]. People living in the dry lowlands of Central Asia (irrigated agricultural land and oases) depend on river waters originating from the Tien Shan mountains [10].

Arid lowlands and deserts, where irrigation during the growing season usually depends on glacial meltwater, are common along the entire border of the Zhetysu Alatau (Dzhungar) mountain range. In our study area, the waters of the Karatal, Koksuy, Lepsy, Aksu, and other rivers are intensively used for irrigation. In the basins of these rivers, the water withdrawal for irrigation of almost 200 thousand hectares is estimated at  $1.3 \text{ km}^3/\text{year}$ . Rational water use for irrigation and hydropower needs is impossible without comprehensive information on the glaciation areas change (shrinkage) and their volume. Glacier shrinkage leads to a reduction in their long-term moisture reserve, glacial runoff decrease, and the violation of the natural self-regulation of river flow. This problem is solved by monitoring modern glaciation, which should be carried out not for 1–2 “reference” glaciers of a mountainous country where field observations are carried out (an example is the well-known Tuyuksu glacier in the Ile Alatau), but for large glacial systems in general, numbering hundreds and thousands of glaciers. It is also necessary to assess the rate of reduction in ice reserves and the prospects for the existence of these systems in the near and distant future [11].

The first detailed inventory of the Zhetysu Alatau glaciers, the Catalog of Glaciers (*Catalogue of Glaciers of the USSR*, 1969, 1970, 1975, and 1980), was published in 1969 and was based on aerial photographs from 1956. Cherkasov (2004) compiled a second glacier inventory using 1:25,000 topographic maps based on aerial photographs taken in 1972. However, two more limited surveys of glaciers conducted in the 1990s and 2000s have not been released [12].

In subsequent years, several authors studied the glacier area change in the entire Zhetysu Alatau and its subregions. They estimated the overall glacier area decrease [13–15]. The study by Severskiy et al. [15] was especially detailed, where the authors conducted a general analysis and assessment of changes in the glaciation areas of the entire Zhetysu Alatau (in 1956, 1972, 1990, 2000, and 2011). They analyzed changes between 1956 and 1972 based on the glacier catalog of the USSR, which was created using topographic maps at a scale of 1:25,000 based on aerial photographs taken in 1972. Our catalog of the Zhetysu Alatau glaciers was carried out for 2000 and 2011, similar to the catalog content mentioned above, on the basis of state survey maps at a scale of 1:25,000, Landsat 7 ETM+ satellite images, a digital elevation model (DEM), and surface reference points. According to their studies, Severskiy et al. [15], in the period 1956–2011, found that the area of glaciers of the Zhetysu Alatau decreased from  $813.9 \text{ km}^2$  [16–19] to  $465.17 \text{ km}^2$ , and the total annual reduction rate was 0.78%. Owing to climate change and other factors, over the past few decades, nearly 97.52% of glaciers in the Tien Shan mountains have been shrinking at a rapid rate [20], characterized by a decrease in the total area and mass of glaciers by about  $27 \pm 15\%$  [4], as well as the fact that, in the near future, this process of shrinking glaciers will continue [21,22].

Despite the vulnerability of the Zhetysu Alatau glaciers to area shrinkage in the region [13], ground monitoring and actual area assessment have not been carried out during recent years since 2012. Thus, a continuous glacier inventory is essential in the Zhetysu Alatau.

The main aim of this article is the investigation of glaciers and their changes in the Kazakh part of the Zhetysu Alatau based on remote sensing data. In particular, the major objectives are: (1) to create an updated catalog of the Zhetysu Alatau glaciers using remotely sensed data, to obtain and analyze the characteristics of glaciers in order to compare them with other previous inventory works, (2) to analyze the glacier area change dynamics from 1956 to 2016, (3) to analyze the main climatic trends (temperature and precipitation), (4) and to correlate the estimated changes in glacier areas with climatic, topographic parameters, and other characteristics.

## 2. Study Area

The Zhetysu Alatau (Dzhungar Alatau) is a mountain system stretching from west–southwest to east–northeast along the state border between Kazakhstan and China. The range length is 450 km, the width fluctuates from 50 to 90 km, and the maximal height reaches up to 4622 m (Semyonov-Tyan-Shansky peak) (Figure 1). The total area of the Zhetysu Alatau mountain ridge, including the river basins of the Borotala Mountains in China, is about 40,000 km<sup>2</sup> [23]. It is located at 45° N, within 79–82°E. Its southern border is the Ile River, the northern one is the Balkhash Plain, and the northeastern one is the Alakol Lake and Dzhungar Gates. The longitudinal valleys of the rivers Koksuy in the west and Borotala in the east divide the Zhetysu Alatau into two large ridges parallel to each other—North Central and South Central [24].

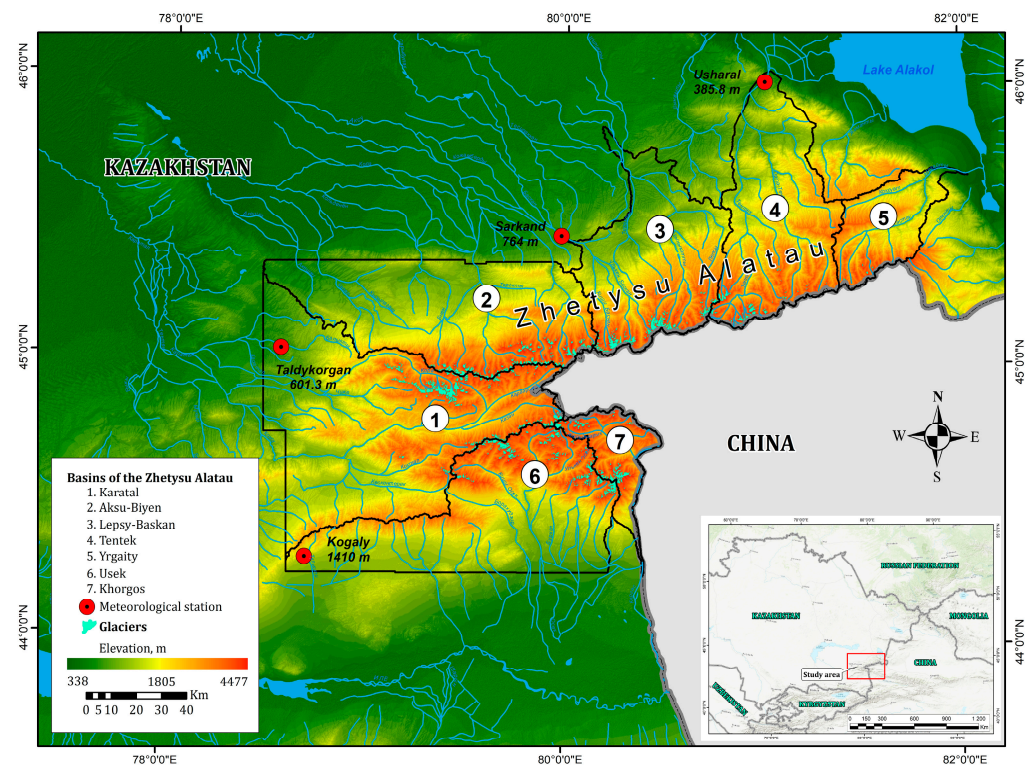


**Figure 1.** An overview map with the boundaries of the basins and the weather station.

The climate of the Zhetysu Alatau is mainly continental. It is under the influence of arctic, polar, and tropical air masses, which undergo significant transformation on the way. Arctic air masses come from the north and northwest, from the Barents and Kara seas. They come mostly in the first half of the winter period. Their invasion is accompanied by a sharp drop in air temperatures.

The average long-term air temperature in the lower part of the glacial zone (at altitudes of 3200–3600 m) during the accumulation period is  $-8$ – $-10$  °C; in the upper part (above 4000 m), it drops to  $-14$ – $-16$  °C. As the terrain rises above sea level, differences in climatic conditions are clearly manifested. According to the climate references [25], the coldest month is January, the temperature of which ranges from  $-7.5$  at meteorological station (MS) Sarkand to  $-13.2$  °C (MS Usharal). The warmest month is July, when the temperature reaches  $24.3$  °C in the foothill areas and  $17.7$  °C in the mountains. The region's climate is characterized by well-developed temperature inversions, i.e., the temperature increases with elevation. The minimum air temperatures drop to an average of  $-18.3$  °C in the flat areas and  $-13.4$  °C in mountainous areas. The absolute minimum reaches  $-44$  °C, and the absolute maximum is  $44$  °C. The warm season, with a mean daily air temperature above  $0$ °, varies from 116 days to 137 days in mountainous areas. The duration of the frost-free period in most of the territory is 123–161 days. Spring frosts stop mainly at the end of

April (23–29 April), and the first autumn frosts in most areas are observed at the end of September and the beginning of October.

The annual rainfall is from 298 mm to 520 mm in the mountains. In the warm season of the year (from April to October), 50–65% of the annual precipitation falls. The average annual wind speed is 1.1–2.7 m/s. Steady snow cover is observed in late November–early December. The snow cover melting is observed in the end of March. The duration of the stable snow cover is 111–155 days. The average of the maximal heights of snow cover does not exceed 15–33 cm during winter [26].

### 3. Materials and Methods

#### 3.1. Utilized Images

We used data from optical satellites such as Landsat ETM+ and Landsat OLI. We also used high-resolution imagery from Google Earth (QuickBird satellite) to define glacier contours in difficult areas and assess the mapping accuracy. We selected only two observation months (10 August to 25 September) due to minimal snow cover. The scenes were taken on cloudless days of this period, but some of the edges of the glaciers were hidden by shadows from the rocks and the walls of the glacial cirque. In total, six Landsat 7 (ETM+) scenes were used for 2001–2012, and three Landsat 8 (OLI) scenes for 2015–2016.

Landsat (level L1T) georeferenced imagery was provided by the USGS Center for Earth Observation and Science (EROS) (<http://earthexplorer.usgs.gov/> (accessed on 20 December 2020)). A panchromatic channel with a resolution of 15 m was used to improve the quality of maps using the pan-sharpening tool (Table 1).

**Table 1.** List of images used in the study.

WRS2 Path-Row	Date	Satellite and Sensor	Spatial Resolution (m)	Suitability of Scenes	Suitability of Scenes
148-029	22 August 2001	Landsat ETM+	15/30/60	Main	
147-029	18 August 2002	Landsat ETM+	15/30/60	Additional information	Seasonal snow
147-029	12 September 2011	Landsat ETM+	15/30/60	Additional information	Filling the gaps
148-029	3 September 2011	Landsat ETM+	15/30/60	Additional information	Filling the gaps
147-029	13 August 2012	Landsat ETM+	15/30/60	Main	
148-029	20 August 2012	Landsat ETM+	15/30/60	Main	
147-029	1 September 2016	Landsat OLI	15/30/60	Main	Seasonal snow, shadow areas
148-029	24 September 2016	Landsat OLI	15/30/60	Main	Seasonal snow, shadow areas
148-029	21 August 2015	Landsat OLI	15/30/60	Additional information	Shadow areas

Due to the unfavorable natural and climatic characteristics of the Landsat 7 ETM+ images for 2001, covering the eastern part of the Zhetysu Alatau, an additional image from the Landsat 7 ETM+ satellite of 2002 was used.

Since Landsat 8 OLI was only launched in 2013, and the Scan Line Corrector (SLC) in the ETM+ instrument (Landsat 7) failed in 2003, the 2012 ETM+ images required pre-processing, namely the Gap filling process, that is, filling in the missing pixels. This procedure was carried out in the ENVI software using the Gap Fill module. The images from 2012 were used as the “master file”, and the images from 2011 were used as the “slave file” (Figure 2).



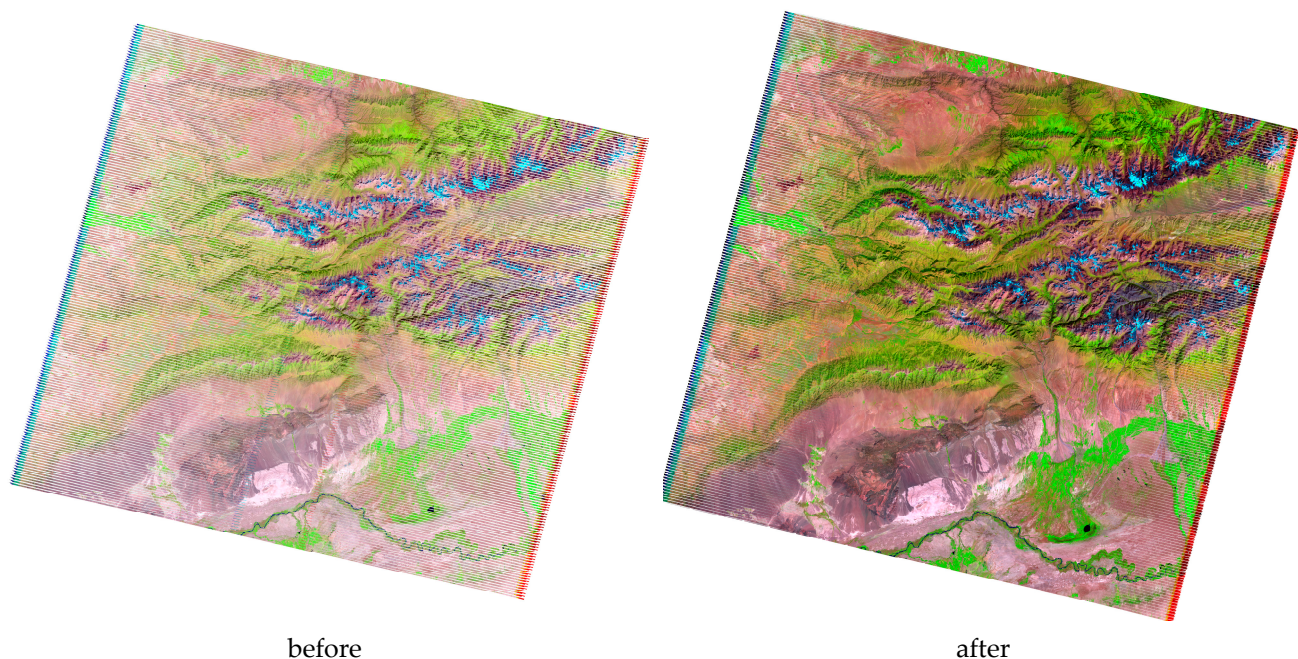


**Figure 2.** Filling gaps in the Landsat ETM+ (2012).

In addition to the 2016 Landsat OLI satellite images, the 2015 Landsat OLI images were used due to improved shadow conditions, which in turn allowed more detailed mapping of the glaciers.

The satellite imagery available on Google Earth for glacier contouring served as a visual guidance tool, with data coming primarily from very-high-resolution optical sensors (Google Earth 2017). Unfortunately, it was not available for all study areas.

The ALOS PALSAR DEM was used to extract watersheds and topographic information for the glacier inventory. For the dynamics of the glacier areas, we analyzed the 2nd edition of the 13th volume of the *Catalog of Glaciers of the USSR (Glaciers On The Territory of Zhetysu Alatau)* 1969, 1970, 1975, and 1980, published on the basis of aerial photographs of 1956.

### 3.2. Climatic Data

An assessment of the dynamics of spatial and temporal changes in the amount of precipitation and temperature indicators in the study area was carried out on the basis of long-term observation data analysis of the Usharal, Taldykorgan, Sarkand, and Kogaly meteorological stations (according to the *Manual on the Global Observing System. Volume I—Global Aspects*, World Meteorological Organization 2015 (WMO-No. 544) observations at the meteorological stations of the RSE “Kazhydromet”, carried out every three hours at the main standard (00:00, 06:00, 12:00, and 18:00) and intermediate times (03:00, 09:00:00, 15:00, and 21:00)). Detailed information about the mentioned meteorological stations is illustrated in Table 2.

We also used data from the Republican Hydrometeorological Fund RSE “Kazhydromet” for the period from 1960 to 2021. A constant upward trend in the mean temperatures was observed throughout Kazakhstan. According to Cherednichenko et al., 2015 [27], the increase in the average annual air temperature is 0.32 °C every decade in Kazakhstan. Atmospheric precipitation demonstrated a slight upward trend (by 2.6 mm/10 years), mainly due to spring period precipitation, when the increase in some western and northern regions is 10–20%/10 years. In autumn, the precipitation amounts decrease in some western and southern regions by 2–12%/10 years. All trends in the average annual and seasonal precipitation are statistically negligible all over Kazakhstan.

**Table 2.** Geographic location of selected weather stations.

	Meteorological Stations (MSs)	Elevation (m)	Coordinates	Description
1	Usharal	385.8	46°10'N, 80°56'E	It is located in the desert plain region of the Alakol depression, Tentek river basin, eastern part of the Zhetysu Alatau.
2	Taldykorgan	601.3	45°01'N, 78°22'E	It is located in the foothill region of the western Zhetysu Alatau (Karatal river basin).
3	Sarkand	764	45°25'N, 79°55'E	It is located on the northern part of the Zhetysu Alatau (Lepsy river basin).
4	Kogaly	1410	44°29'N, 78°39'E	It is located on the southern part of the Zhetysu Alatau (Usek river basin).

The most recommended and useful methods for determining trends in climate change are nonparametric methods [28]. Therefore, for the assessment of the general trend in changes in air temperature and precipitation, we used the nonparametric statistical method of Mann–Kendall with a  $p$ -value of 95%. The calculations were carried out in the R program in the `mk.test2` application. The test detects any upward or downward trends in the time series data. If the  $p$ -value is less than the significance level  $\alpha$  (alpha) = 0.05, it indicates the presence of a trend in the time series, i.e., the result is statistically significant; if the  $p$ -value is greater than the significance level, this indicates that the trend has not been detected.

In addition, the analysis of change tendencies in the characteristics of the climatic regime for the study period was carried out on the basis of calculated linear trends in the series of observations using the least squares method.

### 3.3. Methods

F. Paul [29,30] compared the different methods, including the band ratios of Landsat ETM + (3/5, 4/5) and Landsat OLI (4/6, 5/6), including filters and mapping in shadow areas [31]. According to his study, the ratio of Landsat ETM + (TM 3/5) and Landsat OLI (OLI 4/6) is the most reliable, reproducible, and simple method, in parts even better than manual mapping. Furthermore, this method has been applied by various authors to glaciers around the world [32].

In this regard, we used a semiautomatic method based on the ratio of bands (Figure 3a). The technique is based on using the threshold ratio values of the spectral channels of optical images (Landsat, Sentinel-2) to determine the contour of a glacier. We used the RED/SWIR-1 channels of the Landsat satellite. The threshold value of 2.1 was set manually through visual inspection (the clean-ice and snow patch). To clean up the glacier polygon, we used a median filter (3 by 3 kernel size) (Figure 3b) and then converted it to a vector (Figure 3c).

For mapping glaciers in the shadow areas, we used Band 2 (Blue) with threshold 7400 (set manually by visually checking). For mapping all shadow areas, we applied SRTM HillShade, which calculated using sun azimuth and other parameters, as in Landsat imagery metadata. We obtained glaciers in shadow areas as the intersection of Band 2 > 7400 and Hillshade  $\leq 0$  (less than or equal to 0) (Figure 3d).

Additionally, the delineation of the glacier tongue, covered with debris, was performed using additional data, such as thermal band and geomorphological characteristics obtained from the DEM, as well as Google Earth images. However, debris cover was not a major problem in defining the glacier boundaries, due to the fact that most of the glacier surface in this area is pure ice.

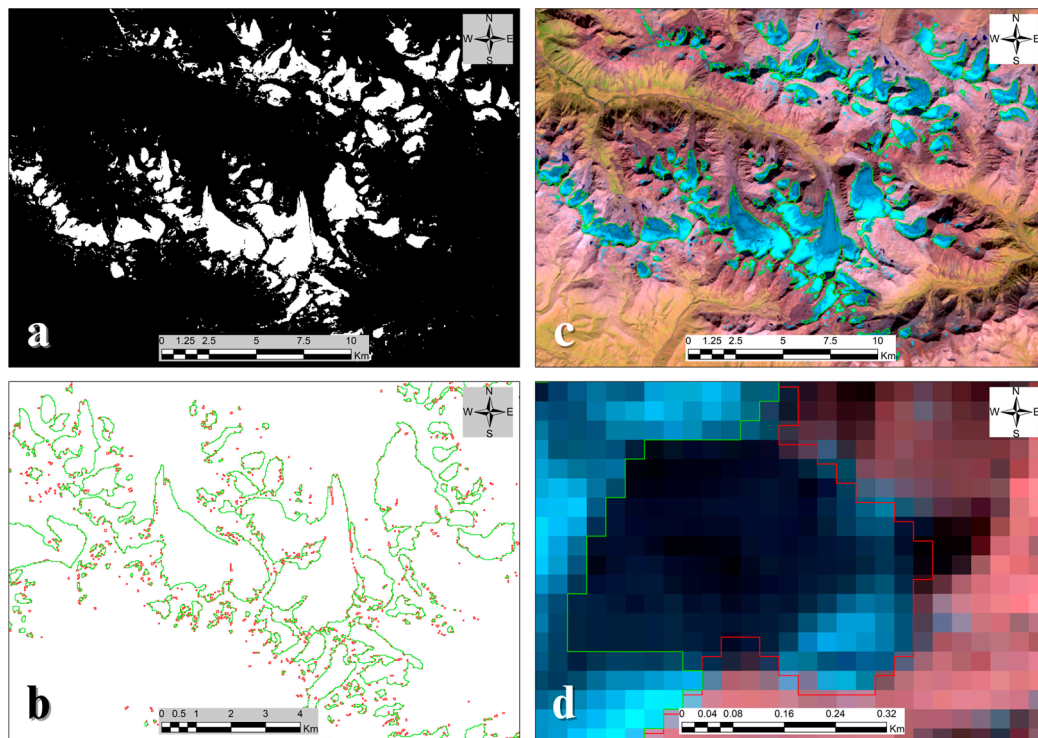


**Figure 3.** Glacier mapping using a semiautomated band ratio technique: (a) TM3/TM5, OLI4/OLI6; (b) after filtering (median filter  $3 \times 3$ ); (c) raster to vector format conversion; (d) mapping of glaciers in the shadow area.

### 3.4. Uncertainty of Mapping

In order to correctly interpret and estimate the importance of the study, the accuracy needs to be evaluated. In our previous study [13], uncertainty was estimated with the buffer method [33,34]. The size of the buffer was chosen to be half of the estimated RMSE, i.e., 7.5 m to each side, and the accuracy was within  $\pm 5\%$  for our study region.

We also determined uncertainty using another independent way, namely, the multiple digitization of glacier outlines, which is the best method to define the accuracy of mapping by one analyst [34]. This method gives the most realistic (analyst-specific) estimate for the provided dataset. Despite the higher workload, this method is recommended for use instead of the literature value or buffer methods. Following Paul et al. (2013) [29], we manually digitized four glaciers five times (one time every day) independently, using a reference dataset with high resolution (Figure 4). Then, the resulting average areas were compared with the area obtained automatically using TM. As a result, the difference between the manually and automatically derived area was around 1–3.5 and 2–4.5%, respectively (Table 3).

**Table 3.** Comparison of glacier area values.

Glaciers	Manually Delineated							Automated with TM. km <sup>2</sup>	Std%	Diff%
	1 Day	2 Day	3 Day	4 Day	5 Day	Mean. km <sup>2</sup>	Mean-koef. km <sup>2</sup>			
a	1.4356	1.4085	1.4271	1.4193	1.4302	1.4241	1.4105	1.3958	2.0	1.4
b	2.7081	2.7114	2.7147	2.7275	2.7253	2.7174	2.6913	2.6621	2.0	1.0
c	4.1658	4.1790	4.1970	4.2279	4.2338	4.2007	4.1604	4.0848	2.8	3.4
d	0.3853	0.3860	0.3877	0.3941	0.3923	0.3891	0.3853	0.3716	4.5	4.0



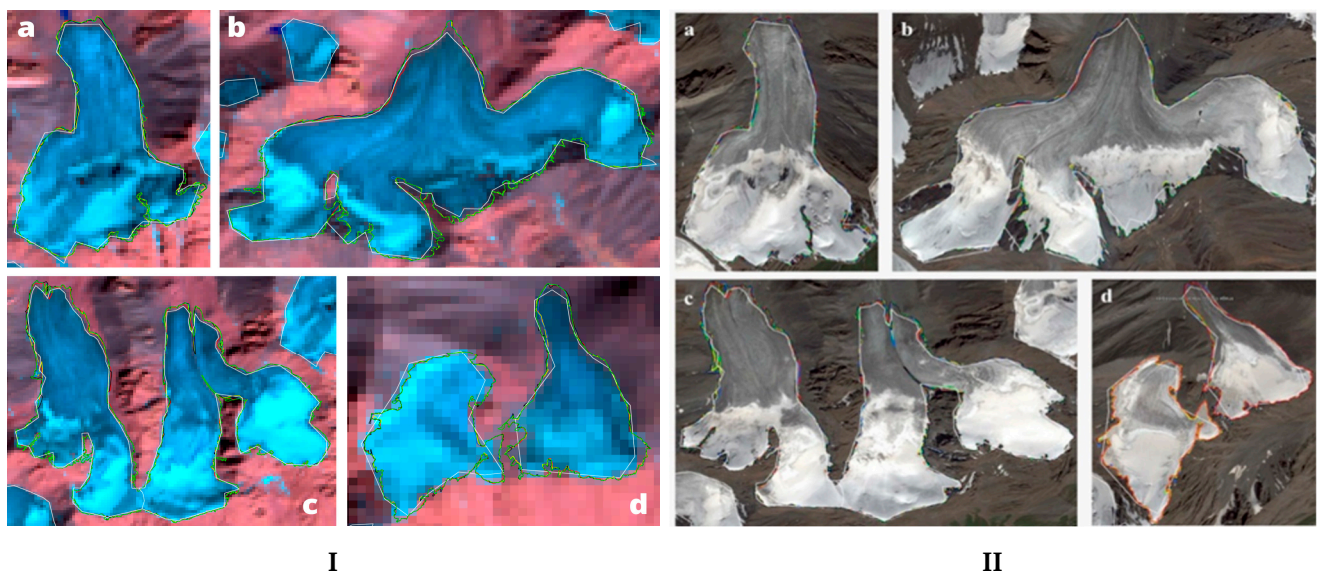


**Figure 4.** Overlay of four (a–d) manually digitized glacier extents (colored) and the white outline is derived automatically from TM: (I) on the Landsat 8 OLI images; (II) on the Google Earth images.

## 4. Results

### 4.1. Glacier Inventory of 2001

According to Landsat data for 2001, we identified and mapped 897 glaciers with an area of more than 0.005 km<sup>2</sup> each, with a total area of  $517.4 \pm 14.5$  km<sup>2</sup> in the basins of 7 large rivers (including sub-basins) of the Zhetysy Alatau (Table 4). Of these,  $126.5 \pm 3.5$  km<sup>2</sup> or 24.4% of the total area of glaciers falls on the western part (Karatal) of the Zhetysy Alatau,  $197.2 \pm 5.5$  km<sup>2</sup> or 38.1% on the northern part (Aksu-Bien and Lepsy-Baskan),  $59.7 \pm 1.7$  km<sup>2</sup> or 11.5% on the eastern part (Tentek and Rgayty), and  $133.9 \pm 3.7$  km<sup>2</sup> or 26% was found in the southern part (Khorgos and Usek) (Figure 5).

**Table 4.** Glacier area change.

Basins	1956	2001	2012	2016	1956–2001	2001–2012	2012–2016	2001–2016	1956–2016	Mean Size in 2001/2016
	Area km <sup>2</sup> (Count)				Area Decrease % (% yr <sup>−1</sup> )					
1	2	3	4	5	6	7	8	9	10	11
Karatal	202.5 (285)	126.5 ± 3.5 (231)	110.3 ± 3.1 (221)	102.6 ± 2.9 (220)	−37.5 (0.8)	−12.8 (−1.2)	−7 (−1.7)	−18.9 (−1.3)	−49.3 (−0.8)	0.55/0.47
Aksu Bien	140.4 (135)	93.4 ± 2.6 (133)	83.1 ± 2.3 (127)	77.1 ± 2.2 (127)	−33.5 (−0.7)	−11 (−1)	−7.2 (−1.8)	−17.5 (−1.2)	−45.1 (−0.8)	0.70/0.60
Lepsy-Baskan	154 (116)	103.8 ± 2.9 (112)	93.7 ± 2.6 (111)	88.4 ± 2.5 (105)	−32.6 (−0.7)	−9.7 (−0.9)	−5.7 (−1.4)	−14.9 (−1)	−42.6 (−0.7)	0.91/0.83
Tentek	75.2 (94)	49.7 ± 1.4 (85)	41.8 ± 1.2 (73)	36.9 ± 1.0 (58)	−33.9 (−0.8)	−15.8 (−1.4)	−12.6 (−3.1)	−26.4 (−1.8)	−51.4 (−0.9)	0.57/0.63
Rgaitis	13.1 (22)	10 ± 0.3 (21)	8.2 ± 0.2 (18)	6.9 ± 0.2 (17)	−23.5 (−0.5)	−18.4 (−1.7)	−16.2 (−4.1)	−31.6 (−2.1)	−47.7 (−0.8)	0.47/0.40
Usek	144.8 (233)	84.9 ± 2.4 (219)	73.4 ± 2.1 (202)	64.6 ± 1.8 (197)	−41.4 (−0.9)	−13.6 (−1.2)	−12 (−3)	−23.9 (−1.6)	−55.4 (−0.9)	0.38/0.32
Khorgos	83.5 (100)	49 ± 1.4 (96)	43.2 ± 1.2 (90)	38.5 ± 1.1 (89)	−41.3 (−0.9)	−11.9 (−1.1)	−11 (−2.7)	−21.6 (−1.4)	−53.9 (−0.9)	0.51/0.43
Total	813.6 (985)	517.4 ± 14.5 (897)	453.7 ± 12.7 (842)	414.6 ± 11.6 (813)	−36.4 (−0.8)	−12.3 (−1.1)	−8.6 (−2.2)	−19.9 (−1.3)	−49 (−0.8)	0.57/0.51
Glaciers <0.005 km <sup>2</sup>	18.9 (385)	5.1 ± 0.14 (143)	3.7 ± 0.10 (96)	3 ± 0.08 (83)	−72.9 (−1.6)	−27.4 (−2.5)	−19.3 (−4.8)	−41.4 (−2.8)	−84.1 (−1.4)	0.04/0.03



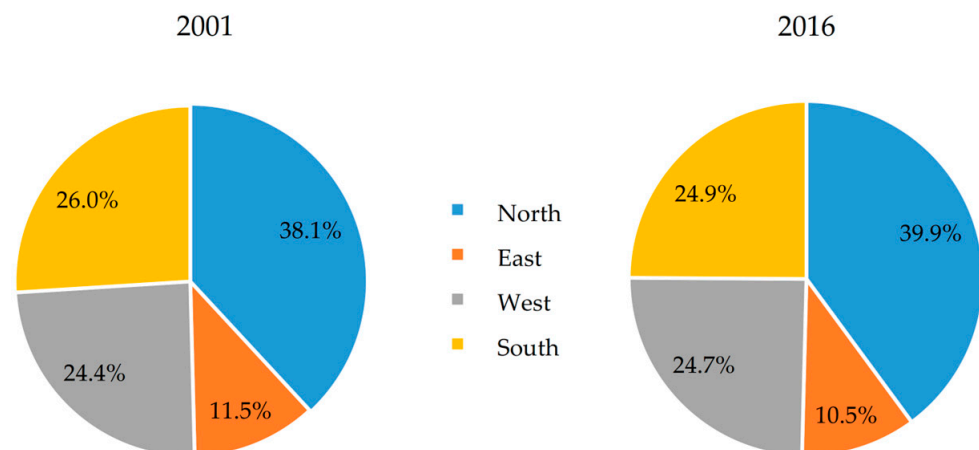


**Figure 5.** Glacier distribution in the Zhetysu Alatau between regions.

The average size of the glaciers for the entire mountainous region was  $0.57 \text{ km}^2$ , with the glaciers of the  $1.0\text{--}5.0 \text{ km}^2$  size class prevailing, with a total area of  $221.5 \pm 6.2 \text{ km}^2$  (Figure 5), which is  $42.8\% \pm 2.8$  of the total area. Of these,  $38\% \pm 2.8$  was concentrated in the northern part (the basins of the Aksu-Bien and Lepsy-Baskan rivers) of the Zhetysu Alatau.

The larger glacier sizes ( $0.7\text{--}0.91 \text{ km}^2$ ) were concentrated in the northern part of the Zhetysu Alatau (the basins of the Lepsy-Baskan and Aksu-Bien rivers), while the average sizes of the glaciers in the southern (Usek) ( $0.38 \text{ km}^2$ ) and eastern part (Rgayty— $0.47 \text{ km}^2$ ) were smaller (Table 4).

Glaciers with a size class of  $0.1\text{--}0.5 \text{ km}^2$  were the most numerous (381 glaciers) in 2001 (Figure 6b).

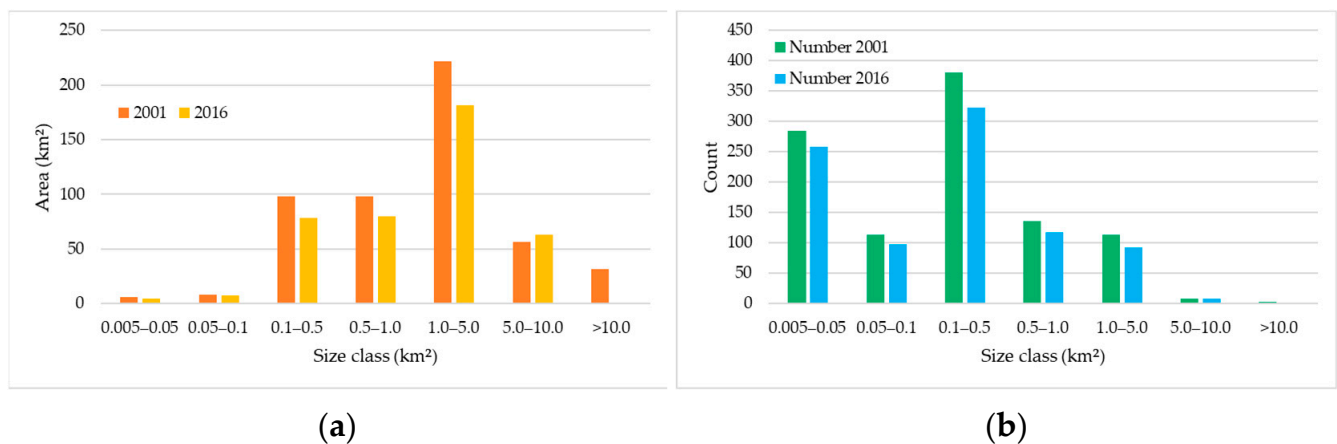


**Figure 6.** Dynamics of glaciers: area (a); number (b) changes for seven size classes in the Zhetysu Alatau in 2001 and 2016.

Most glaciation areas of the Zhetysu Alatau faced north (north, northwest, and north-east) (Figure 7a,b) and were located at altitudes between 3000 and 4000 m.a.s.l. (Figure 8).

Glaciers with northern, northeastern, and northwestern exposure were the most extensive in the Zhetysu Alatau, covering  $163.55 \pm 4.6 \text{ km}^2$ ,  $121.32 \pm 3.4 \text{ km}^2$ , and  $105.48 \pm 3 \text{ km}^2$ , respectively, and they accounted for  $75.4 \pm 2.8\%$  of all glaciers (Figure 7b). The southern, southeastern, and southwestern sides occupied  $13.61 \pm 0.4 \text{ km}^2$ ,  $20.96 \pm 0.6 \text{ km}^2$ , and  $14.72 \pm 0.4 \text{ km}^2$ , respectively, and together, they accounted for  $9.5 \pm 2.8\%$  of all glaciers. The western side occupied  $32.27 \pm 0.9 \text{ km}^2$ , or  $6.1 \pm 2.8\%$ , and the eastern side,  $47.20 \pm 1.3 \text{ km}^2$ , or  $9\%$ , respectively (Figure 7b).

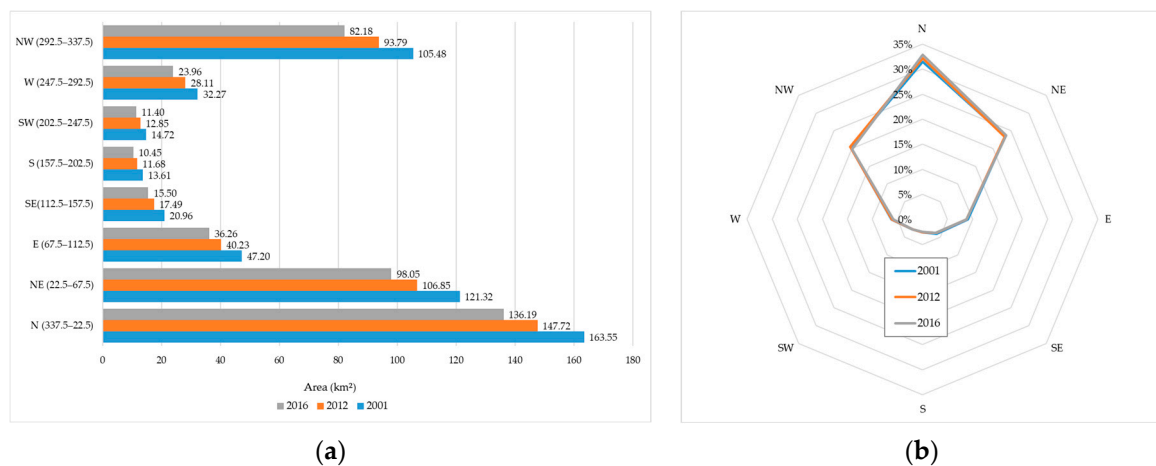


**Figure 7.** Glacier area change distribution by exposition in the Zhetysu Alatau in 2001, 2012, and 2016: (a) area, km<sup>2</sup>; (b) area, (%).

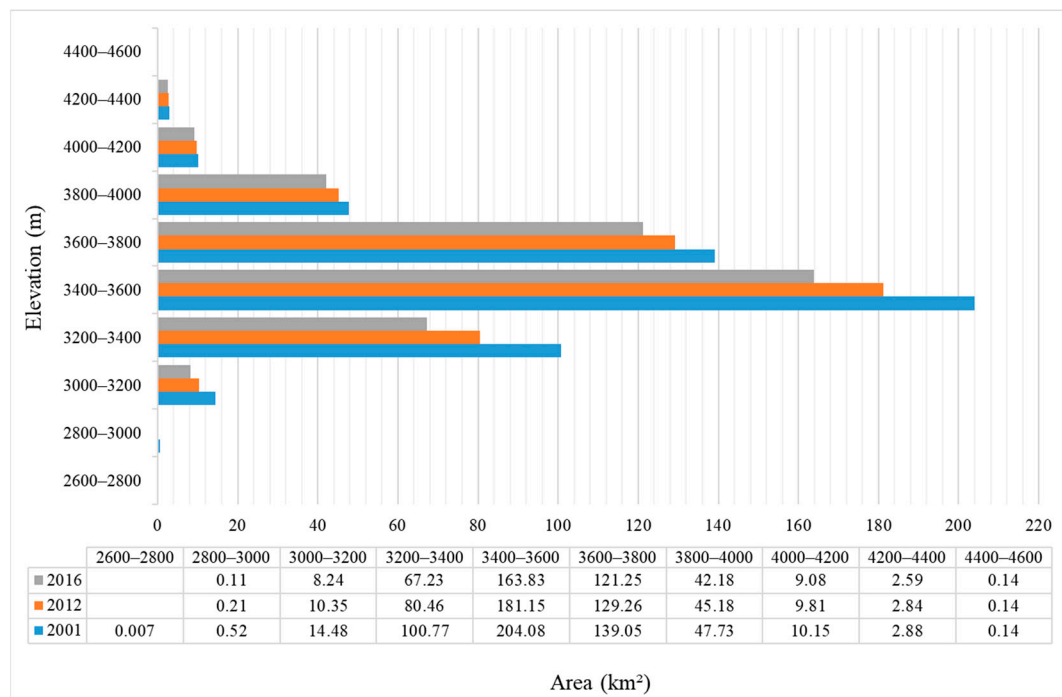


**Figure 8.** Glacier area distribution and changes by elevation in the Zhetysu Alatau in 2001, 2012, and 2016.

About  $39.4 \pm 2.8\%$  of the glaciers of the Zhetysu Alatau were located at altitudes of 3400–3600 m, almost 26.9% at altitudes of 3600–3800 m and about  $19.5 \pm 2.8\%$  at altitudes of 3200–3400 m (Figure 8).

In 2001, according to Landsat data, three glaciers with an area greater than 10 km<sup>2</sup> were identified and mapped in the Zhetysu Alatau. Two of them were located in the northern part (in the Lepsy river basin) of the Kolesnik glacier ( $10.3 \pm 0.3$  km<sup>2</sup>) and Bereg ( $10.9 \pm 0.3$  km<sup>2</sup>), and one in the western part (in the Karatal river basin) of the Bezsonov glacier ( $10.3 \pm 0.3$  km<sup>2</sup>).

#### 4.2. Glacier Inventory of 2016

In 2016, 813 glaciers with a total area of  $414.6 \pm 11.6$  km<sup>2</sup> were identified and mapped in the Zhetysu Alatau (Table 4). Of these,  $102.6 \pm 2.9$  km<sup>2</sup> or  $24.7 \pm 2.8\%$  of the total area of glaciers falls on the western part (Karatal) of the Zhetysu Alatau,  $165.5 \pm 4.6$  km<sup>2</sup> or

$39.9 \pm 2.8\%$  on the northern part (Aksu-Bien and Lepsy-Baskan),  $43.8 \pm 1, 2 \text{ km}^2$  or  $10.5\%$  in the eastern part (Tentek and Rgaity), and  $103.1 \pm 2.9 \text{ km}^2$  or  $24.9 \pm 2.8\%$  was found in the southern part (Khorgos and Usek) (Table 4, Figure 5).

In 2016, glaciers with a size of  $1.0\text{--}5.0 \text{ km}^2$  ( $181.2 \pm 5 \text{ km}^2 \sim 43.7 \pm 2.8\%$ ) predominated in terms of total occupied area, and glaciers with size of  $0.1\text{--}0.5 \text{ km}^2$  predominated in number (322 glaciers). However, the area of glaciers from the group of  $5.0\text{--}10.0 \text{ km}^2$  increased, and there were no glaciers with an area of more than  $10 \text{ km}^2$  in 2016 in the Kazakhstan part of the Zhetysu Alatau (Figure 6a).

The average height of glaciers ranged from 3580 m above sea level (northern slope) to 3640 m (southern slope); on average, the glacier location was at an altitude of 3615 m above sea level. Most glacier areas ( $316.9 \pm 8.9 \text{ km}^2$ ) in 2016 belonged to northern exposure slopes (N, NW, and NE), while the relative number and areas of glaciers facing the southern exposure parts (S, SW, and SE) were very small (Figure 7a,b).

The glacier ends were located at a mean minimum height of 3407 m.a.s.l., and their average maximal height was at 3746 m.a.s.l. Figure 9a illustrates the distribution of glacier area by the maximum and minimum heights. This means that large valley glaciers have a lower tongue and smaller glaciers have a higher tongue [13]. Additionally, Figure 9b illustrates the spatial spreading of the average height of glaciers greater than  $0.01 \text{ km}^2$  in 2016.

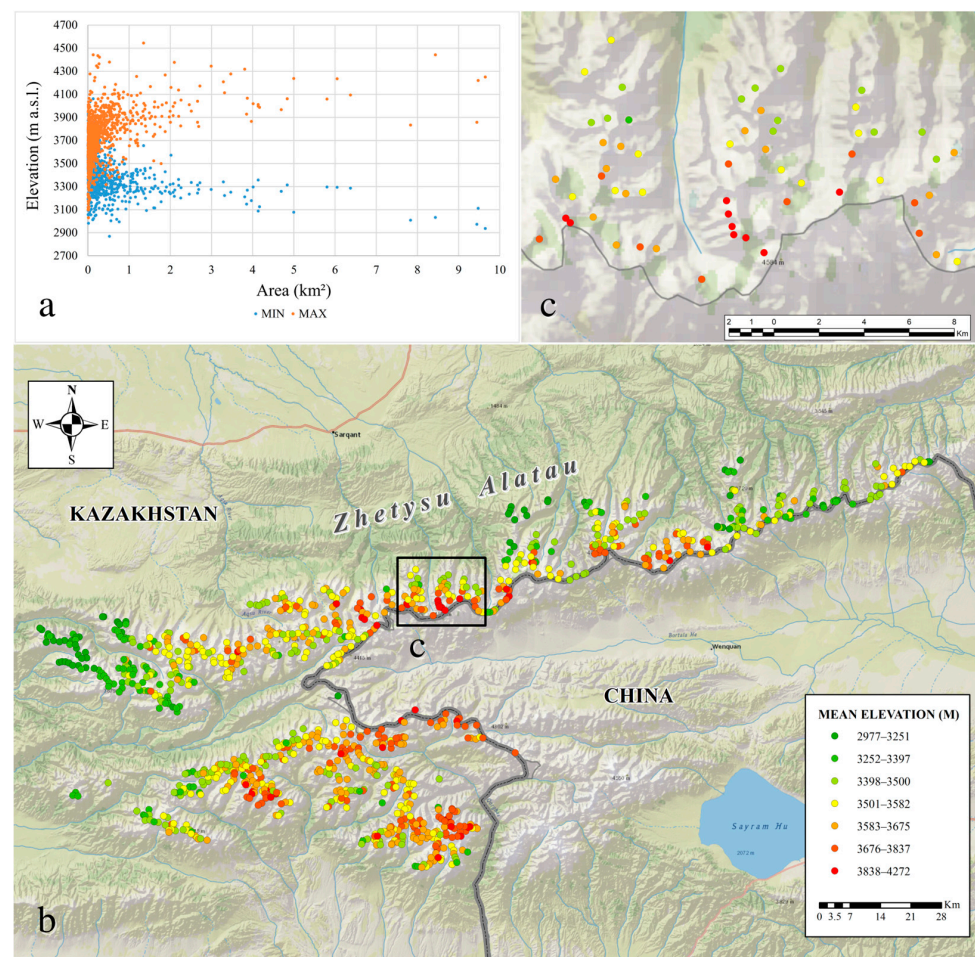


**Figure 9.** Corresponding distribution of glaciers of Zhetysu Alatau in the maximum and minimum altitude zones: (a) distribution of glacier area by the maximum and minimum heights; (b) distribution map of the glaciers average height; (c) an enlarged example of glaciers distribution by mean elevation in the selected area.

In 2016, there were three large glaciers along the Zhetysu Alatau with a total area of 28.6 km<sup>2</sup>. Two of them were the Kolesnik ( $9.6 \pm 0.3$  km<sup>2</sup>) and Bereg ( $9.5 \pm 0.3$  km<sup>2</sup>) glaciers in the northern part (in the Lepsy river basin) and Bezsonov ( $9.4 \pm 0.3$  km<sup>2</sup>) in the western part (in the Karatal river basin). As we have already noted, in 2016, there was no glacier with an area greater than 10 km<sup>2</sup> along the Zhetysu Alatau.

#### 4.3. Glacier Changes in 2001–2016

As a part of this study, 897 glaciers were identified in 2001 and 813 in 2016, which were listed in the glacier catalog with a total area of  $517.4 \pm 14.5$  and  $414.6 \pm 11.6$  km<sup>2</sup>, respectively (Table 4). The study results demonstrate that changes in the glacier areas of the Zhetysu Alatau had a significant decrease during the period from 2001 to 2016. Between 2001 and 2016, the total loss of glaciers was  $102.8 \pm 2.9$  km<sup>2</sup> or  $19.9 \pm 2.8\%$  ( $-1.3\%$  yr<sup>-1</sup>).

The highest rates of shrinkage of the glacier area were in the eastern (Rgaity and Tentek) and southern (Usek and Khorgos) parts of the Zhetysu Alatau.

For the period 2001–2016, the glacier area decreased by  $31.6 \pm 2.8\%$  ( $-2.1\%$  year<sup>-1</sup>) from  $59.7 \pm 1.7$  km<sup>2</sup> to  $43.8 \pm 1.2$  km<sup>2</sup> in the eastern part, i.e., in the Rgaity river basin, and by  $26.4 \pm 2.8\%$  ( $-1.8\%$  year<sup>-1</sup>) in the Tentek river basin.

The reduction rate of glacier areas in the northern (Aksu-Bien and Lepsy-Baskan) and western (Karatal) parts of the Zhetysu Alatau was relatively low. Between 2001 and 2016, the glacier areas belonging to the Karatal river basin (western) decreased by  $18.9 \pm 2.8\%$  ( $-1.3\%$  year<sup>-1</sup>), in the Aksu-Bien rivers (northern), this shrinkage was  $17.5 \pm 2.8\%$  ( $-1.2\%$  yr<sup>-1</sup>). The smallest reduction in the glacier area in the Zhetysu Alatau was noted in the Lepsy-Baskan river basin, belonging to the northern part. Between 2001 and 2016, the glacier area in this basin decreased by  $14.9 \pm 2.8\%$ , and the annual reduction rate was 1% per year.

The average size of the Zhetysu Alatau glaciers in 2001 was 0.58 km<sup>2</sup>, while in 2016, the average size decreased by 0.51 km<sup>2</sup>. There was a decrease in the average size of glaciers in all areas; however, only the glaciers of the Tentek river basin (eastern part) increased from 0.57 km<sup>2</sup> to 0.63 km<sup>2</sup> on average. This happened due to the shrinking of small glaciers in the basin. As an example, in 2001, there were 90 glaciers in the Tentek river basin with a total area of 11.1 km<sup>2</sup> up to 0.5 km<sup>2</sup> in size, and in 2016, their total area was 5.7 km<sup>2</sup>—almost halved—and 45 glaciers remained.

The analysis of the relative change in area compared to the initial area of the glacier indicated a large relative loss of smaller glaciers (from 0.01 to 0.1 km<sup>2</sup>) (Figure 10). For larger glaciers (>1.0 km<sup>2</sup>), the loss factors were smaller and more similar. The difference in shrinkage rate between the northern and western slopes was insignificant.

However, there were wide variations in losses, especially for smaller glaciers, while there were also glaciers of all size classes that only slightly decreased. The total area loss was higher for larger glaciers, and the average glacier height increased by 24 m, while the average minimal glacier height increased by 42 m from 3367 to 3409 m.a.s.l. over the period 2001–2016.

#### 4.4. Temperature and Precipitation Trends

The resulting estimates of air temperature trends showed that the temperature increase occurred at all stations in all seasons and months of the year. However, there were some peculiarities in the rate of air temperature increase (Table 5). The table shows that the most noticeable increase in the average annual temperature was in the desert plain zone of the Alakol depression (MS Usharal), and the average rate of change was 0.29 °C/10 years. The lowest rates of temperature change were observed in the mountainous regions of the Zhetysu Alatau (0.12 °C/10 years—MS Kogaly). The trends in summer temperatures (June–August) showed that in mountainous and foothill areas, they had the highest values and ranged from 0.19 °C/10 years (MS Kogaly) to 0.25 °C/10 years (MS Taldykogan), and the lowest were at Usharal MS (0.12 °C/10 years). An analysis of changing trends showed that a steady increase in air temperature has been observed in the study area in recent



decades; the only exception was the Sarkand MS, where a slight decrease in precipitation was found. At the same time, in 2019 and 2020, at the three MSs of Taldykorgan, Usharal, and Kogaly, there was a deficit in atmospheric precipitation. At the same time, the smallest anomalies were observed at the MS Usharal (12–64 mm), and the largest was observed at the mountain station of Kogaly, 183 mm, which is 65% of the norm.

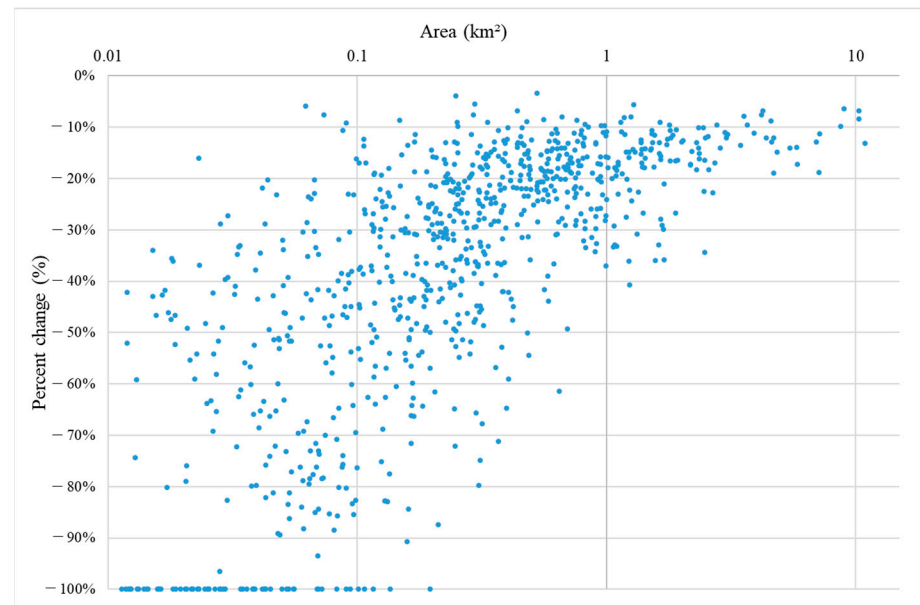


**Figure 10.** Scatterplot of relative glacier changes compared to initial glacier size for 813 glaciers between 2001 and 2016.

**Table 5.** Average annual and summer rates of change in air temperature ( $^{\circ}\text{C}/10$  years) and precipitation ( $\text{mm}/10$  years) in 1960–2021.

No.	Meteorological Stations	Average Annual Rate of Air Temperature Change $^{\circ}\text{C}/10$ Years	Average Summer Air Temperature Change Rate $^{\circ}\text{C}/10$ Years	Average Annual Rate of Change in Precipitation, $\text{mm}/10$ Years
1	Taldykogan	0.28	0.25	8.5
2	Kogaly	0.18	0.19	9.3
3	Usharal	0.20	0.20	−2.2
4	Usharal	0.29	0.12	11.4

Thus, in contrast to the air temperature, the change in the precipitation regime in the study area gives a more variegated picture. The time series of annual precipitation anomalies for the period 1960–2021 give a general idea of the nature of modern changes in the precipitation regime. There have been no long-term trends over the last 40 years; there was an alternation of short periods with positive and negative anomalies in the amount of precipitation.

The significance of trends for both air temperature and precipitation was assessed for the summer months, as well as for the average annual and summer periods. An analysis of the data in Tables 6 and 7 showed that there was a significant upward trend in the average annual temperature in the study area. This was confirmed by the nonparametric Mann–Kendall statistic, which gave a positive Z-statistic. The average annual values of Z-statistics for air temperature reached 4.2276 (MS Usharal).

**Table 6.** Mann–Kendall statistics of average annual and summer (June–August) air temperatures for the study area.

Station	Mann–Kendall Stats	June	July	August	Mean Summer Period (June–August)	Annual Mean
<b>Air Temperature</b>						
Taldykorgan	Z-statistic	2.9339	3.0857	3.7235	3.8145	3.7295
	<i>p</i> -value	0.003347	0.002031	0.0001965	0.0001364	0.0001919
	Significance	(**)	(**)	(***)	(***)	(***)
Kogaly	Z-statistic	2.8003	2.7152	2.6483	3.5837	4.2033
	<i>p</i> -value	0.005106	0.006623	0.00809	0.0003388	0.00002631
	Significance	(**)	(**)	(**)	(***)	(***)
Sarkand	Z-statistic	2.8913	2.1745	2.2596	3.4379	3.2132
	<i>p</i> -value	0.003836	0.02967	0.02385	0.0005862	0.001312
	Significance	(**)	(*)	(*)	(***)	(**)
Usharal	Z-statistic	2.1138	1.0508	1.6219	2.4418	4.2276
	<i>p</i> -value	0.03453	0.2933	0.1048	0.01462	0.00002362
	Significance	(*)	N.S.	N.S.	(*)	(***)

\*\*\*:  $\alpha = 0.001$ ; \*\*:  $\alpha = 0.01$ ; \*:  $\alpha = 0.05$ ;  $\alpha = 0.1$  level of significance; N.S.—nonsignificant.

**Table 7.** Mann–Kendall statistics of average annual and summer (June–August) values of atmospheric precipitation for the study area.

Station	Mann–Kendall Stats	June	July	August	Mean Summer Period (June–August)	Annual Mean
<b>Precipitation</b>						
Taldykorgan	Z-statistic	0.11541	0.40699	0.94162	0.69853	1.1116
	<i>p</i> -value	0.9081	0.684	0.3464	0.4848	0.2663
		(N.S.)	(N.S.)	(N.S.)	(N.S.)	(N.S.)
Kogaly	Z-statistic	0.48594	−0.31586	0.99015	0.84431	0.62564
	<i>p</i> -value	0.627	0.7521	0.3221	0.3985	0.5315
		(N.S.)	(N.S.)	(N.S.)	(N.S.)	(N.S.)
Sarkand	Z-statistic	−0.6378	0.14578	0.82617	−0.12149	−0.14578
	<i>p</i> -value	0.5236	0.8841	0.4087	0.9033	0.8841
		(N.S.)	(N.S.)	(N.S.)	(N.S.)	(N.S.)
Usharal	Z-statistic	0.90517	0.21867	0.49812	1.0995	1.7979
	<i>p</i> -value	0.3654	0.8269	0.6184	0.2715	0.07219
		(N.S.)	(N.S.)	(N.S.)	(N.S.)	(N.S.)

N.S.—nonsignificant.

The average annual trend changes were assessed as significant, since all values were less than  $p$ -value  $< 0.05$ . The same picture was observed in the summer period (June–August). However, if we consider the change in trends by month, there were some differences. Significant positive trends were noted at the three studied meteorological stations (Taldykorgan, Kogaly, and Sarkand); the  $p$ -values were significantly less than 0.05. At Usharal MS, there was a significant trend only in June; in June and August, the trends

were insignificant. The results obtained are consistent with the results obtained in the Ishfaq Farooq (2021) study. Ishfaq Farooq [14,35] studied the air temperature time series for Kazakhstan using the M-K statistical test. The results showed that there was a significant increase in the average annual temperature in Kazakhstan from 1970 to 2017.

The results of the Mann–Kendall test showed that there were no statistically significant linear trends in precipitation for the period under study, at almost all stations, although strong interannual variability was observed in the time course. Statistically insignificant trends were observed at Sarkand MS in the average annual and summer season, but negative trends were noted (Z-statistic:  $-0.12149$  in summer;  $-0.14578$  per year). Similar results were obtained for other regions of Kazakhstan by Talipova et al. (2021) [36] and Shahgedanova (2018) [37]. Thus, we can conclude that climate change for the study area was observed in the form of an increase in air temperature and statistically insignificant positive trends in changes in precipitation.

## 5. Discussion

An intensive reduction in glacier area was confirmed by many previous studies [2,4,6,10,15,20,24,32,38–45]. However, our results show rates of area reduction of about  $-0.8\% \text{ a}^{-1}$  for the period 1956–2001, and  $-1.3\% \text{ a}^{-1}$  for the period 2001–2016, which are the highest values among all the glacial zones of the world and Central Asia, including Altai and Pamir [6,33,36,37]. It is important to note that the rate of decline increased rapidly, and amounted to  $-0.8\%$ ,  $-1.1\%$ ,  $2.2\%$ , and  $-1.3\% \text{ a}^{-1}$  for the periods 1956–2001, 2001–2012, 2012–2016, and 2001–2016, respectively. If we compare the rate of reduction in the area of glaciers in the study area with other glacial regions of the world, then significant differences can be observed. For example, according to the studies by Tielidze and Wheate (2018) [46], the reduction in the area of glaciers in the Greater Caucasus over the period 1960–1986 amounted to  $11.5\%$  ( $-0.44\% \text{ a}^{-1}$ ), and for 1986–2014, this figure was  $19.5\%$  ( $-0.69\% \text{ a}^{-1}$ ). In the research by Tennant et al. (2012) [47], glacier reduction in the Canadian Rockies was  $-28.3\%$  ( $-0.4\% \text{ a}^{-1}$ ) in the period of 1919–1985,  $-7.6\%$  ( $-0.5\% \text{ a}^{-1}$ ) in the period of 1985–2001, and  $-9.9\%$  ( $2.0\% \text{ a}^{-1}$ ) in the period of 2001–2006. In the European Alps, according to Paul et. al. (2020) [48], the total glacier area shrunk from  $2060 \text{ km}^2$  in 2003 to  $1783 \text{ km}^2$  in 2015/16, i.e., by  $-13.2\%$  ( $-1.1\% \text{ a}^{-1}$ ).

However, the features of the geographical location of the Tien Shan mountain system, in particular the natural zone, as well as the climatic conditions, are significantly different from the above-mentioned mountain systems. That is, the mountain system is located in the arid and semiarid region of Central Asia, surrounded by deserts. In addition, the speed of acceleration is significantly higher compared to other ranges of the Tien Shan mountain system [5,15,39,40,42].

Such a significant reduction in the areas of glaciers is fully consistent with other studies, which found that the greatest area loss occurred primarily in the peripheral areas with low-altitude ranges [10,49]. The study by Aizen et al. (2006) [43], for 1977–2003 in the inner region of Tien Shan, and Narama et al. (2006) [44], for 1971–2002 in the western Tien Shan, indicated a glacial decrease of 8–9% or  $0.26\text{--}0.29\% \text{ a}^{-1}$ , while glacier reduction in the peripheral ranges of the northern Tien Shan was remarkably faster. For example, in the Ile and Kungey Alatau, the glacier reduction speed was  $-0.73\% \text{ a}^{-1}$  for the period of 1955–1999 [32]. The southern part of the Zhetysu Alatau was studied by Kokarev and Shesterova (2014) [49]; the calculated rate was about  $-0.86\%$  per year.

The glaciers of the outer Tien Shan receive the greatest amount of precipitation, and they are very sensitive to even the slightest temperature changes due to the high rate of mass transfer. On the contrary, the glaciers of the inner Tien Shan react to climate change with a longer delay, since the accumulation and, consequently, the mass turnover of predominantly cold glaciers are relatively small [10,50–53].

This may be due to the peculiarities of the geographical location of the Zhetysu Alatau, as well as the morphometric parameters of glaciers (the type and size of glaciers), the location along the altitudinal strip, and factors such as climate. An increase in air

temperature also has implications for snow cover, such as a decrease in snow amounts and an increasing intensity of snowmelt [2,54,55].

Regions with predominantly small glaciers are more sensitive to changes due to the shorter response time of glaciers to climate change [56,57]. It has also been reported that smaller glaciers with a large edge area-to-length ratio are shrinking faster than larger glaciers at the same rate of melt [58]. In the Zhetysu Alatau, the vast majority of glaciers are small, at less than 1 km<sup>2</sup> in size. Small glaciers cover more than half of the total area, which is common in midlatitudes.

An additional reason for the greater loss of area may be the lower height of the glaciers of the Zhetysu Alatau. An increase in mean annual temperatures without a significant increase in precipitation will shift the ELA about 150 m upwards per degree [59]. At low altitudes, this upward shift in the ELA increases the risk of the entire glacier area falling into the ablation zone (Figure 11). A reduction in glaciers was found at all altitudes of the study area during the study period. However, the greatest changes in the area were shown by glaciers lying on the slopes of the western and northwestern exposures. Most of the glaciers lying on the slopes of the southern exposures were outside the study area, but those that were not showed a noticeable reduction.

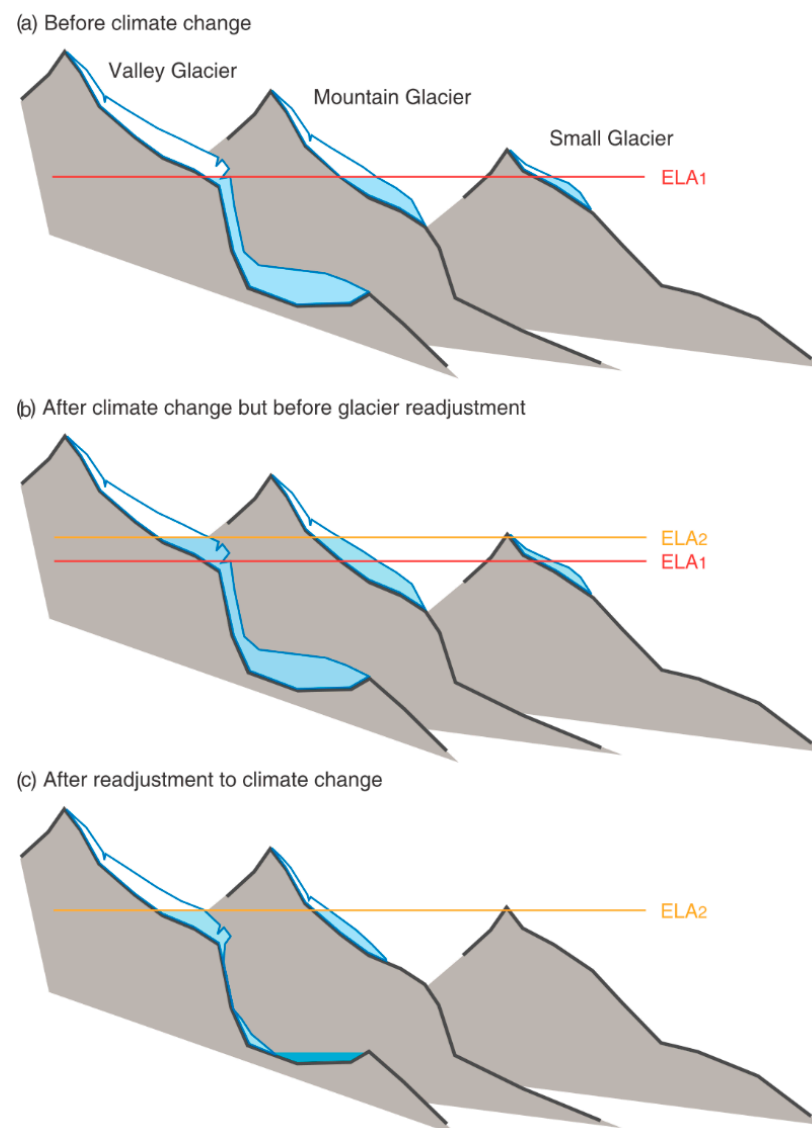


**Figure 11.** Schematic of the response of the three types of glaciers to climate change (from IPCC, 2013) [59].



Moreover, because of the western orientation, the Zhetysu Alatau ranges are also under the influence of warm western air masses originating over deserts located to the south of Lake Balkhash [54,60]. The exposure to moist air masses and dominating wind directions is strongly controlling the ELA elevation on ice [61]. Furthermore, the long-distance westerly winds are a carrier of fine-grained loess from the deserts of Central Asia to Tien Shan [60,62], polluting the glacial surfaces and intensifying the melting rate [59]. The frequency of dust storms directed to the Zhetysu Range has increased during the last few decades [62], so the shrinkage rate of our study area, located in the western Zhetysu Alatau, is almost three times as severe ( $-0.86\%$  per year) as the Bortala River in the eastern Zhetysu Alatau ( $-0.32\%$  per year) [63].

The rates of temperature change were observed in the mountainous areas of Zhetysu Alatau (Kogaly MS), where the average rate of change was  $0.12\text{ }^{\circ}\text{C}/10\text{ years}$ . The trends in summer temperature changes (June–August) showed that mountainous and foothill areas had the highest values, which ranged from  $0.19\text{ }^{\circ}\text{C}/10\text{ years}$  (Kogaly MS) to  $0.25\text{ }^{\circ}\text{C}/10\text{ years}$  (Taldykogan MS). A warming climate leads to increasing glacier melt and as well as less snow accumulation, which in turn causes a lower albedo in the glacier surface [63–65]. The upward trend in temperature caused an increase in rainfall rate rather than snowfall in the high-altitude zones, leading to a decrease in accumulation and an acceleration of ablation, especially during summer [65].

## 6. Conclusions

We have presented a new and updated catalog of glaciers for the Zhetysu Alatau range for the period of 2001–2016. Glaciers were detected in all seven river basins for the Zhetysu Alatau using Landsat satellite images from 2001 to 2016. With area loss rates of about  $-0.8\%$  and  $-1.3\% \text{ a}^{-1}$  for the periods of 1956–2001 and 2001–2016, our results showed a higher rate than other regions of the Central Asian mountains, including Tien Shan, Altai, and Pamir. In addition, the rates of area shrinkage were significantly higher than other ranges of the Tien Shan mountain system, which were  $-0.8\%$ ,  $-1.1\%$ ,  $2.2\%$ , and  $-1.3\% \text{ a}^{-1}$  for the periods of 1956–2001, 2001–2012, 2012–2016, and 2001–2016, respectively.

For a more detailed analysis of the reason for the sharp reduction in the glacier, we analyzed climate data using the nonparametric Mann–Kendall test. Analyzing weather station climatic data, we found a significant increase in temperature at all stations. The trends in summer temperature changes (June–August) showed that mountainous and foothill areas had the highest values, ranging from  $0.19\text{ }^{\circ}\text{C}/10\text{ years}$  (Kogaly MS) to  $0.25\text{ }^{\circ}\text{C}/10\text{ years}$  (Taldykogan MS). An analysis of the trends in change showed that a steady increase in air temperature has been observed in the study area over the past decades.

It was found that climatic conditions play a main role in the state of glaciers. The location of the region under study on the periphery of the mountain system has less favorable conditions than the inner ranges. Moreover, a significant increase in temperature and a slight change in precipitation played a main role in the negative balance of glaciation in the Zhetysu Alatau.

**Author Contributions:** Conceptualization, S.N., A.K. and G.F.; methodology, S.N., A.K. and A.N.; software, K.Z., A.M. and S.N.; validation A.K. and S.N.; investigation, S.N., A.K. and K.Z.; data curation, A.M., A.N., K.Z. and D.C.; writing—original draft preparation, K.Z., A.K. and N.S.; writing—review and editing, A.K., K.Z. and G.I.; visualization, A.M. and K.Z.; supervision, A.K.; project administration, A.K.; funding acquisition, A.K. All authors have read and agreed to the published version of the manuscript.

**Funding:** This research has been funded by the Science Committee of the Ministry of Education and Science of the Republic of Kazakhstan within the framework of the projects AP08856470 and AP14872134, and supported by the Postdoctoral Fellowship provided by Al-Farabi Kazakh National University. The APC was funded by the project budget.

**Data Availability Statement:** The Landsat ETM+ and Landsat OLI images used in this study can be downloaded from the United States Geological Survey at <https://earthexplorer.usgs.gov/> (accessed on 20 December 2020). The Shuttle Radar Topography Mission (SRTM) 90 m DEM used in this study can be downloaded from CGIARCSI consortium for spatial information at <https://cgiarcsi.community/> (accessed on 20 December 2020). The ALOS PALSAR 12.5 m DEM used in this study can be downloaded from the Alaska Satellite Facility at <https://asf.alaska.edu> (accessed on 20 December 2020). High-resolution optical images with 3D representation used in this study are available in the program Google Earth. *Glacier Inventory of the USSR* (1969, 1970, 1975, and 1980) is available at <https://www.geokniga.org/books/> (accessed on 20 December 2020).

**Acknowledgments:** We are grateful to the providers of free data for this study: Alaska Satellite Facility (ASF), United States Geological Survey (USGS), and others. Thanks are due to DING Xiao-li, Chair Professor of Geomatics, Department of Land Surveying and Geo-Informatics, The Hong Kong Polytechnic University for his scientific consult and encouragement. We also acknowledge Baygurin Zhaksybek for his help during the preparation of the manuscript.

**Conflicts of Interest:** The authors declare no conflict of interest.

## References

1. Barnett, T.P.; Adam, J.C.; Lettenmaier, D.P. Potential impacts of a warming climate on water availability in snow-dominated regions. *Nature* **2005**, *438*, 303–309. [CrossRef]
2. Sorg, A.; Bolch, T.; Stoffel, M.; Solomina, O.; Beniston, M. Climate change impacts on glaciers and runoff in Tien Shan (Central Asia). *Nat. Clim. Chang.* **2012**, *2*, 725–731. [CrossRef]
3. Viviroli, D.; Dürri, H.H.; Messerli, B.; Meybeck, M.; Weingartner, R. Mountains of the world, water towers for humanity: Typology, mapping, and global significance. *Water Resour. Res.* **2007**, *43*, 1–13. [CrossRef]
4. Farinotti, D.; Longuevergne, L.; Moholdt, G.; Duethmann, D.; Mölg, T.; Bolch, T.; Vorogushyn, S.; Güntner, A. Substantial glacier mass loss in the Tien Shan over the past 50 years. *Nat. Geosci.* **2015**, *8*, 716–722. [CrossRef]
5. Aizen, V.B.; Aizen, E.M.; Kuzmichonok, V.A. Glaciers and hydrological changes in the Tien Shan: Simulation and prediction. *Environ. Res. Lett.* **2007**, *2*, 045019. [CrossRef]
6. Aizen, V.B.; Kuzmichonok, V.A.; Surazakov, A.B.; Aizen, E.M. Glacier changes in the Tien Shan as determined from topographic and remotely sensed data. *Glob. Planet. Chang.* **2007**, *56*, 328–340. [CrossRef]
7. Hagg, W.; Braun, L.N.; Weber, M.; Becht, M. Runoff modelling in glacierized Central Asian catchments for present-day and future climate. *Nord. Hydrol.* **2006**, *37*, 93–105. [CrossRef]
8. Karthe, D.; Chalov, S.; Borchardt, D. Water resources and their management in central Asia in the early twenty first century: Status, challenges and future prospects. *Environ. Earth Sci.* **2015**, *73*, 487–499. [CrossRef]
9. Kaser, G.; Großhauser, M.; Marzeion, B. Contribution potential of glaciers to water availability in different climate regimes. *Natl. Acad. Sci. USA* **2010**, *107*, 20223–20227. [CrossRef]
10. Narama, C.; Käab, A.; Duishonakunov, M.; Abdrakhmatov, K. Spatial variability of recent glacier area changes in the Tien Shan Mountains, Central Asia, using Corona (~1970), Landsat (~2000), and ALOS (~2007) satellite data. *Glob. Planet. Chang.* **2010**, *71*, 42–54. [CrossRef]
11. Vilesov, E.; Severskiy, I. Degradation of the Dzhungar (Zhetysu) Alatau Glaciation in the Second Half of the XX Century. *Ice Snow* **2013**, *53*, 12–20.
12. Severskiy, I.; Vilesov, E.; Kokarev, A.; Shesterova, I.; Morozova, V.; Kogutenko, L.; Usmanova, Z. Glacial systems of the Balkhash-Alakol basin: State, modern changes. *Quest. Geogr. Geoecology* **2012**, *2*, 31–40.
13. Kaldybayev, A.; Chen, Y.; Vilesov, E. Glacier change in the Karatal river basin, Zhetysu (Dzhungar) Alatau, Kazakhstan. *Ann. Glaciol.* **2016**, *57*, 11–19. [CrossRef]
14. Kaldybayev, A.; Chen, Y.; Issanova, G.; Wang, H.; Mahmudova, L. Runoff response to the glacier shrinkage in the Karatal river basin, Kazakhstan. *Arab. J. Geosci.* **2016**, *9*, 208. [CrossRef]
15. Severskiy, I.; Vilesov, E.; Armstrong, R.; Kokarev, A.; Kogutenko, L.; Usmanova, Z.; Morozova, V.; Raup, B. Changes in glaciation of the Balkhash-Alakol basin, central Asia, over recent decades. *Ann. Glaciol.* **2016**, *57*, 382–394. [CrossRef]
16. Cherkasov, P. *Glacier Inventory of the USSR. Lake Balkhash Basin, Part 4*; Hydrometeorological Publishing House: Leningrad, Russia, 1975; Volume 13.
17. Cherkasov, P. *Glacier Inventory of the USSR. Lake Balkhash Basin, Part 5*; Hydrometeorological Publishing House: Leningrad, Russia, 1980; Volume 13.
18. Cherkasov, P. *Glacier Inventory of the USSR. Lake Balkhash Basin, Part 6*; Hydrometeorological Publishing House: Leningrad, Russia, 1970; Volume 13.
19. Cherkasov, P.; Erasov, V. *Glacier Inventory of the USSR. Lake Balkhash Basin, Part 7*; Hydrometeorological Publishing House: Leningrad, Russia, 1969; Volume 13.
20. Chen, Y.; Li, W.; Deng, H.; Fang, G.; Li, Z. Changes in Central Asia's Water Tower: Past, Present and Future. *Sci. Rep.* **2016**, *6*, 35458. [CrossRef] [PubMed]

21. Pritchard, H.D. Asia's shrinking glaciers protect large populations from drought stress. *Nature* **2019**, *569*, 649–654. [\[CrossRef\]](#)
22. Sorg, A.; Huss, M.; Rohrer, M.; Stoffel, M. The days of plenty might soon be over in glacierized Central Asian catchments. *Environ. Res. Lett.* **2014**, *9*, 104018. [\[CrossRef\]](#)
23. Vilesov, E.; Morozova, V.; Seversky, I. *Glaciation of the Dzungarian (Zhetysu) Alatau: Past, Present, Future*; KazNU: Almaty, Kazakhstan, 2013.
24. Yudichev, M. *Dzungarian Alatau. Materials on Geology and Minerals of Kazakhstan*; KazFAN USSR: Leningrad, Russia, 1940; Volume 14.
25. Ministry of Energy of the Republic of Kazakhstan United Nations Development Programme in Kazakhstan Global Environment Facility. *Seventh National Communication and Third Biennial Report of the Republic of Kazakhstan to the UN Framework Convention on Climate Change*; Ministry of Energy of the Republic of Kazakhstan United Nations Development Programme in Kazakhstan Global Environment Facility: Astana, Kazakhstan, 2017; p. 290.
26. Ministry of Ecology, Geology and Natural Resources of the Republic of Kazakhstan; Republican State Enterprise «Kazhydromet»; Scientific Research Center. *Annual Bulletin of Monitoring of the Climate State and Climate Change in Kazakhstan: 2021*; Research Center of RSE «Kazhydromet»: Astana, Kazakhstan, 2022; p. 76.
27. Cherednichenko, A.; Cherednichenko, A.; Vilesov, E.N.; Cherednichenko, V.S. Climate change in the City of Almaty during the past 120 years. *Quat. Int.* **2015**, *358*, 101–105. [\[CrossRef\]](#)
28. Hollander, M.; Wolfe, D.A. *Nonparametric Statistical Methods*; John Wiley & Sons.: Hoboken, NJ, USA, 1999.
29. Paul, F.; Barrand, N.E.; Baumann, S.; Berthier, E.; Bolch, T.; Casey, K.; Frey, H.; Joshi, S.P.; Kononov, V.; Le Bris, R.; et al. On the accuracy of glacier outlines derived from remote-sensing data. *Ann. Glaciol.* **2013**, *54*, 171–182. [\[CrossRef\]](#)
30. Racoviteanu, A.E.; Paul, F.; Raup, B.; Khalsa, S.J.S.; Armstrong, R. Challenges and recommendations in mapping of glacier parameters from space: Results of the 2008 global land ice measurements from space (GLIMS) workshop, Boulder, Colorado, USA. *Ann. Glaciol.* **2009**, *50*, 53–69. [\[CrossRef\]](#)
31. Paul, F.; Kääb, A. Perspectives on the production of a glacier inventory from multispectral satellite data in Arctic Canada: Cumberland Peninsula, Baffin Island. *Ann. Glaciol.* **2005**, *42*, 59–66. [\[CrossRef\]](#)
32. Bolch, T. Climate change and glacier retreat in northern Tien Shan (Kazakhstan/Kyrgyzstan) using remote sensing data. *Glob. Planet. Chang.* **2007**, *56*, 1–12. [\[CrossRef\]](#)
33. Bolch, T.; Yao, T.; Kang, S.; Buchroithner, M.F.; Scherer, D.; Maussion, F.; Huintjes, E.; Schneider, C. A glacier inventory for the western Nyainqentanglha range and the Nam Co Basin, Tibet, and glacier changes 1976–2009. *Cryosphere* **2010**, *4*, 419–433. [\[CrossRef\]](#)
34. Paul, F.; Bolch, T.; Briggs, K.; Kääb, A.; McMillan, M.; McNabb, R.; Nagler, T.; Nuth, C.; Rastner, P.; Strozzi, T.; et al. Error sources and guidelines for quality assessment of glacier area, elevation change, and velocity products derived from satellite data in the Glaciers\_cci project. *Remote Sens. Environ.* **2017**, *203*, 256–275. [\[CrossRef\]](#)
35. Farooq, I.; Shah, A.R.; Salik, K.M.; Ismail, M. Annual, Seasonal and Monthly Trend Analysis of Temperature in Kazakhstan During 1970–2017 Using Non-parametric Statistical Methods and GIS Technologies. *Earth Syst. Environ.* **2021**, *5*, 575–595. [\[CrossRef\]](#)
36. Talipova, E.; Shrestha, S.; Alimkulov, S.; Nyssanbayeva, A.; Tursunova, A.; Isakan, G. Influence of climate change and anthropogenic factors on the Ile River basin streamflow, Kazakhstan. *Arab. J. Geosci.* **2021**, *14*, 1756. [\[CrossRef\]](#)
37. Shahgedanova, M.; Afzal, M.; Severskiy, I.; Usmanova, Z.; Saidaliyeva, Z.; Kapitsa, V.; Kasatkin, N.; Dolgikh, S. Changes in the mountain river discharge in the northern Tien Shan since the mid-20th Century: Results from the analysis of a homogeneous daily streamflow data set from seven catchments. *J. Hydrol.* **2018**, *564*, 1133–1152. [\[CrossRef\]](#)
38. Kriegel, D.; Mayer, C.; Hagg, W.; Vorogushyn, S.; Duethmann, D.; Gafurov, A.; Farinotti, D. Changes in glacierisation, climate and runoff in the second half of the 20th century in the Naryn basin, Central Asia. *Glob. Planet. Chang.* **2013**, *110*, 51–61. [\[CrossRef\]](#)
39. Zhang, Q.; Chen, Y.; Li, Z.; Li, Y.; Xiang, Y.; Bian, W. Glacier changes from 1975 to 2016 in the Aksu River Basin, Central Tianshan Mountains. *J. Geogr. Sci.* **2019**, *29*, 984–1000. [\[CrossRef\]](#)
40. Zhang, Q.; Chen, Y.; Li, Z.; Fang, G.; Xiang, Y.; Li, Y.; Ji, H. Recent changes in water discharge in snow and glacier melt-dominated rivers in the Tianshan mountains, Central Asia. *Remote Sens.* **2020**, *12*, 2704. [\[CrossRef\]](#)
41. Kutuzov, S.; Shahgedanova, M. Glacier retreat and climatic variability in the eastern Terskey-Alatau, inner Tien Shan between the middle of the 19th century and beginning of the 21st century. *Glob. Planet. Chang.* **2009**, *69*, 59–70. [\[CrossRef\]](#)
42. He, Y.; Yang, T.-b.; Ji, Q.; Chen, J.; Zhao, G.; Shao, W.-W. Glacier variation in response to climate change in Chinese Tianshan Mountains from 1989 to 2012. *J. Mt. Sci.* **2015**, *12*, 1189–1202. [\[CrossRef\]](#)
43. Aizen, V.B.; Kuzmichenok, V.A.; Surazakov, A.B.; Aizen, E.M. Glacier changes in the central and northern Tien Shan during the last 140 years based on surface and remote-sensing data. *Ann. Glaciol.* **2006**, *43*, 202–213. [\[CrossRef\]](#)
44. Narama, C.; Shimamura, Y.; Nakayama, D.; Abdrakhmatov, K. Recent changes of glacier coverage in the western Terskey-Alatau range, Kyrgyz Republic, using Corona and Landsat. *Ann. Glaciol.* **2006**, *43*, 223–229. [\[CrossRef\]](#)
45. Unger-Shayesteh, K.; Vorogushyn, S.; Farinotti, D.; Gafurov, A.; Duethmann, D.; Mandychyev, A.; Merz, B. What do we know about past changes in the water cycle of Central Asian headwaters? A review. *Glob. Planet. Chang.* **2013**, *110*, 4–25. [\[CrossRef\]](#)
46. Tielidze, L.G.; Wheate, R.D. The Greater Caucasus Glacier Inventory (Russia, Georgia and Azerbaijan). *Cryosphere* **2018**, *12*, 81–94. [\[CrossRef\]](#)
47. Tennant, C.; Menounos, B.; Wheate, R.; Clague, J.J. Area change of glaciers in the Canadian rocky mountains, 1919 to 2006. *Cryosphere* **2012**, *6*, 1541–1552. [\[CrossRef\]](#)


48. Paul, F.; Rastner, P.; Azzoni, R.S.; Diolaiuti, G.; Fugazza, D.; Bris, R.L.; Nemec, J.; Rabatel, A.; Ramusovic, M.; Schwaizer, G.; et al. Glacier shrinkage in the Alps continues unabated as revealed by a new glacier inventory from Sentinel-2. *Earth Syst. Sci. Data* **2020**, *12*, 1805–1821. [[CrossRef](#)]
49. Kokarev, A.; Shesterova, I. Present-day changes of mountain glaciers on the southern slope of the Dzhungarian Alatau range. *Ice Snow* **2015**, *128*, 54. [[CrossRef](#)]
50. Dolgushin, L.; Osipova, G. The Nature of the World: Glaciers. Mysl. Moscow, USSR. 1989; Volume 447. Available online: [https://www.studmed.ru/dolgushin-l-d-osipova-g-b-ledniki\\_e961d16f14e.html](https://www.studmed.ru/dolgushin-l-d-osipova-g-b-ledniki_e961d16f14e.html) (accessed on 1 March 2023).
51. Liu Chaozhai; Han Tianding Relation between recent glacier variations and climate in the Tien Shan Mountains, Central Asia. *Ann. Glaciol.* **1992**, *16*, 11–16. [[CrossRef](#)]
52. Pieczonka, T.; Bolch, T. Region-wide glacier mass budgets and area changes for the Central Tien Shan between ~1975 and 1999 using Hexagon KH-9 imagery. *Glob. Planet. Chang.* **2015**, *128*, 1–13. [[CrossRef](#)]
53. Li, B.; Zhu, A.X.; Zhang, Y.; Pei, T.; Qin, C.; Zhou, C. Glacier change over the past four decades in the middle Chinese Tien Shan. *J. Glaciol.* **2006**, *52*, 425–432. [[CrossRef](#)]
54. Aizen, V.B.; Aizen, E.M.; Melack, J.M.; Dozier, J. Climatic and hydrologic changes in the Tien Shan, central Asia. *J. Clim.* **1997**, *10*, 1393–1404. [[CrossRef](#)]
55. Qin, D.; Liu, S.; Li, P. Snow cover distribution, variability, and response to climate change in western China. *J. Clim.* **2006**, *19*, 1820–1833. [[CrossRef](#)]
56. Bahr, D.B.; Pfeffer, W.T.; Sassolas, C.; Meier, M.F. Response time of glaciers as a function of size and mass balance: 1. Theory. *J. Geophys. Res. Solid Earth* **1998**, *103*, 9777–9782. [[CrossRef](#)]
57. Ye, B.; Ding, Y.; Liu, C. Response of valley glaciers in various sizes and their runoff to climate change. *J. Glaciol.* **2003**, *49*, 1–7.
58. Granshaw, F.D.; Fountain, A.G. Glacier change (1958–1998) in the North Cascades National Park Complex, Washington, USA. *J. Glaciol.* **2006**, *52*, 251–256. [[CrossRef](#)]
59. Ciais, P.; Sabine, C.; Bala, G.; Bopp, L.; Brovkin, V.; Canadell, J.; Chhabra, A.; DeFries, R.; Galloway, J.; Heimann, M.; et al. The physical science basis. Contribution of working group I to the fifth assessment report of the intergovernmental panel on climate change. *Chang. IPCC Clim.* **2013**, *375*, 20160321. [[CrossRef](#)]
60. Vandenberghe, J.; Renssen, H.; van Huissteden, K.; Nugteren, G.; Konert, M.; Lu, H.; Dodonov, A.; Buylaert, J.P. Penetration of Atlantic westerly winds into Central and East Asia. *Quat. Sci. Rev.* **2006**, *25*, 2380–2389. [[CrossRef](#)]
61. Hagg, W.; Mayer, C.; Lambrecht, A.; Kriegel, D.; Azizov, E. Glacier changes in the Big Naryn basin, Central Tian Shan. *Glob. Planet. Chang.* **2013**, *110*, 40–50. [[CrossRef](#)]
62. Gulnura, I.; Abuduwaili, J.; Oleg, S. Deflation processes and their role in desertification of the southern Pre-Balkhash deserts. *Arab. J. Geosci.* **2014**, *7*, 4513–4521. [[CrossRef](#)]
63. Wang, L.; Li, Z.; Wang, F.; Edwards, R. Glacier shrinkage in the Ebinur lake basin, Tien Shan, China, during the past 40 years. *J. Glaciol.* **2014**, *60*, 245–254. [[CrossRef](#)]
64. Ageta, Y.; Kadota, T. Predictions of changes of glacier mass balance in the Nepal Himalaya and Tibetan Plateau: A case study of air temperature increase for three glaciers. *Ann. Glaciol.* **1992**, *16*, 89–94. [[CrossRef](#)]
65. Fujita, K.; Ageta, Y. Effect of summer accumulation on glacier mass balance on the Tibetan Plateau revealed by mass-balance model. *J. Glaciol.* **2000**, *46*, 244–252. [[CrossRef](#)]

**Disclaimer/Publisher’s Note:** The statements, opinions and data contained in all publications are solely those of the individual author(s) and contributor(s) and not of MDPI and/or the editor(s). MDPI and/or the editor(s) disclaim responsibility for any injury to people or property resulting from any ideas, methods, instructions or products referred to in the content.



## Review

# Application of Artificial Intelligence in Glacier Studies: A State-of-the-Art Review

Serik Nurakynov <sup>1,2,\*</sup> , Aibek Merekeyev <sup>1</sup>, Zhaksybek Baygurin <sup>2</sup>, Nurmakhambet Sydyk <sup>1</sup> and Bakytzhan Akhmetov <sup>3</sup>

<sup>1</sup> Institute of Ionosphere, Almaty 050000, Kazakhstan

<sup>2</sup> Department of Surveying and Geodesy, Satbayev University, Almaty 050000, Kazakhstan

<sup>3</sup> School of Mechanical and Aerospace Engineering, Nanyang Technological University, 50 Nanyang Ave, Singapore 639798, Singapore

\* Correspondence: snurakynov@ionos.kz

**Abstract:** Assessing glaciers using recent and historical data and predicting the future impacts on them due to climate change are crucial for understanding global glacier mass balance, regional water resources, and downstream hydrology. Computational methods are crucial for analyzing current conditions and forecasting glacier changes using remote sensing and other data sources. Due to the complexity and large data volumes, there is a strong demand for accelerated computing. AI-based approaches are increasingly being adopted for their efficiency and accuracy in these tasks. Thus, in the current state-of-the-art review work, available research results on the application of AI methods for glacier studies are addressed. Using selected search terms, AI-based publications are collected from research databases. They are further classified in terms of their geographical locations and glacier-related research purposes. It was found that the majority of AI-based glacier studies focused on inventorying and mapping glaciers worldwide. AI techniques like U-Net, Random forest, CNN, and DeepLab are mostly utilized in glacier mapping, demonstrating their adaptability and scalability. Other AI-based glacier studies such as glacier evolution, snow/ice differentiation, and ice dynamic modeling are reviewed and classified. Overall, AI methods are predominantly based on supervised learning and deep learning approaches, and these methods have been used almost evenly in glacier publications over the years since the beginning of this research area. Thus, the integration of AI in glacier research is advancing, promising to enhance our comprehension of glaciers amid climate change and aiding environmental conservation and resource management.

**Keywords:** remote sensing; artificial intelligence; machine learning; glacier mapping; snow/ice differentiation; ice dynamics modeling



**Citation:** Nurakynov, S.; Merekeyev, A.; Baygurin, Z.; Sydyk, N.; Akhmetov, B. Application of Artificial Intelligence in Glacier Studies: A State-of-the-Art Review. *Water* **2024**, *16*, 2272. <https://doi.org/10.3390/w16162272>

Academic Editors: Jueyi Sui and Richard Smardon

Received: 17 June 2024

Revised: 26 July 2024

Accepted: 6 August 2024

Published: 12 August 2024



**Copyright:** © 2024 by the authors. Licensee MDPI, Basel, Switzerland. This article is an open access article distributed under the terms and conditions of the Creative Commons Attribution (CC BY) license (<https://creativecommons.org/licenses/by/4.0/>).

## 1. Introduction

Glaciers worldwide are at serious risk due to climate change. For instance, the mass loss of mountain glaciers between 2006 and 2016 resulted in a global sea-level contribution of  $335 \pm 144$  Gt per year [1]. Even though the rate of glacier loss is dependent on the region, it is expected to have significant environmental and social impacts [2,3]. In fact, nearly 10% of the world's population residing in mountainous regions depends on glaciers as a crucial water source, where they are utilized for agriculture, industry, hydropower generation, and domestic use [4,5]. Moreover, meltwater from glaciers contributes to the sustenance of rivers, lakes, and wetlands, supporting diverse aquatic life forms. Additionally, glaciers play a crucial role in regulating local microclimates [6], influencing vegetation patterns and providing a habitat for various species, thereby shaping the composition and dynamics of terrestrial ecosystems [7]. Therefore, evaluating and estimating changes in glaciers plays a crucial role in projecting future scenarios, particularly in regions where both the environment and society depend on them.

For a few decades, organizations and scientists have been developing inventories for glaciers throughout the world. For instance, the World Glacier Inventory (WGI) contains data for over 130,000 glaciers, providing information on parameters such as geographic location, area, length, orientation, elevation, and classification, primarily derived from aerial photographs and maps. However, the WGI inventory can provide a glacier distribution in the second half of the 20th century [8]. Similarly, the Randolph Glacier Inventory (RGI) serves as another valuable database for glaciers; however, its temporal coverage is limited as most of the glaciers were mapped around the 2000s [9]. Therefore, these inventories can only serve as baseline datasets, as they are unable to capture the latest changes in glacier dynamics. However, in the last decade, there has been a proactive effort to generate additional localized data using remote sensing methods, aimed at enhancing the temporal accuracy in monitoring glacier changes [10].

Methods relying on optical, synthetic aperture radar (SAR), and multisource datasets are well known in glacier mapping. Optical imagery (OI) is considered as the primary technique utilized for glacier extraction, leveraging the significant contrast between the minimal spectral reflectance of ice and snow in the shortwave infrared and their high reflectance within the visible spectrum [11,12]. However, its efficacy is constrained by weather variability and the difficulty in distinguishing glaciers, especially those covered with debris from surrounding rocks of mountains, due to their comparable spectral characteristics [13]. To address these challenges, SAR data are utilized in glacier extraction, leveraging two main principles. One principle focuses on the lower coherence observed in glaciers, both clean and debris-covered, compared to the higher coherence of surrounding bedrock, with commonly used data sources including Sentinel-1 and ALOS PALSAR [14,15]. However, the processing of SAR coherence is complex and limited by the presence of non-steady deformation processes. Additionally, SAR imaging can be hindered by factors such as layover and shadow effects in steep terrain, which may obscure certain glacier features and impede accurate mapping [16]. Furthermore, combining different data sources (i.e., multisource approach) from SAR, OI, and digital elevation models (DEMs) provides valuable insights into glacier dynamics and changes [17]. However, the multi-source method involves various drawbacks related to data integration complexity, temporal and spatial mismatch, cost and accessibility, data consistency and quality, as well as interpretation and validation challenges. Addressing these disadvantages requires careful consideration of data processing techniques, quality assessment measures, and validation procedures to ensure robust and accurate glacier mapping results [18].

Transitioning from traditional methods to artificial intelligence (AI) techniques marks a significant advancement in glacier mapping and monitoring. Indeed, studies have shown that AI methodologies demonstrate notable efficacy in classifying remote sensing (RS) data through feature extraction and selection, particularly in hyperspectral images [19,20]. These AI techniques have yielded promising outcomes across various RS applications, including tree delineation [21], land cover classification [22], building detection [23,24], fault diagnosis [25], and fault-tolerant control [26]. Moreover, within the realm of glacier studies, AI methods have also found applications in mapping large glaciers from RS data.

Recently, various advanced methods have been actively employed for evaluating changes in glacier-covered regions and ice formations during specific periods. Among these methods, segmentation techniques that rely on visual interpretation and RS are the most frequently used [27–29]. Moreover, these evaluations have begun to be studied using decision-tree, supervised, and unsupervised methods [30]. In the same way, band ratios and manual on-screen digitalization are utilized to classify debris-covered glaciers [31]. Furthermore, a number of researchers have suggested semi-automatic methods for classification purposes, and more recently, unmanned aerial vehicles (UAVs) have been employed to map glaciers with increased precision [32].

These AI algorithms offer powerful tools for glacier mapping applications, enabling researchers to analyze large-scale glacier datasets more efficiently and accurately than traditional manual methods. By leveraging the capabilities of AI, scientists can gain deeper

insights into glacier dynamics, contribute to climate change research, and support informed decision making in environmental management [33]. Therefore, reviewing the latest works in this new area is necessary to understand the research trends in terms of AI methods applied for glacier studies.

In this study, we conduct a state-of-the-art review of the most recent research papers that have applied artificial intelligence (AI) methods in glacier studies. According to our observations, the application of AI methods for glacier studies has been active since 2019. The main reasons may be the increased access and availability of open-source AI tools such as Pytorch [34], Tensorflow [35], and Keras [36] for the general audience and continuous improvements in image-based AI techniques, which have significantly accelerated in the last few years [37]. This makes the recent works particularly relevant and of interest given the latest advancements.

Thus, the objective of the current state-of-the-art review is to understand the trend of AI-based method applications in glacier studies, as well as the types and classification of AI methods, and to evaluate the size and variety of glacier datasets used for training and validation in addition to the accuracy and efficiency of the selected AI methods in studying glaciers. Moreover, the reviewed works are classified based on the type of glacier studies, providing the reader with clear guidance on the AI methods applied for the relevant studies. For each type of glacier study that uses AI, the research works are reviewed and discussed in chronological order, offering valuable insights into how this research field is evolving over time. Additionally, comparative analyses are carried out for each type of AI-based glacier study. Hence, in the next section, the readers may learn about the approach to finding the research works among AI-based glacier studies, understanding the reviewed works in a general manner, and gaining knowledge from classification charts and illustrations. Furthermore, in the subsequent sections, the classified works are discussed in more detail, followed by a discussion section. Finally, conclusive remarks, including future works, are presented in the conclusion section.

## 2. Review Approach and Overview of the Collected Works

To find research works that apply AI methods and techniques to glacier studies, we used search terms and expressions such as “Glacier Deep Learning”, “Glacier Machine Learning”, “Artificial Intelligence in glacier studies”, “Glacier studies with Neural Networks”, and “Neural Network-based glacier studies” in various databases (Figure 1). Specifically, we conducted searches in databases such as Elsevier, Wiley, Springer, Taylor & Francis, IEEE, Copernicus Group, and MDPI. According to the Scimago Journal Rank ([www.scimagojr.com](http://www.scimagojr.com)), these publishers, under the category of Earth-Surface Processes, host the leading journals that publish environmental science, geology, and glaciology research works. Additionally, we used these terms and expressions in the Google search engine to find similar works in other databases to ensure comprehensive coverage. As shown in the flowchart, the research articles found are firstly classified in chronological order.

Furthermore, according to the inventory data of RGI [38], there are 19 glacier regions in the world, as shown in Figure 2. Once all the works are collected in chronological order, the second step in classification involves dividing them based on these regions. Such classification can be considered reasonable since the accuracy of AI models usually depends on the geological location of the training datasets, and they are often less accurate when tested on another dataset from a different location [39]. Thus, among the glacier regions studied using AI methods, the most prominent are those in South West and South East Asia, designated as Region 14 and 15, respectively, followed by Central Europe and other regions. This is clearly can be noticed in the second column of the Sankey Diagram illustrated in Figure 3. Furthermore, considering the main classification of the reviewed works, we focus on the purpose of AI applications in glacier studies (Figure 3), which are mainly divided into (i) inventory and mapping, (ii) glacier evolution, (iii) snow/ice differentiation, and (iv) ice dynamics modeling. Therefore, the main part of the current work, Section 3, is divided into subsections based on these classifications of glacier studies.

# Glacier AI review

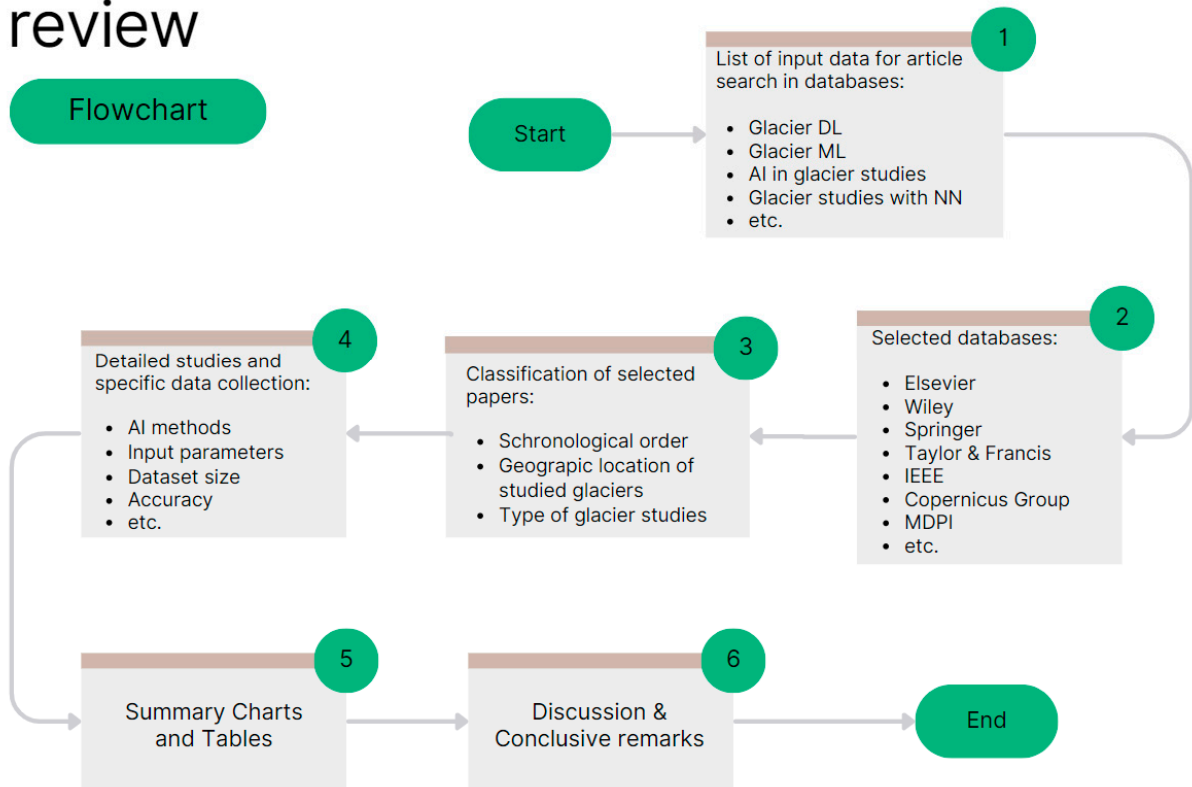


**Figure 1.** Flowchart for illustration of the methods used in the current review work.

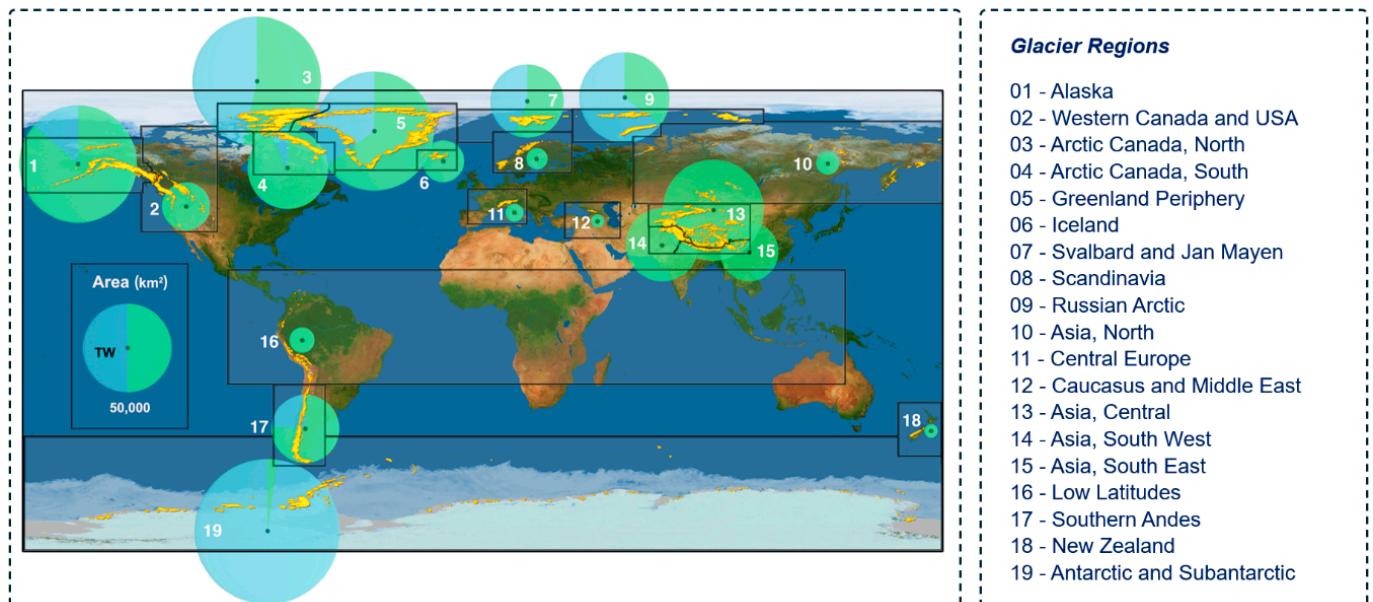


**Figure 2.** Glacier regions in the world (modified from [38]).



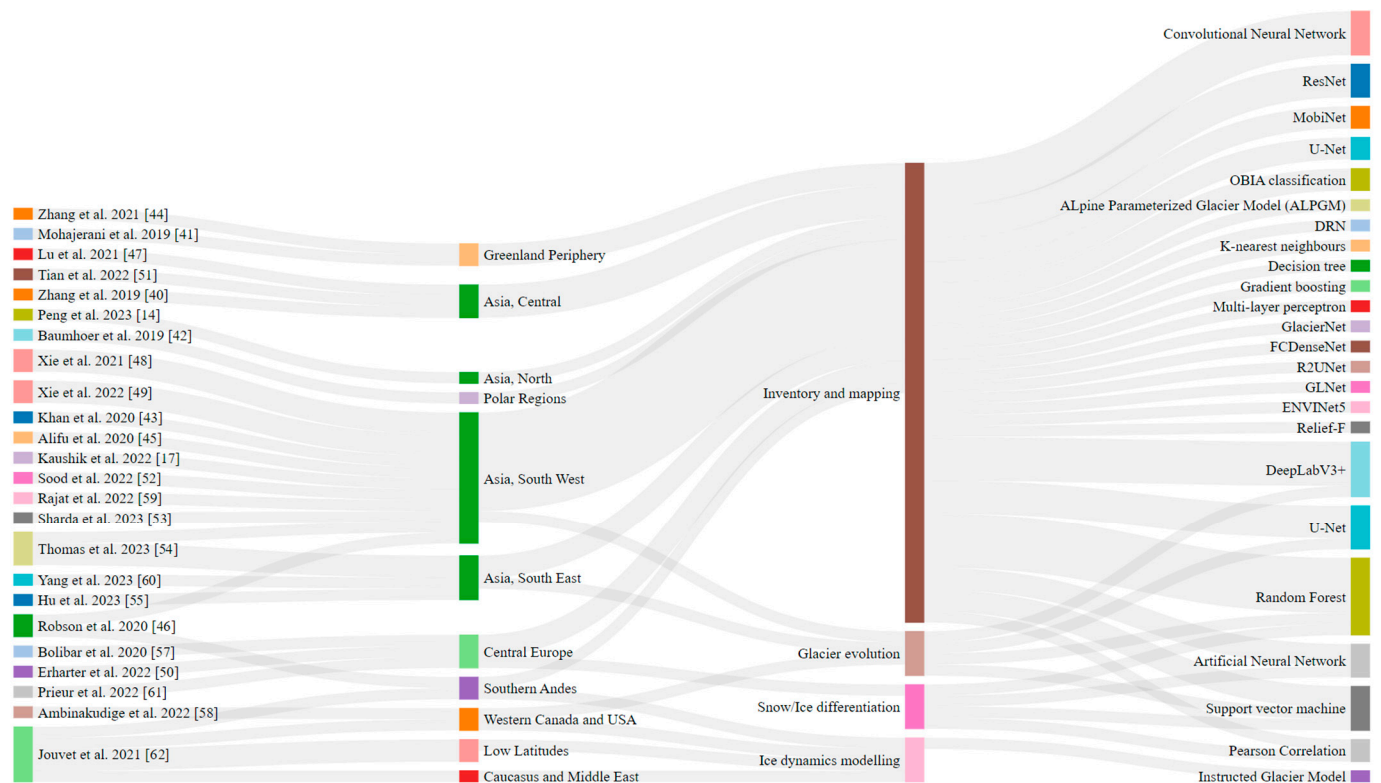


**Figure 3.** Classification of the collected research works based on glacier regions, type of glacier study, and AI models using a Sankey Diagram.

Inventory development and mapping of glaciers represent one of the most extensively studied areas within the field of AI-based glacier studies, and this is clearly shown in the Sankey diagram (Figure 3). Among the collected and reviewed works, XX papers dealt with the application of AI methods for inventory and mapping of glaciers. Thus, researchers and scientists have increasingly utilized AI methods such as machine learning (ML) techniques and deep learning (DL) techniques to automate the process of mapping glaciers, creating detailed inventories, and monitoring changes in glacier extent over time.

On the other hand, monitoring glacier evolution becomes crucial for understanding environmental changes, especially as glaciers worldwide are affected by the consequences of climate change. Therefore, in the latest works, applications of AI in this area can be found since AI offers powerful tools for continuously tracking glacier dynamics, enabling researchers to gain insights into changes in glacier extent, volume, and behavior over time.

There are certain unique applications of AI in snow/ice differentiation and ice dynamics modeling that allow us to distinguish glaciers from snow layers and simulate ice volume changes, mass balance, and their coupling to assess the development of icefields and ice sheets. Therefore, they are considered as separate areas of glacier studies in the current review work.

As shown in the flowchart (Figure 1), while reviewing each research work, the main findings—such as the location and type of the glacier, its classification/type based on GLIMS (Global Land Ice Measurements from Space) if applicable, the selected AI model, the input parameters, the datasets and dataset sizes, the accuracy of the model, and the software used to develop and run the AI model—are summarized in Table 1. Such a tabulated summary is highly suitable for a quick comparison of AI-based works, and it contains all the main findings in the form of organized data for readers to evaluate the past works and plan their future research.

Table 1. Summary of the review.

Author	Location	Glacier Location Name	Studied Glacier Types	Classification by GLIMS Manual	AI Model	Parameters	Dataset Size	Accuracy	Software
Glacier inventory and mapping									
2019 Zhang et al. [40]	Parlung Zangbo Basin, China	Tibetan Plateau glacier	<ul style="list-style-type: none"><li>Non/partially debris-covered glaciers</li><li>Fully debris-covered glaciers</li></ul>	N/A	Random forest (RF)	<ul style="list-style-type: none"><li>Landsat-8 images</li><li>Normalized difference vegetation index (NDVI)</li><li>Normalized Difference Water Index (NDWI)</li><li>Normalized Difference Snow Index (NDSI)</li><li>GF-1 PMS imagery</li><li>Digital Elevation Model (DEM)</li><li>11 topographic parameters</li></ul>	2755	RF-98.6% (ovearall)	EnMAP-Box + DLL
2019 Mohajerani et al. [41]	Greenland	Jakobshavn, Sverdrup, Kangerlussuaq, Helheim	<ul style="list-style-type: none"><li>Tidewater glaciers</li></ul>	N/A	U-Net	<ul style="list-style-type: none"><li>Landsat images</li></ul>	Training data: images from Jakobshavn, Sverdrup and Kangerlussuaq. Test data: images from Helheim glacier	Mean deviation of 96.3 m from the true calving fonts	Python
2019 Baumhoer et al. [42]	Antarctica	<ul style="list-style-type: none"><li>Sulzberg ice shelf</li><li>Skackleton ice shelf</li><li>Wilkes Land</li><li>Victoria Land</li><li>Getz ice shelf</li><li>Ekstromisen</li><li>Wordie ice shelf</li><li>Oats land</li><li>Marie Byrd land</li></ul>	<ul style="list-style-type: none"><li>Ice shelves, dynamic glaciers</li></ul>	N/A	Modified U-Net	<ul style="list-style-type: none"><li>Sentintel-1, TanDEM-X digital elevation model</li></ul>	38 pre-processed Sentinel-1 scenes 90m resolution TanDEM-X	Average f1-score = 90%	N/A

Table 1. Cont.

Author	Location	Glacier Location Name	Studied Glacier Types	Classification by GLIMS Manual	AI Model	Parameters	Dataset Size	Accuracy	Software
2020 Khan et al. [43]	Hunza Basin, Pakistan	Batura glacier	<ul style="list-style-type: none"><li>Glaciers</li><li>Debris-covered glaciers</li><li>Non-glaciated areas</li></ul>	N/A	<ul style="list-style-type: none"><li>Support vector machine (SVM)</li><li>Artificial neural network (ANN)</li><li>RF</li></ul>	<ul style="list-style-type: none"><li>NDVI</li><li>NDSI</li><li>NDWI</li><li>New band ratio (NBR)</li><li>Mean</li><li>Variance</li><li>Homogeneity</li><li>Contrast</li><li>Dissimilarity</li><li>Entropy</li><li>Energy</li><li>Correlation</li><li>Angular second momentum</li><li>Slope</li><li>Aspect</li><li>Evaluation</li><li>Land surface temperature</li></ul>	2,688,723 pixels  Training: 70% Testing: 30%	Kappa: SVM = 0.89 ANN = 0.92 RF = 0.95  f-measure: SVM = 91.86% ANN = 92.05% RF = 95.06%	N/A
2021 Zhang et al. [44]	Greenland	Jakobshavn Isbræ, Kangerlussuaq, Helheim glaciers	Tidewater outlet glaciers	Tidewater outlet glacier	<ul style="list-style-type: none"><li>U-Net</li><li>DeepLabv3+ with ResNet</li><li>DRN</li><li>MobiNet</li></ul>	<p>Optical:</p> <ul style="list-style-type: none"><li>Landsat-8</li><li>Sentinel-2</li></ul> <p>Synthetic aperture radar images:</p> <ul style="list-style-type: none"><li>Envisat</li><li>ALOS-1</li><li>TerraSAR-X</li><li>Sentinel-1</li><li>ALOS-2</li></ul>	Training: 110 Landsat-8, 13 ALOS-1, 76 TSX, 140 Sentinel-1  Testing: 74 Landsat-8, 52 Sentinel-2, 48 Envisat, 17 TSX, 90 Sentinel-1, 14 ALOS-2	Test-error studies: DRN-DeepLabv3+ is the lowest  Refer to Table 3 from [44] for full test results	Python  Open-source in GitHub: <a href="https://github.com/enzezhang/FrontDL3">https://github.com/enzezhang/FrontDL3</a> (accessed on 7 July 2024)

Table 1. Cont.

Author	Location	Glacier Location Name	Studied Glacier Types	Classification by GLIMS Manual	AI Model	Parameters	Dataset Size	Accuracy	Software
2020 H. Alifu et al. [45]	Karakoram—Pakistan Shaksgam Valley, China	North-western Karakoram region and Shaksgam Valley glaciers	Debris-covered glaciers	Valley, Mountain glaciers	Machine learning classifiers (MLC): - K-nearest neighbors (KNN) - Support vector machine (SVM) - Decision tree (DT), - Gradient boosting (GB) - Random forest (RF) - Multi-layer perceptron (MLP)	<ul style="list-style-type: none"><li>• Sentinel-2A</li><li>• Landsat-8</li><li>• Sentinel-1A</li><li>• ALOS DEM</li><li>• Geomorphometric parameters</li><li>• Thermal Infrared images</li><li>• GAMDAM dataset</li></ul>	Area 1: 2000 to 20,000 points. Area 2: 20,000 points	RF-97%	Python
						<ul style="list-style-type: none"><li>• Sentinel-2: Blue, Green, Red, Near-Infrared, and shortwave Infrared bands</li><li>• SAR coherence data</li></ul>	Not clear	<ul style="list-style-type: none"><li>• User’s accuracy: 65.9%</li><li>• Producer accuracy: 71.4%</li></ul>	Google Tensorflow
2021 Lu et al. [47]	China	High Mountain Asia	Debris-covered glaciers	Mountain glacier	RF CNN	<ul style="list-style-type: none"><li>• Landsat 8</li><li>• NDVI</li><li>• NDWI</li><li>• NDSI</li><li>• Elevation</li><li>• Slope</li><li>• Aspect</li><li>• Shaded relief</li></ul>	Eastern Pamir: 7499 samples  Nyainqentanglha: 3099 samples	Eastern Pamir and Nyainqentanglha  User’s accuracy: <ul style="list-style-type: none"><li>• RF = 91.59%, 92.53%</li><li>• CNN = 87.96%, 78.75%</li><li>• RF-CNN = 97.90%, 90.60%</li></ul> Producer’s accuracy: <ul style="list-style-type: none"><li>• RF = 97.17%, 98.86%</li><li>• CNN = 98.69%, 97.53%</li><li>• RF-CNN = 98.33%, 74.54%</li></ul>	Python



Table 1. Cont.

Author	Location	Glacier Location Name	Studied Glacier Types	Classification by GLIMS Manual	AI Model	Parameters	Dataset Size	Accuracy	Software
2021 Xie et al. [48]	Kashmir Region.	Karakoram glaciers	DCG	Mountain, Valley glaciers	<ul style="list-style-type: none"><li>GlacierNet</li><li>Mobile-Unet</li><li>Res-UNet</li><li>FCDenseNet</li><li>R2UNet</li><li>DeepLabV3+</li></ul>	<ul style="list-style-type: none"><li>Landsat 8</li><li>ALOS DEM</li><li>Slope–azimuth divergence index</li><li>Slope angle</li><li>Tangential curvature profile</li><li>Unspphericity curvature</li></ul>	N/A	<div>IOU:</div> <ul style="list-style-type: none"><li>DeepLabV3+ = 0.8623</li><li>GlacierNet = 0.8599</li><li>Mobile-UNet = 0.8531</li><li>ResUNet = 0.8399</li><li>FCDenseNet = 0.8265</li><li>R2UNet = 0.8204</li><li>Accuracy: DeepLabV3+ = 0.9684</li><li>GlacierNet = 0.9677</li><li>Mobile-UNet = 0.9660</li><li>ResUNet = 0.9636</li><li>FCDenseNet = 0.9597</li><li>R2UNet = 0.9582</li></ul>	N/A
	Nepal region	Nepal glaciers							
2022 Xie et al. [49]	Northern Pakistan	Central Karakoram	DCG	Mountain, Valley glaciers	CNN	<ul style="list-style-type: none"><li>11 bands of Landslide 8 DEM</li><li>Unspphericity Profile</li><li>curvature Tangential curvature</li><li>Slope angle</li><li>Slope azimuth divergence index</li></ul>		<div>Accucary:</div> <ul style="list-style-type: none"><li>GlacierNet: 0.9677</li><li>DeepLabV3+: 0.9684</li><li>GlacierNet &amp; DeepLabV3+: 0.9685</li><li>GlacierNet2: 0.9735</li></ul>	
2022 Erhardter [50]	Austria Apls	Vienna, Burgenland, Lower Austria, Upper Austria	RG	Mountain glaciers	ANN with U-net	<ul style="list-style-type: none"><li>DEM</li><li>Orthophotos</li></ul>	<div>5769 RGs:</div> <ul style="list-style-type: none"><li>3722 training</li><li>800 validation</li></ul>	<ul style="list-style-type: none"><li>Ranged values using probability map</li></ul>	Python, Keras

Table 1. Cont.

Author	Location	Glacier Location Name	Studied Glacier Types	Classification by GLIMS Manual	AI Model	Parameters	Dataset Size	Accuracy	Software
2022 Kaushik et al. [17]	12 sites across Himalaya	Himalayan glaciers	Glacier lake	N/A	GLNet—Deep convolutional neural network	<ul style="list-style-type: none"><li>• Sentinel-2: B, G, R, NIR, and SWIR)</li><li>• Landsat 8</li><li>• Elevation</li><li>• Slope</li></ul> NDWI	660 images	Accuracy = 0.98 Precision = 0.95 REcall f-score = 0.95	
2022 Tian et al. [51]	Pamir Plateau		RG	Mountain glaciers	Channel attention U-net (U-net+cSE)	<ul style="list-style-type: none"><li>• Landsat 8</li></ul> SRTM DEM data	7821 images	Accuracy: U-net = 0.9756 GlacierNet = 0.9689 U-net + cSE = 0.9774	
2022 Sood et al. [52]	Bara Shigri, Himachal Pradesh, India			Valley glacier	ENVINet5	<ul style="list-style-type: none"><li>• Landsat 8</li></ul>		Accuracy = 91.89% Kappa = 0.8778	
2022 Sharda et al. [53]	Karakoram Range, Pakistan		DCG	Mountain, Valley, Icefields	<ul style="list-style-type: none"><li>• Relief-F</li><li>• Pearson correlation</li></ul> Hybrid RF-Corr	<ul style="list-style-type: none"><li>• Landsat 8</li><li>• SRTM 1-Arc Second GDEM</li><li>• Pamir and Karakoram inventories</li><li>• GLIMS database</li></ul>		up to 99.8%	<ul style="list-style-type: none"><li>• MATLAB eCognition developer software</li></ul>
2023 Peng et al. [14]	Qilian Mountains, China		Not specified		U-net with LGT encoder and LGCB decoder	<ul style="list-style-type: none"><li>• SAR (Sentinel-1), Optical (Sentinel-2)</li><li>• Image band indices</li><li>• DEM</li><li>• NDSI</li><li>• NDWI</li><li>• NDVI</li></ul>	2072 glaciers: <ul style="list-style-type: none"><li>• Training: 70%</li><li>• Testing: 30%</li></ul>	Accuracy: U-Net: 0.725 DeepLab V3+: 0.924 Attention DeepLab V3+: 0.960 Swin Transformer: 0.962 Proposed model: 0.972	NA

Table 1. Cont.

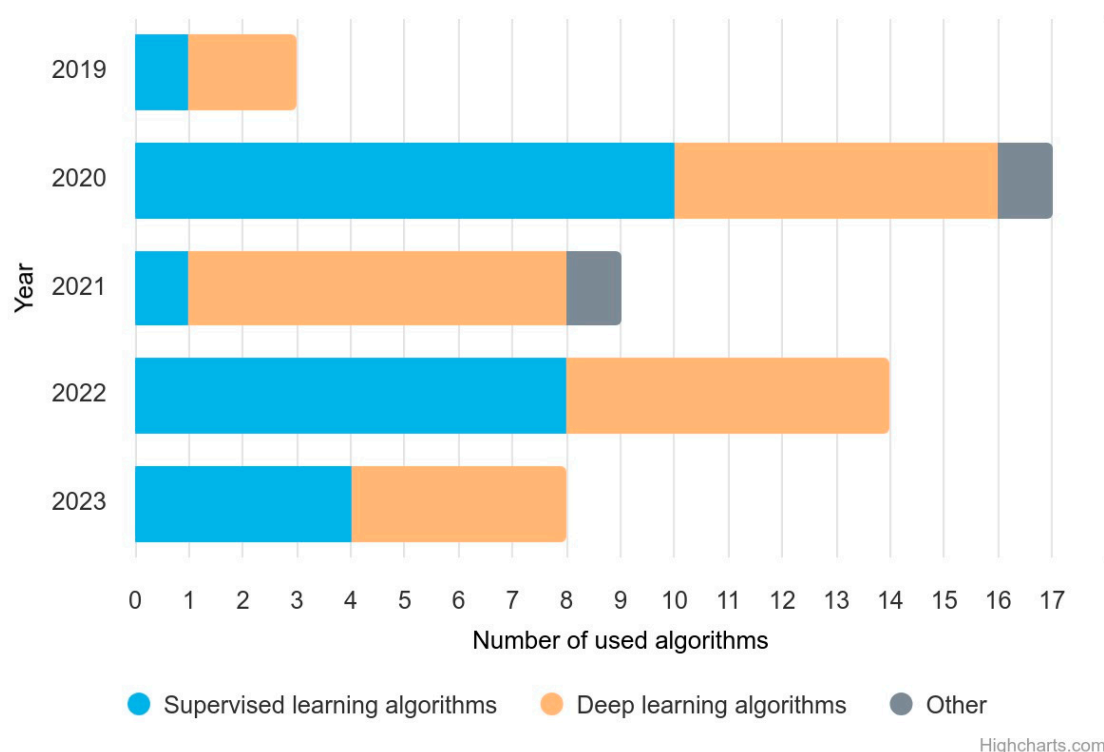
Author	Location	Glacier Location Name	Studied Glacier Types	Classification by GLIMS Manual	AI Model	Parameters	Dataset Size	Accuracy	Software
2023 Thomas et al. [54]	Khumbu—Nepal, China Manaslu—Nepal Hunza—Pakistan		DCG	Valley, Mountain, Icefields, Cirque	CNN with OBIA classification	<ul style="list-style-type: none"><li>• Sentinel-2</li><li>• Landsat-8</li><li>• ALOS DEM</li><li>• Corona KH-4B</li><li>• Geomorphometric data</li></ul>	69,500 samples Supraglacial debris-20,000 Non-glacial material-20,000 Vegetation-10,000 Lakes-7500 Clean ice glacier-5000 Snow cover-5000 Shadows-2000	<ul style="list-style-type: none"><li>• CNN-OBIA—93.8%</li></ul>	Trimble’s eCognition Developer 10.2 TensorFlow library
2023 Hu et al. [55]	Western Kunlun Mountains, China	Western Kunlun Mountains	Rock glaciers	N/A	DeepLabv3+ with Xception71 backbone	<ul style="list-style-type: none"><li>• Sentinel-2,</li><li>• ALOS-1 PALSAR</li><li>• InSAR data</li><li>• Google Earth images</li></ul>	Training (90%): 2007 images; Validation (10%): 223 images;	N/A	N/A
Monitoring of glacier evolution									
2022, 2020 Bolibar et al. [56,57]	French Alps	Écrins, Vanoise, Mont-Blanc glaciers	Mountain Glaciers	Mountain Glacier	Alpine Parameterized Glacier Model (ALPGM) based on ANN	<ul style="list-style-type: none"><li>• DEM</li><li>• Glacier boundary shape files</li><li>• SMB values</li><li>• Glacier topographical data</li></ul>	32 glaciers in French Alps	47% in space 58% in time	Python
2022 Ambinakudige and Intsiful [58]	Columbia Icefields, Canada			Icefields	SVM RF MLC	<ul style="list-style-type: none"><li>• Landsat 8</li><li>• NDSI</li><li>• NDVI</li><li>• NDSI</li><li>• NDII</li></ul>	1985, 1991, 2013, and 2020 Landsat satellite images  70% training 30% validation	Accuracy: RF = 99.8% MLC = 99.7% SVM = 99.7%  Kappa: RF = 0.995 MLC = 0.993 SVM = 0.994	N/A
2022 Rajat et al. [59]	Himachal Pradesh, India	Himalayan mountains		Mountain glaciers	U-Net	<ul style="list-style-type: none"><li>• Landsat</li><li>• Indian Remote sensing</li><li>• DEM</li></ul>	75% training 25% validation	F1 score: 95%	N/A

Table 1. Cont.

Author	Location	Glacier Location Name	Studied Glacier Types	Classification by GLIMS Manual	AI Model	Parameters	Dataset Size	Accuracy	Software
2023 Yang et al. [60]	Southeast Tibet	Zelongnong ravine	Glacier Debris Flow susceptibility	Valley, Cirque	<ul style="list-style-type: none"><li>DeepLabv3+ [FCN (fully convolutional networks)]</li></ul> DCNN	<ul style="list-style-type: none"><li>SRTM X DEM</li><li>SRTM C</li><li>TanDEM-x DEM</li><li>Landsat 7/8</li></ul> GLIMS		<ul style="list-style-type: none"><li>MIOU (Mean Intersection over Union)—92.15%</li><li>MPA (Mean Pixel Accuracy)—95.89%</li></ul>	
Snow/ice differentiation									
2022 Prieur C. [61]	Zermatt, Switzerland	Mont Rose massif	Temperate glacier/snow lines	Temperate glaciers	<ul style="list-style-type: none"><li>Feed forward NN</li><li>SVM linear kernel</li><li>SVM Gaussian kernel</li></ul> Random forest	<ul style="list-style-type: none"><li>Copernicus DEM</li><li>Landsat 8</li></ul> Alps’ glacier inventory from 2015	- Ice/snow—270,000 pixels - Glacier—200,000 pixels - Mountain shadow—140,000 pixels	<ul style="list-style-type: none"><li>Feed forward NN—98%</li><li>SVM linear kernel—98.7%</li><li>SVM Gaussian kernel—99%</li></ul> Random forest—99.8%	-
Ice dynamics modeling									
2021 Juvet et al. [62]	<ul style="list-style-type: none"><li>Andes</li><li>Canada</li><li>Caucasus</li><li>Colombi</li><li>Ethiopia</li></ul>			Icefields, Valley glaciers	Instructed Glacier Model (IGM) using CNN	-		≈20 direct speedup using CNN	Python



As supervised AI methods, random forest, ANNs (artificial neural networks), and support vector machines (SVMs) are commonly used, while deep learning methods such as U-Net, DeepLab, and CNNs (convolutional neural networks) represent another type of AI technique frequently used in glacier studies, as can be noted from the chart in Figure 3. Both supervised learning and deep learning methods have been actively used for years and have been deployed at nearly the same rate, except in 2021, when deep learning methods were dominant (Figure 4). In the next section, which is the main part, the reader will be able to access a summary of each work along with detailed tabulated information (Table 1) on the types of glaciers studied, their geographical locations, their classification according to the GLIMS glacier manual, the AI methods applied, the input parameters, the datasets used, and the accuracy of the studies.



**Figure 4.** Yearly classification of AI algorithms applied for glacier studies.

### 3. AI-Based Glacier Studies

#### 3.1. AI for Glacier Inventory and Mapping

Glacier inventory and mapping represent a promising area of application of AI, offering a transformative approach for optimizing the efficiency and accuracy of glacier monitoring efforts. Through extensive training on a variety of datasets, including satellite imagery, digital elevation models (DEMs), and historical records, AI models can quickly learn to recognize various glacier features, delineate glacier boundaries, and quantify glacier extent with unprecedented accuracy. This capability not only speeds up the creation of glacier inventories and maps, but also improves the reliability and consistency of glacier monitoring data, which are critical for understanding glacier dynamics, assessing climate impacts, and making environmental management decisions. A summary of the works on glacier inventory and mapping can be found in the first section of Table 1.

Earlier works in AI-based glacier inventory and mapping start from 2019, and one of them was written by Zhang et al. [40]. In their work, the authors studied glaciers in the Parlung Zangbo basin located within the Tibetan Plateau. The glacier data were collected from Landsat-8 images with 30 to 100 m spatial resolutions, and the image textures were analyzed using the Grey Level Co-occurrence Matrix (GLCM). Moreover, the authors calculated the Normalized Difference Water Index (NDWI), Normalized Difference Vegetation

Index (NDVI), and Normalized Difference Snow Index (NDSI) and used them as a dataset together with topographic parameters from ASTER Global Digital Elevation Model (GDEM V2), including other DEMs such as TanDEM-X and Shuttle Radar Topography Mission (SRTM) DEM to obtain elevation change data. Random forest (RF) with 100 decision trees was selected as the AI method as shown in Figure 5, and there were three steps, preprocessing, RF classification, overlaying of classification results, and accuracy assessment, to achieve the final mapping. The overall accuracy of the RF classification was 98.6%. The study showed 1476 glaciers spanning 2011.32 km<sup>2</sup> in the Parlung Zangbo basin, where 20.7% of the glacier region was debris-covered and it was between 4600 m and 4800 m above sea level (a.s.l.). Additionally, 77.5% of the glaciers (1558.79 km<sup>2</sup>) were located between 4600 m and 5600 m a.s.l., with smaller glaciers (<1 km<sup>2</sup>) mostly found at lower elevations.

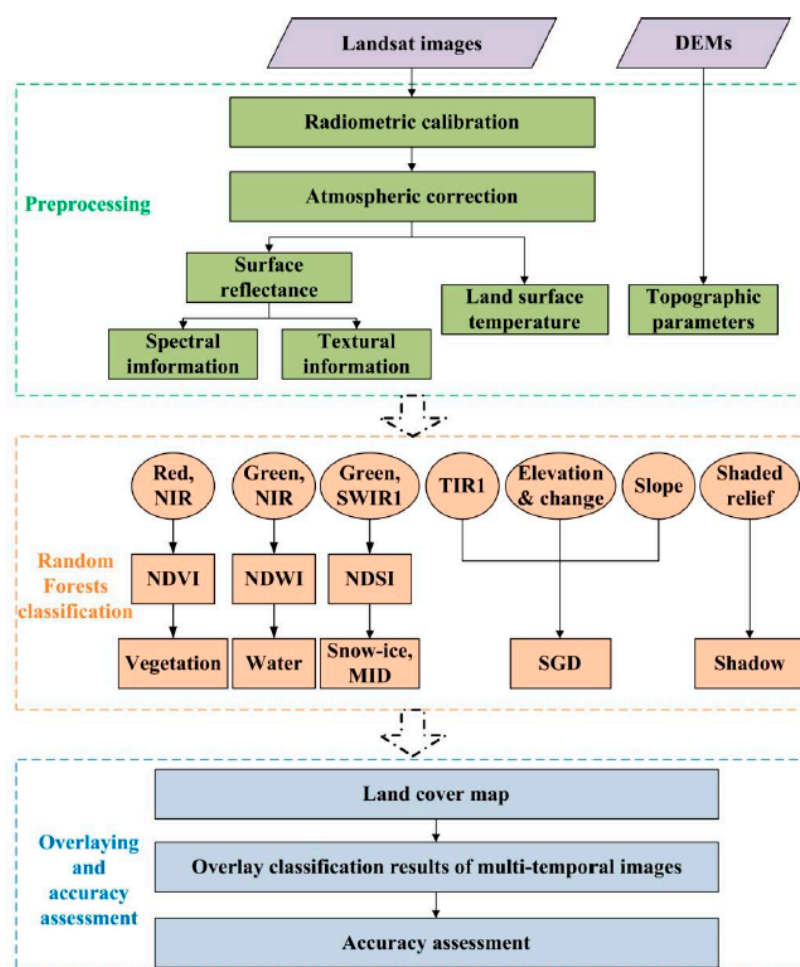


**Figure 5.** Flowchart for glacier mapping by Zhang et al. [40].

Mohajerani et al. [41] developed an ML toolkit that utilizes CNNs with a modified U-Net architecture for automatic detection of glacier calving front margins from satellite imagery (Figure 6). This approach was trained on a dataset of Landsat images of Greenland periphery glaciers. The study utilized Landsat 5, 7, and 8 imagery, focusing on the “green” and “panchromatic” bands, respectively. The optimized 29-layer deep neural network incorporated  $3 \times 3$  ReLU convolutional layers, 0.2 Dropout layers for regularization, and  $2 \times 2$  MaxPooling for downsampling and upsampling layers. A sample-weighted loss function and data augmentation techniques were also employed to enhance the performance. The model’s effectiveness was evaluated not only on validation datasets, but also on a new glacier with higher spatial resolution to assess transferability across different fjord geometries. After training on the Jakobshavn, Sverdrup, and Kangerlussuaq glaciers, the network

was tested on the Helheim glacier, achieving a mean deviation error of 96.3 m (1.97 pixels on average). This accuracy was comparable to manual delineation errors (92.5 m) and significantly outperformed traditional edge-detection methods like the Sobel filter.

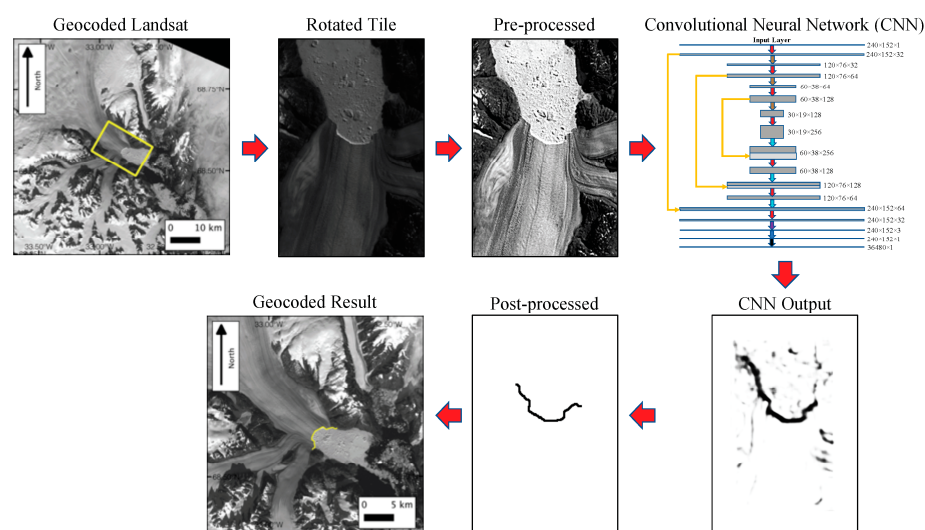


**Figure 6.** Outline of the methodology by Mohajerani et al. [41].

The study highlights the advantages of using DL for glacier mapping, particularly in enhancing the efficiency and accuracy of detecting calving fronts. The modified U-Net architecture employed in this research effectively segments the calving fronts from satellite images, providing a robust tool for continuous monitoring. The automated system allows for the rapid delineation of calving fronts, which is essential for understanding regional changes on the ice sheet periphery over several decades. This method not only reduces the manual effort required, but also provides a consistent and scalable solution for processing large volumes of satellite data, paving the way for more detailed seasonal and long-term analyses of glacier dynamics.

Similarly, a modified U-Net model developed by Baumhoer et al. [42] can process dual-polarization Sentinel-1 radar data along with elevation information from the TanDEM-X digital elevation model to accurately delineate the Antarctic coastline (Figure 7). This method outperforms traditional image processing techniques, especially in challenging areas with low contrast between ice and water or the presence of sea ice. The ability to automatically process large volumes of Sentinel-1 data enables the creation of dense time series to track glacier and ice shelf front movements at continental scales.

The automated approach allows for consistent and objective coastline extraction, overcoming the limitations of time-consuming manual delineation and subjective interpretations in complex areas. When tested on multiple sites around Antarctica, the model achieved average deviations of 78–108 m compared to manually drawn coastlines. Importantly, the method demonstrated spatial and temporal transferability, successfully generating a 15-month time series of front positions for the Getz Ice Shelf without additional training. This capability to produce frequent, large-scale measurements of glacier and ice shelf front dynamics is crucial for improving our understanding of ice sheet mass balance, calving processes, and potential sea level rise contributions from Antarctica.

The paper by Khan et al. [43] investigates the application of supervised ML techniques to automatically classify glacier layers using a blend of Sentinel-2 images along with texture, topographical, and spectral data. The study focuses on the Passu watershed in the Hunza Basin, Pakistan. Three well-known supervised ML methods, namely, support vector machine (SVM), artificial neural network (ANN), and RF, were explored for the classification.

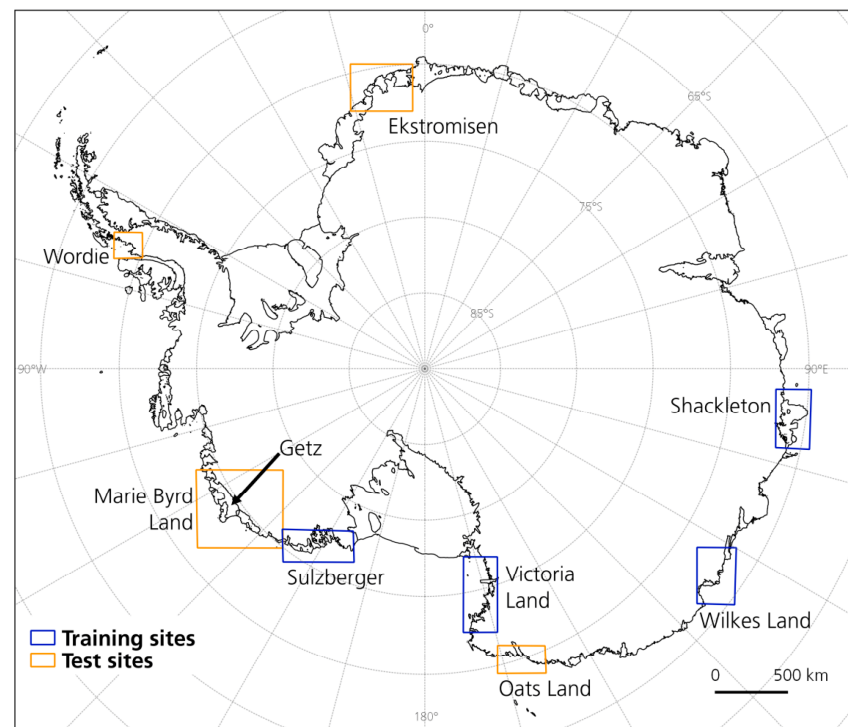


Figure 7. Training and testing sites [42].

Similar to Zhang et al. [40], the method proposed by Khan et al. [43] involves three main steps: feature extraction, machine learning classification, and accuracy assessment. The extracted features encompass spectral reflectance data, textural properties obtained from the GLCM, and topographical attributes acquired from the DEM. The classifiers are then trained and tested on the data, producing classification maps for debris-covered glaciers, usual glaciers, as well as non-glacier areas. The flowchart of the proposed method is provided below in Figure 8. By comparing the output data with the reference data, an accuracy evaluation is conducted.

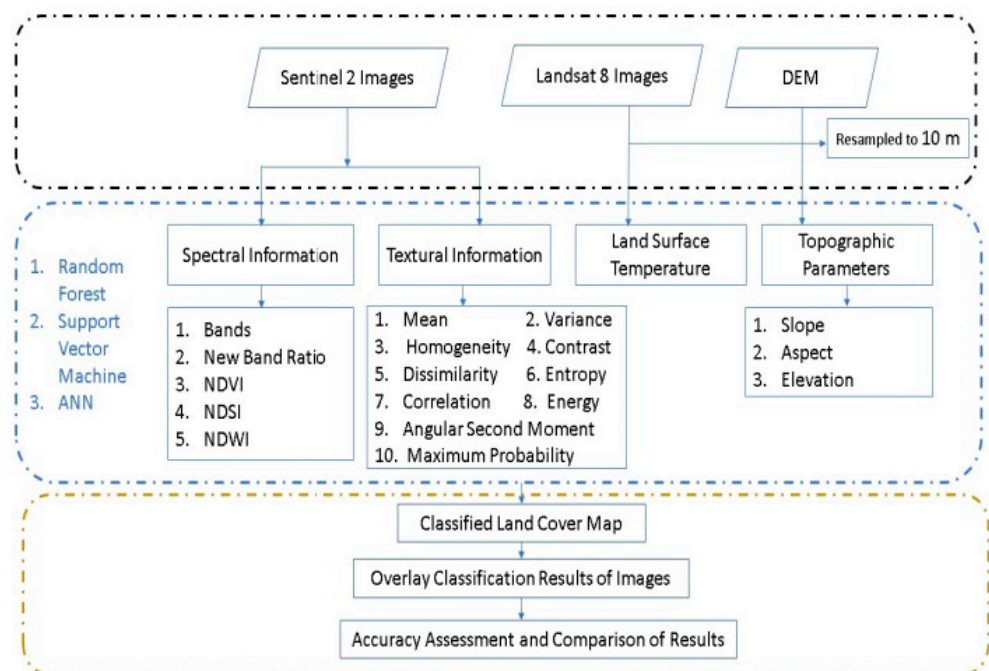
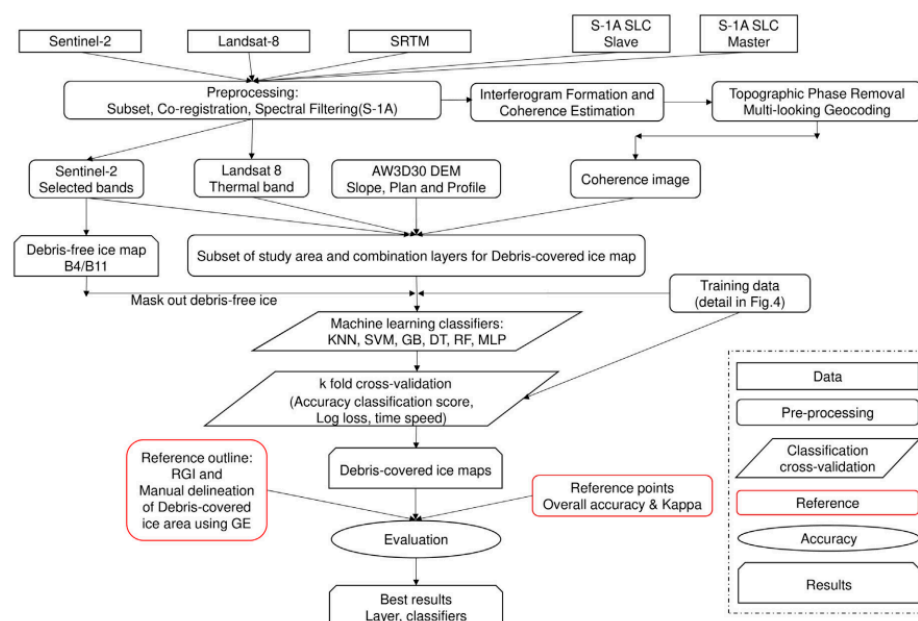


Figure 8. Flowchart of methodology by Khan et al. [43].



The results indicated high accuracy for all classifiers, with RF outperforming SVM and ANN consistently across all classes. The accuracy was measured by means of the Kappa coefficient, or Cohen's Kappa, a statistical technique that evaluates the consistency of agreement between two raters classifying items into mutually exclusive categories. Thus, the overall accuracy, Kappa coefficient, and other indicators demonstrated the effectiveness of the proposed method. For example, the overall accuracy reached as high as 92.77%, and the Kappa value was 0.92. A comparison with existing glacier inventory datasets revealed discrepancies, highlighting the need for more consistent and reliable classification approaches. The study suggests that ML approaches, particularly RF, coupled with remote sensing data, offer robust and accurate means of mapping glaciers and debris-covered glaciers, which is crucial for water resource management and hazard assessment.

In another research work, to map debris-covered glaciers, Haireti Alifu et al. [45] developed an ML-based classification technique. As the multi-sensor input data, they considered SAR coherence, thermal, topographic, and optical data obtained from remote sensing devices to evaluate the accuracy of ML methods such as SVM, decision tree, gradient boosting, and k-nearest neighbors. Furthermore, from Google Earth images, the authors created outlines of debris-covered ice by applying manual delineation (Figure 9). Northwestern region of Karakoram in Pakistan (Location 1) and Shaksam Valley in Western China (Location 2) were selected as areas for testing the ML methods. In particular, datasets from the testing locations, such as RGI-based vector data and GAMDAM glacier inventory, were used for validation purposes.



**Figure 9.** Proposed flowchart of the methodology [45].

The analysis included how training data size affected (up to 20,000) the accuracy of the selected ML-based classification methods, and they were compared between each other to select the most effective method. The outcomes obtained from this increased volume of training data indicated that RF attained greater accuracy, nearly 97%, compared to the GB and SVM methods. Furthermore, the data points increased from 2000 to 20,000, increasing the accuracy of the mapping by 1–2%. When isolated pixels were excluded from the dataset, the accuracy was further improved by up to 1.5%.

In another work [46], the authors combined a CNN with object-based image analysis (OBIA) to predict rock glaciers (RG) in an automated way. Thus, the CNN produced a prediction raster or heatmap, with pixel values ranging from 0 to 1, as shown in Figure 10. Further, OBIA was used to classify objects from the generated heatmaps. In fact, OBIA, a

common remote sensing method, segments images into homogeneous objects for subsequent classification.

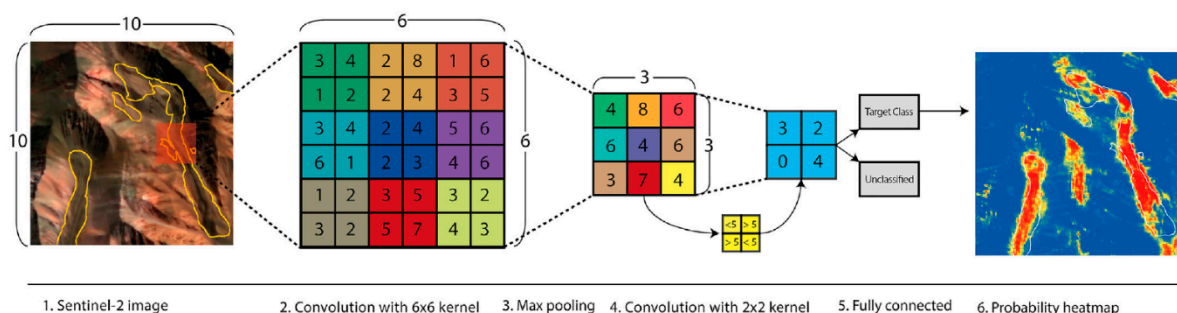


**Figure 10.** The illustration of CNN with a heatmap output for RG evaluation [46].

Two areas with glaciers, namely, the La Laguna (Chile) and Poiqu (Central Himalaya) catchments, were considered for AI-based RG mapping (Figure 11). The La Laguna catchment, located at the Elqui River's headwaters in Chile, encompasses glaciers and RG, contributing 4–13% of the annual streamflow in an elevation range of about 4000 to 6000 m across an area of approximately 140 km<sup>2</sup> and hosting 105 RGs. On the other hand, the Poiqu catchment, a transboundary watershed in the Himalayas draining into Nepal and the Ganges River, spans over 2000 km<sup>2</sup> with elevations from 1100 to over 8000 m, featuring a variety of glaciers. The study focuses on approximately 1500 km<sup>2</sup>, including about 140 rock glaciers, with sizes ranging from <0.01 to >1 km<sup>2</sup>. Approximately 30% of manually interpreted outlines from the Pléiades imagery (RG\_Man) were used for training. The rock glaciers from the La Laguna and Poiqu catchments had sizes of 2.3 km<sup>2</sup> and 6.1 km<sup>2</sup>, respectively, while an additional 0.7 km<sup>2</sup> was extracted from the Pléiades subset. All these outlines were integrated with adjacent polygons, merged, and small ones were removed. To evaluate the accuracy, the leftover polygons—50 from La Laguna, 117 from Poiqu, and 7 from the Poiqu Pléiades subset—were utilized. Around 300 random training points were created within the RG outlines, along with extra points representing debris-covered glaciers, pristine ice glaciers, and stable terrains. As a result, the CNN\_OBIA classification technique detected a combined 108 rock glaciers, encompassing an area of 26.0 square kilometers, out of the total 120 (spanning 20.3 square kilometers in the validation dataset (RG\_Man) across both study areas. This led to an overestimation of 28.0%, with the end-user's and producer's accuracy indicating a relatively high percentage of correctly identified rock glaciers, but with some instances of false positives.

The study by Lu et al. [47] focused on mapping debris-covered glaciers (DCG) around the Tibetan Plateau, in particular, High Mountain Asia (HMA). The selected AI models were RF and CNN. The study employed data from Landsat 8 OLI, thermal infrared sensors, GDEM (Reflection Radiometer Global Digital Elevation Model), and ASTER (Advanced Spaceborne Thermal Emission) for the mapping of debris-covered glaciers on the Tibetan Plateau, namely, in the Eastern Pamir and Nyainqentanglha areas. Various classification models, including RF and CNN, were compared and integrated to achieve the best classification performance. The relationship between debris coverage and ML model parameters was investigated, revealing that debris coverage directly influences model performance and aids in detecting both active and idle DCG.

The authors proposed an approach combining RF and CNN models, referred to as an RF-CNN composite classifier, to enhance the classification accuracy of debris-covered glaciers. By leveraging the respective advantages of the RF and CNN models, the RF-CNN composite classifier achieved promising results, providing valuable insights for glacier mapping and boundary extraction. The study demonstrates that the performance of ML techniques and the accuracy of glacier extraction are closely tied to the intensity

of debris coverage, highlighting the importance of considering local characteristics in mapping efforts.

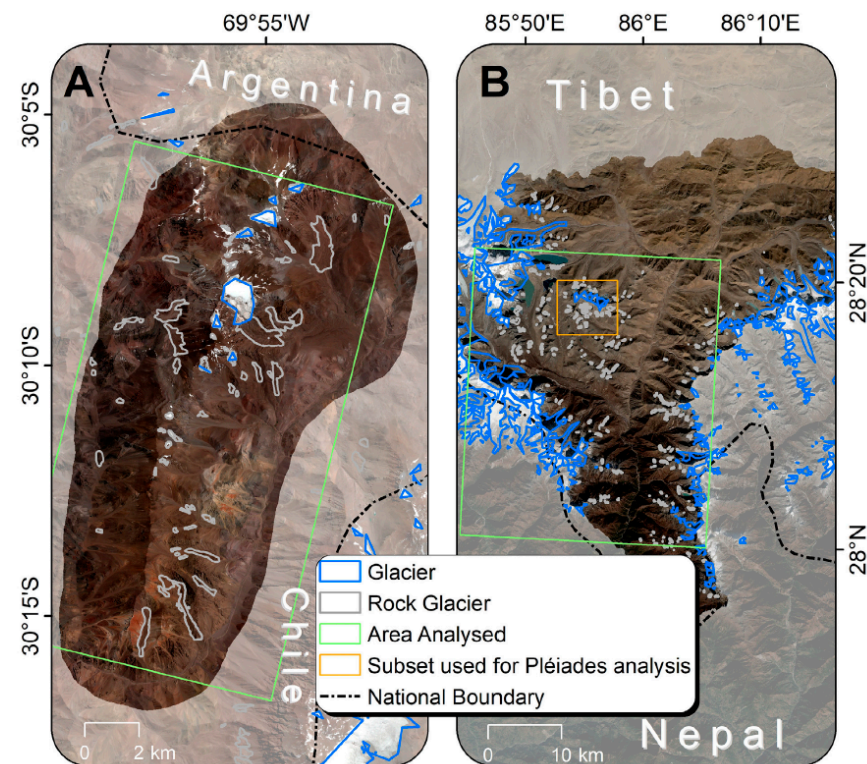


**Figure 11.** Study areas: La Laguna catchment, Chile, and Poiqu catchment, Central Himalaya, by Robson et al. [46].

Furthermore, the study evaluated the performance of the RF-CNN model against existing glacier inventory datasets, showcasing its effectiveness in accurately delineating debris-covered glaciers. The results indicated that the RF-CNN model outperformed individual classifiers, offering a more reliable approach for glacier mapping. The study underscored the significance of machine learning methods in improving the efficiency and accuracy of glacier mapping, laying the groundwork for future research in this field. Future work will focus on refining the RF-CNN model and exploring its applicability to SAR images for enhanced glacier classification.

Xie et al. [48] compared the performance of GlacierNet with other CNN-based methods such as Mobile-UNet, Res-UNet, FCDenseNet, R2UNet, and DeepLabV3+. Each model underwent training using 15% of the total study area, specifically focusing on the Karakoram glaciers (shown in Figure 12), followed by evaluation across twelve glaciers (represented as yellow dots in figure) beyond the training domain. These glaciers exhibited diverse surface and topographical characteristics.

Due to computational intensity, the input image for GlacierNet was sub-sampled by means of a sliding window approach with a stride of 32 and sizes of  $256 \times 256$  or  $512 \times 512$ . As the input consisted of multi-channel images, the networks were configured with an input layer comprising 17 channels instead of the typical 3 channels for RGB images. The CNN output is a binary image representing the input data category, which was then combined into a larger binary image as shown in Figure 13. Additional refinement steps, including region size thresholding, water index-based removal of excess water pixels, and hole filling, were applied to enhance the accuracy.



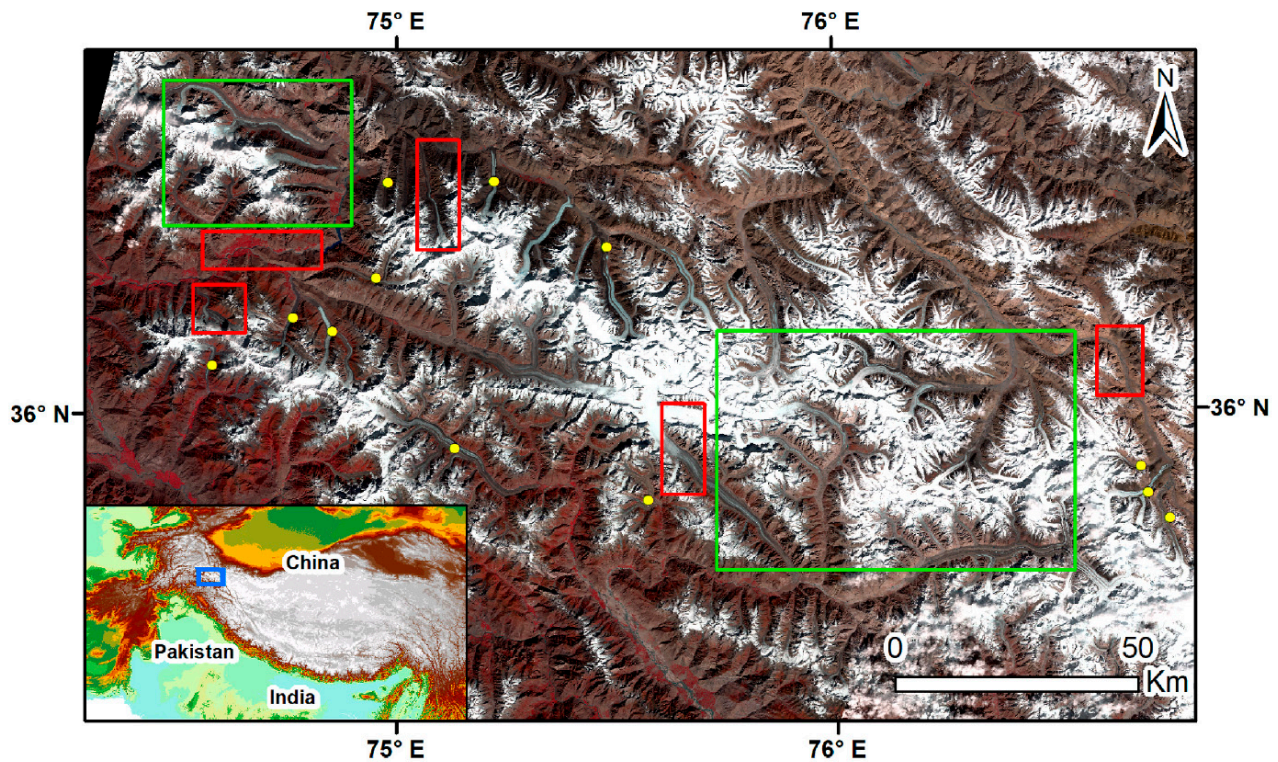


Figure 12. Selected area for the study by Xie et al. [48], Central Karakoram.

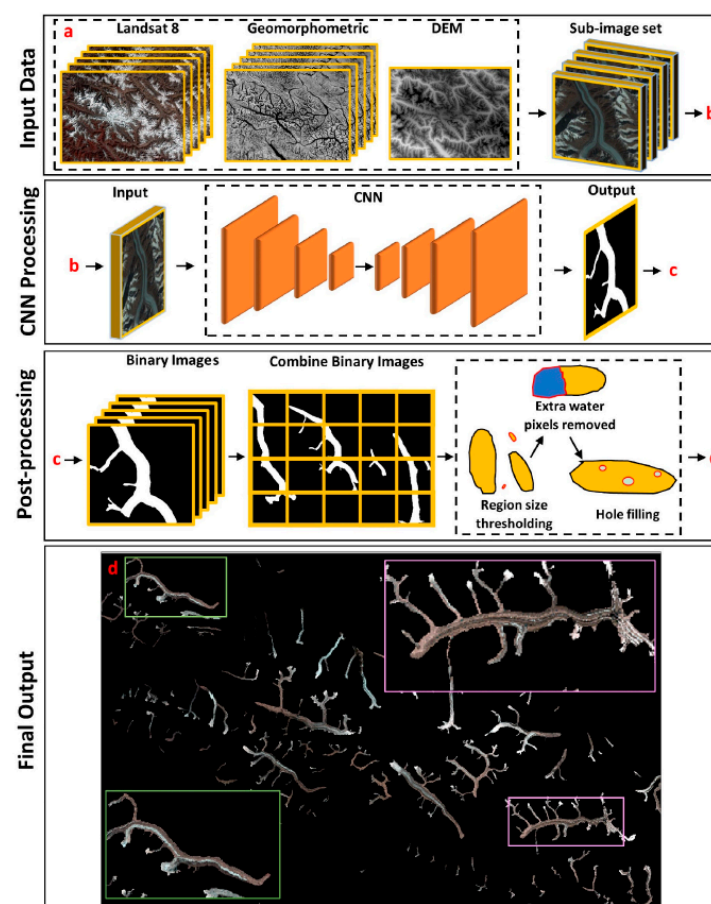


Figure 13. GlacierNet architecture [48].



The analysis revealed DeepLabV3+ as the frontrunner, demonstrating the highest intersection over union (IOU), F-measure, kappa, and accuracy values, with GlacierNet following closely behind. The authors noted variations in performance among the models concerning the estimation of melting zones and terminus, with DeepLabV3+ exhibiting superior performance in this regard. Notably, terminus estimation emerged as a significant challenge across the compared models, prompting suggestions for potential enhancements in network architecture to address this issue.

Furthermore, computational expenses were assessed, revealing FCDenseNet and R2UNet as the most resource-intensive, DeepLabV3+ as moderately demanding, and Mobile-UNet and GlacierNet occupying the lower end of the computational cost spectrum, akin to Res-UNet.

The authors highlighted the suitability of DeepLabV3+ for large-scale glacier mapping tasks, noting its superior performance compared to other models. The GlacierNet emerged as a viable option for regional-scale mapping. The careful selection of training data was emphasized as pivotal given its significant impact on overall model performance.

Later, Xie et al. [49] upgraded the previous model and presented a multi-model learning architecture, GlacierNet2, for glacier mapping. The architecture is based on data subsampling and DL using CNN models such as GlacierNet and DeepLabV3+, and it can estimate the terminus, ablation, and snow-covered accumulation zones of glaciers (SCAZ). Glaciers of central Karakoram in northern Pakistan were selected to test the predictive performance of GlacierNet2. Two scenes of Landslide 8 from September and October of 2016 were used. Notably, mapping glaciers is most achievable in the September–October timeframe due to the end of the ablation season. The architecture has a 17-channel input, which receives the following data: 11 bands of Landsat 8; a digital elevation model (DEM); and five layers of geomorphometric parameters such as unsphericity, profile, tangential curvatures, slope angle, and slope azimuth divergence index. Thus, GlacierNet2 showed the best accuracy in terms of mapping the ablation zone relative to DeepLabV3+ and GlacierNet.

Erhardter et al. [50] applied ANN based on U-net architecture to map rock glaciers of Austria. The dataset they used consisted mainly of DEM and orthophotos obtained from Google Maps satellite images. The inventory consisted of 5769 rock glaciers covering an overall area of 303 km<sup>2</sup> from Austrian states such as Vorarlberg, Salzburg, Tyrol, Styria, Carinthia, and the alpine of Upper Austria. The inputs were images 512 × 512 in pixel size, with a rough precision of 2 m, meaning the overall size of an image was 1 × 1 km. The slope maps were computed using the QGIS software based on DEM data. On the other hand, in the second channel, the greyscale orthophotos were inputted, allowing the landscape's surface and vegetation characteristics to be evaluated. Therefore, the output data consisted of a 512 × 512 binary raster, indicating whether each pixel represented a rock glacier or not. As shown in Figure 14, the U-Net architecture consisted of five contracting and five expanding blocks. It employs 2D convolution layers, batch normalization, and max pooling to reduce the image dimensions. The center part utilizes two conv2d layers, a two-dimensional convolution operation in neural networks that extracts features from images using sliding filters to produce feature maps. This is essential for tasks like image classification, object detection, and image segmentation, and is highly suitable for glacier studies. The final output is generated through a last conv2d layer with sigmoid activation (i.e.,  $f(x) = 1/(1 + e^{-x})$ ), producing a binary output to predict RGs. ANN was trained using the Adam optimizer at a learning rate of 0.0001. To evaluate the accuracy of the model, the dice similarity coefficient (DSC) was used, where 0 and 1 referred to dissimilarity and perfect similarity, respectively, between the ground truth and ANN output.

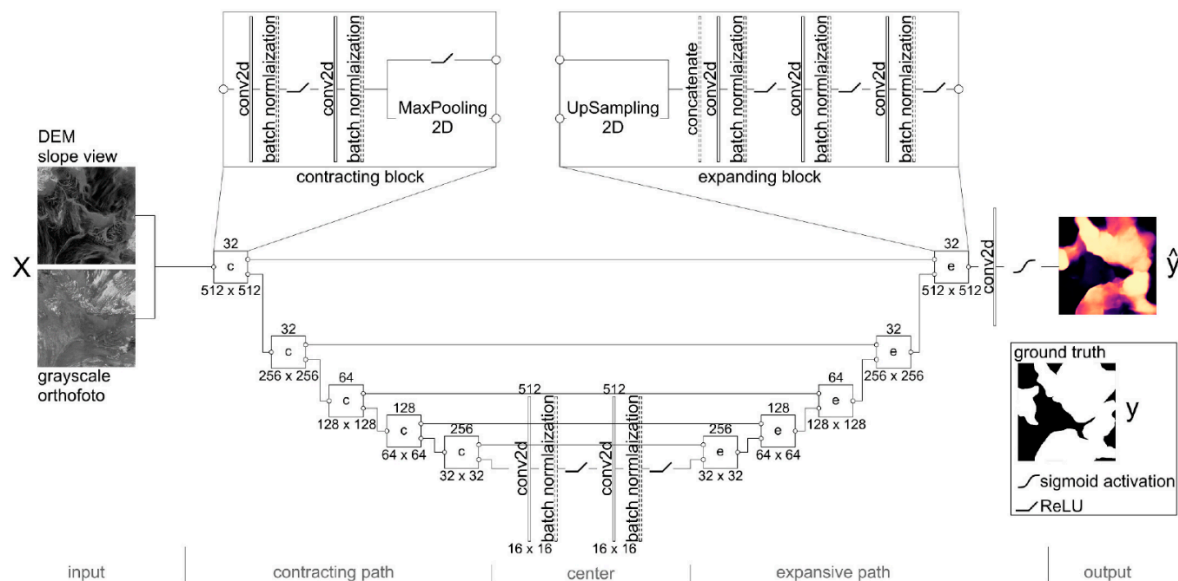


**Figure 14.** ANN architecture U-Net used to map rock glaciers in Austria by Erhardter et al. [50].

Figure 15 illustrates RG examples and an ANN-based probability map. Thus, after testing thresholds ranging from 0 to 1 in steps of 0.05, the authors identified 0.4 as the optimal value to divide results into two categories: values  $\leq 0.4$  represented no rock glacier, and values  $> 0.4$  indicated the existence of a rock glacier. It should be noted that a maximum DSC of 0.616 was obtained at a threshold of 0.4.

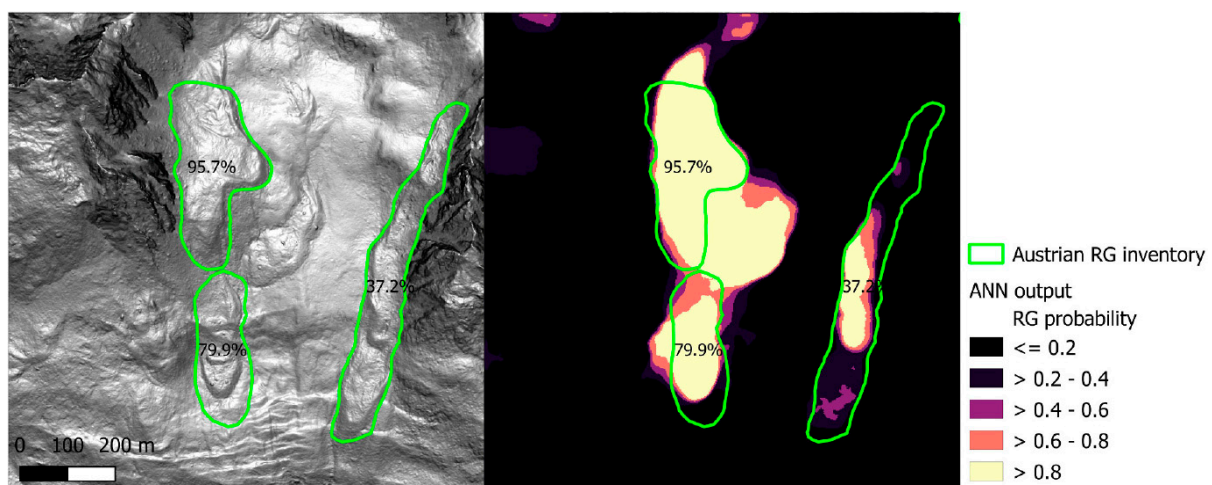


**Figure 15.** RG examples from North Tyrolean “Wurmeskar”, Austria (left), and RG probability map based on ANN (right) developed by Erhardter et al. [50].

Kaushik et al. [17] trained a deep CNN (DCNN), named GLNet, using a dataset of 660 images from multiple sources such as DEM, thermal, microwave, and other remote sensing techniques, as shown in Figure 16. The dataset was obtained from 12 locations within and around the Himalayan glaciers, and the overall selected region was divided into four testing sites.

The GLNet demonstrated a strong performance overall, achieving high accuracy, F1 scores, and correctness in mapping glacial lakes across multiple test sites. However, challenges such as erroneous predictions in certain areas, particularly related to shadows and wet ice pixels, were observed, leading to false positive and false negative results in some instances. One of the evaluation results is shown in Figure 17, specifically for site 3, in eastern Himalaya. Despite these challenges, the model showed an improvement in

its performance over different test sites, highlighting its potential, but also the need for continued refinement to address specific limitations.

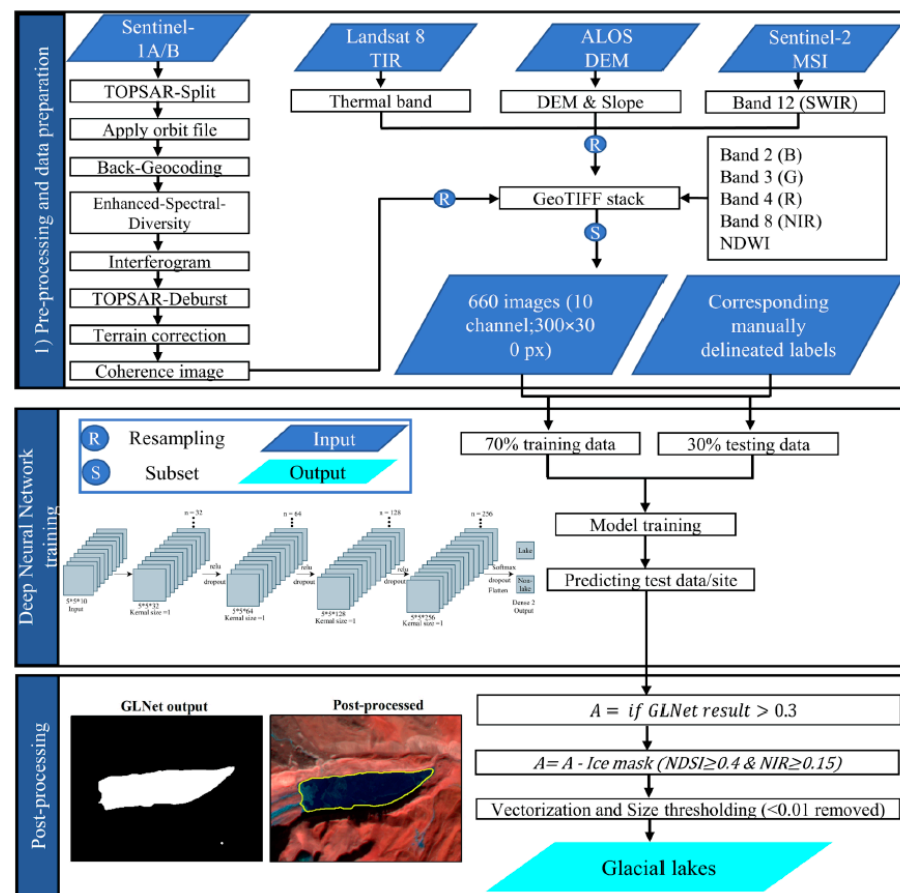


Figure 16. A general representation of the workflow for the GLNet technique [17].

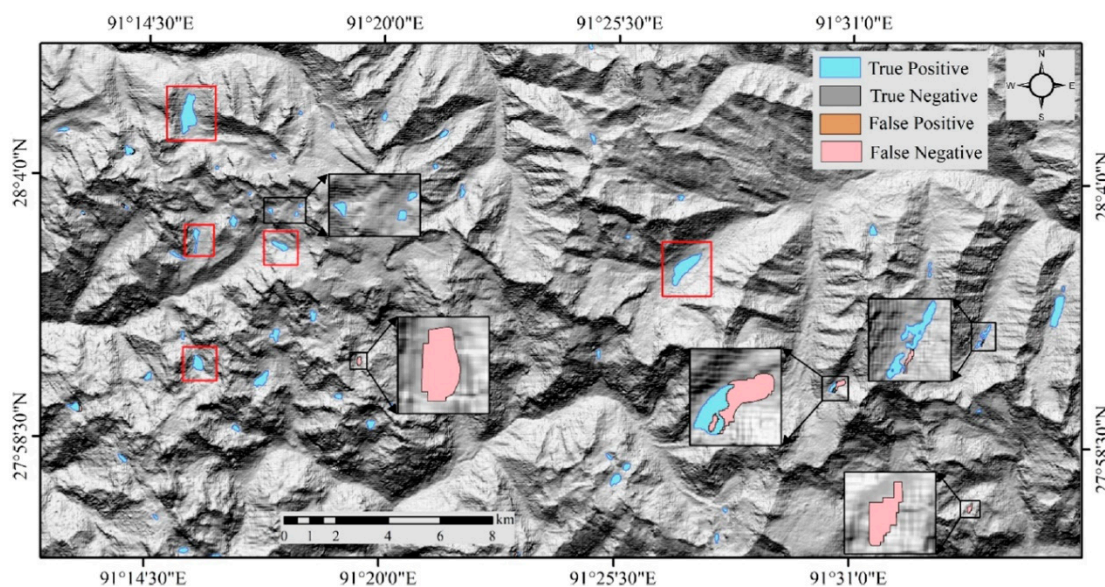


Figure 17. Glacial lakes in the Eastern Himalaya's test site 3 were mapped and compared with the reference data to identify errors in false positives and false negatives [17].

Tian et al. [51] proposed an enhanced U-Net model, incorporating a channel-attention mechanism, for glacier mapping and evaluated its performance using Landsat 8 OLI and

Shuttle Radar Topography Mission (SRTM) digital elevation model (DEM) data obtained for the Pamir Plateau.

The results demonstrate that the channel-attention U-Net model achieved superior accuracy in glacier identification compared to the standard U-Net and GlacierNet models. Furthermore, fine-tuning with a conditional random field (CRF) model effectively reduced background misidentification, enhancing the overall accuracy of glacier extraction. Evaluation metrics such as accuracy, recall, and F1-score validated the effectiveness of the proposed approach, with the channel-attention U-Net model outperforming other methods, albeit with a slight reduction in recall due to its focus on glacier features.

The Pamir Plateau, characterized by its high altitude and extensive glacier coverage, served as the study area, highlighting the relevance of the research in a region highly vulnerable to climate change. Utilizing Landsat 8 OLI imagery and SRTM DEM data, the study ensured data consistency and accuracy, which are critical for reliable glacier mapping. The incorporation of ground-truth data from the Global Land Ice Measurements from Space (GLIMS) database enhanced the reliability of the findings, despite temporal discrepancies necessitating manual modifications.

Despite the promising results, the study acknowledges certain limitations, such as challenges in distinguishing glaciers from similar geological features like water bodies and debris-covered glaciers. Additionally, issues like cloud cover and shadows pose challenges to optical remote sensing-based glacier mapping, requiring careful selection of input imagery. Future research directions include exploring additional data sources, such as synthetic aperture radar (SAR) images, and further refining the model to address specific challenges like the underestimation of debris-covered glaciers.

Sood et al. [52] proposed a deep learning classifier ENVINet5 based on U-Net architecture for glacier monitoring over the Bara Shigri glacier and compared that to the ANN model. ENVINet5 and ENVI Net-Multi are based on the U-Net model and are specifically designed for single-class and multi-class classification, respectively (Figure 18). ENVINet5 utilizes a mask-based encoder–decoder architecture, incorporating features such as convolutional layers, feature fusion, dimensionality reduction, co-convolution, and  $1 \times 1$  convolutions. On the other hand, ENVINet-Multi is tailored for classifying multiple class categories, leveraging the spectral and spatial properties of input datasets along with field data knowledge. These architectures demonstrate the potential of deep learning in handling complex classification tasks in remote sensing. The overall accuracy of the ENVINet-5 was 91.89%, while ANN had 88.38%, and the kappa coefficient was 0.8778 versus 0.8241. The authors mentioned that errors using the ENVINet-5 are high due to the spatial resolution of the input data and parameter selection during the training process. Furthermore, the results may be affected by clouds or topographic effects. Therefore, these effects should be tested.

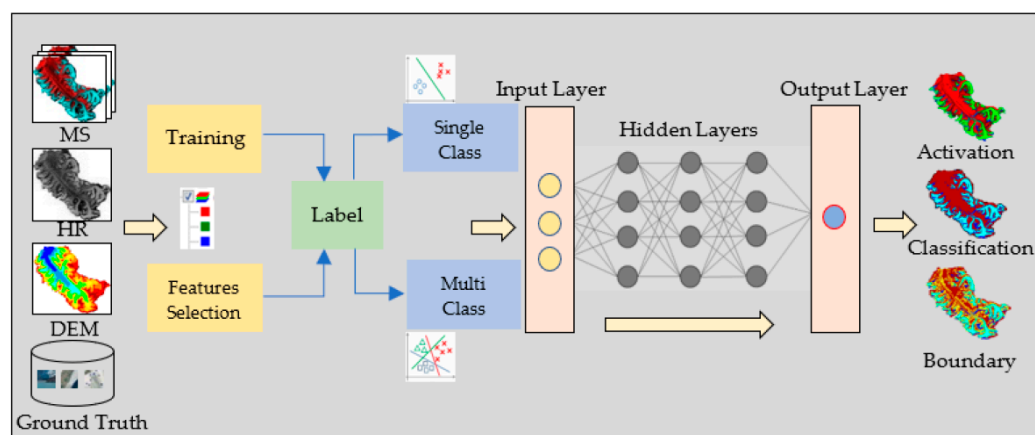
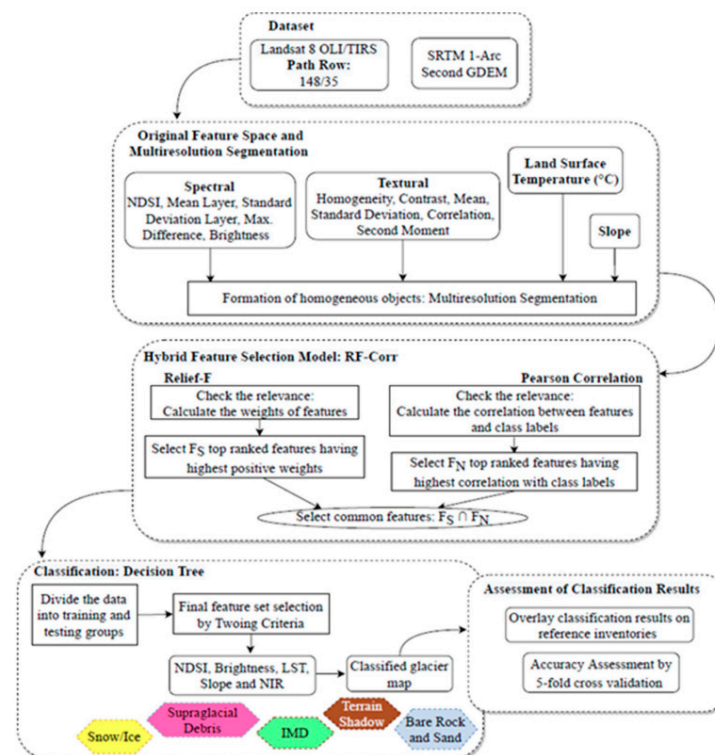


Figure 18. The flowchart of the model [52].



In another work, a hybrid feature selection (FS) approach was created to reduce classifier intricacy and enhance prediction accuracy by Sharda et al. [53]. This method automatically selects the optimal feature set and removes irrelevant or redundant features. Additionally, a supervised ML-based classifier was integrated to automatically select threshold parameters. This reduced the need for trial-and-error iterations in choosing suitable threshold values for assigning objects to various classes.

The FS method they created involved three stages: initial screening, identifying shared features, and fine-tuning. The integration of Relief-F and Pearson correlation filter-based methods improved the feature space. Additionally, the DT classifier enhanced the refined feature space using the Twoing split criteria. The suggested ML-based automatic classification approach, as depicted in Figure 19, underwent testing in the Central Karakoram Region and demonstrated significant resilience across all glacier types.



**Figure 19.** Flowchart of the hybrid feature selection mechanism for automatic object-based glacier mapping [53].

They developed method consisted of three stages: an initial screening stage, a selection of general properties stage, and a refining stage. Thus, the feature space was optimized by means of Pearson correlation and Relief-F algorithms. Twoing split criteria were used in the decision tree classifier (DT) classifier to optimize the feature space. Thus, the developed ML-based automatic classification method was validated based on the glacier data from the Central Karakoram area and further demonstrated accurate results in other selected glaciers. The efficiency of the hybrid FS method was assessed by computing the prediction accuracy via 5-fold cross-validation. Compared to the Relief-F and Pearson correlation approaches, the hybrid model showed a minor enhancement in classification accuracy of 0.04% for the Siachen glacier and 0.17% for other glaciers.

Peng et al. [14] introduced a transformer-based DL method using a U-Net architecture with a Local–Global Transformer encoder and Local–Global CNN Blocks in the decoder, integrating global and local information. Out of 2740 glaciers covering 1514.01 km<sup>2</sup> in Qilian Mountains, China, those between 1 and 10 km<sup>2</sup> accounted for the largest glacierized areas (832.52 km<sup>2</sup>); our study focuses on 2072 glaciers larger than 0.05 km<sup>2</sup>, totaling 1498.06 km<sup>2</sup>.

Thus, trained on Sentinel-1, Sentinel-2, HMA DEM, and SRTM DEM data, the DL model achieved 0.972 accuracy.

Thomas et al. [54] introduced a method for mapping debris-covered glaciers (DCG) that combined a CNN and object-based image analysis into a single categorizing workflow. This method was applied to open-source datasets, including thermal (Landsat-8), multispectral (Sentinel-2), interferometric coherence (Sentinel-1), and geomorphometric records (Figure 20). Central Himalayan areas in China and Nepal, including the Karakoram glaciers in Pakistan, were selected to apply and test the developed method.

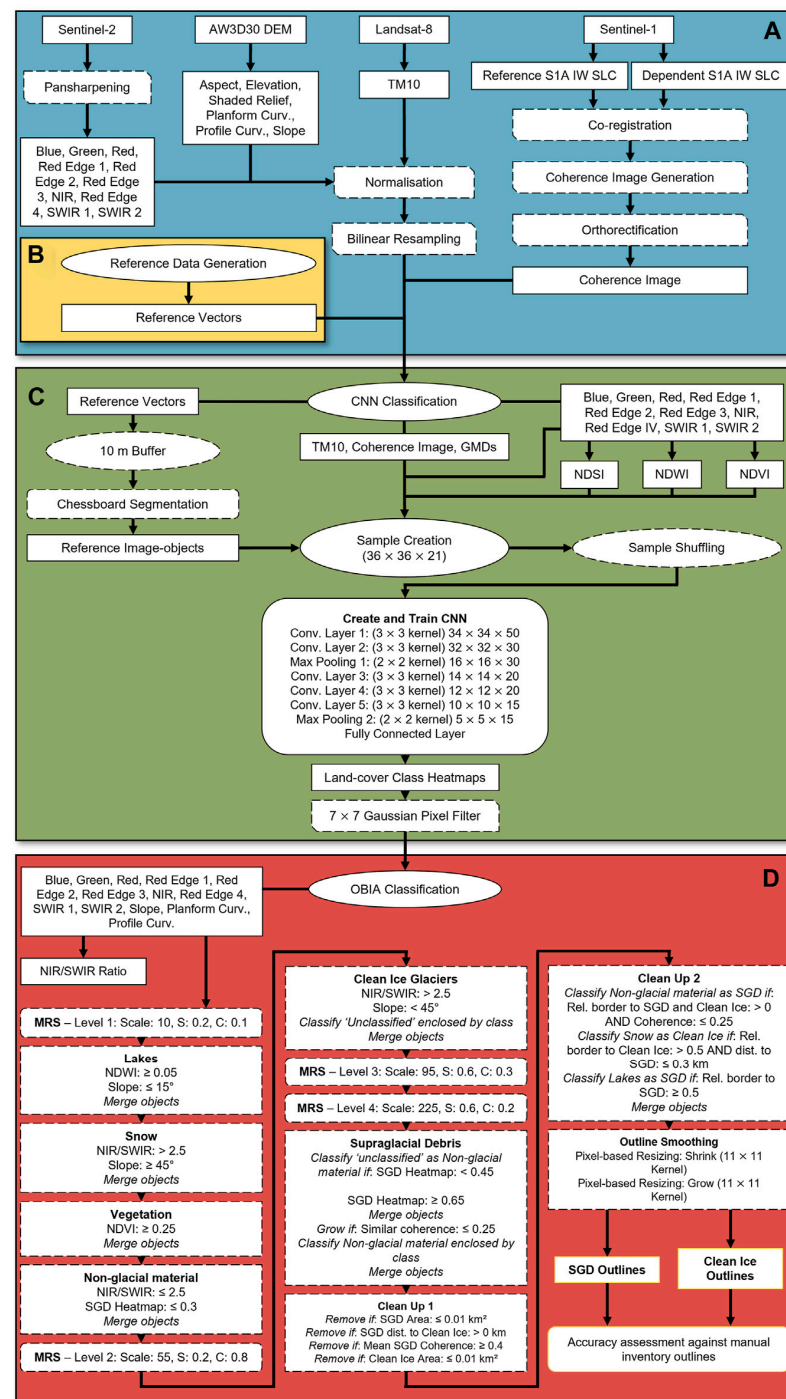


**Figure 20.** Flow chart of the developed approach. The steps include dataset pre-processing, reference vector dataset generation, convolutional neural network classification, and object-based image analysis refinement [54].

A precision–recall graph was produced for supraglacial debris outlines in the Khumbu region, initially delineated without object-based image analysis (OBIA), with a set probability heatmap threshold of  $\geq 0.65$ . Furthermore, the recall and precision accuracies increased by 0.9% and 4.2%, as shown by the precision–recall curve. As a result, the F-score accuracy was improved up to 2.6%, meaning that by utilizing OBIA after CNN classification, one can access more accurate mapping of DCG extents compared to relying solely on CNN classification.

However, as the authors stated, the complex topography and precipitous slopes in certain sections of the selected areas led to errors of omission in mapping DCG termini. Specifically, the CNN-OBIA method underestimated the locations of glacier termini with gradients exceeding  $24^\circ$  in the Hunza region and steep tributaries covered with debris in the Manaslu area. These challenging terrains posed difficulties for the CNN, as there was limited variation within the samples of supraglacial debris, hindering accurate classification.

In another study [55] of the Western Kunlun Mountains, researchers combined Interferometric Synthetic Aperture Radar (InSAR) techniques with a DL model, DeepLabv3+, to create a comprehensive inventory of rock glaciers. The workflow for automatic mapping of rock glaciers is shown in Figure 21. The deep learning method improved the mapping efficiency by automating identification and delineation tasks, while also overcoming limitations of InSAR-based methods such as coherence loss and insensitivity to certain movement directions.

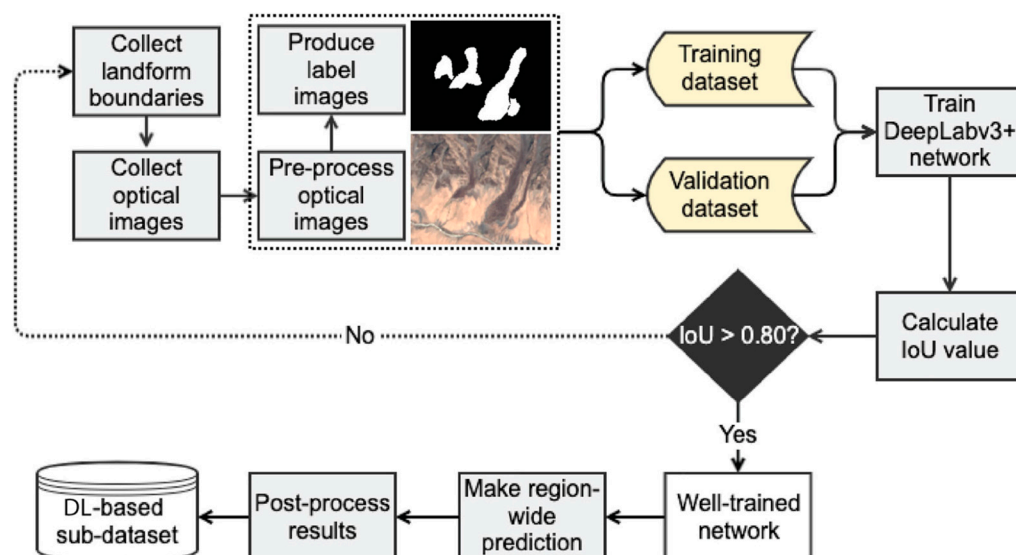


Figure 21. Workflow diagram [55].

The combined AI and remote sensing approach enabled the first regional-scale mapping of rock glaciers in this arid mountain range, resulting in an inventory of 413 rock glaciers. Of these, 290 were active rock glaciers mapped manually using InSAR, while 123 were newly identified and delineated by the DL model applied to Sentinel-2 optical imagery. This semi-automated workflow allowed for consistent mapping across a large, remote area where field studies are challenging. The resulting inventory provides valuable baseline data on rock glacier distribution, morphology, and kinematics that can inform further research on permafrost, climate change impacts, and water resources in this high mountain region.

Thus, as can be seen from the reviewed works dedicated to inventorying and mapping glaciers, traditional ML classifiers such as RF, SVM, KNN, DT, GB, and MLP were applied. These methods mostly rely on structured data and use algorithmic approaches for classification. In contrast, CNNs and their variants, such as U-Net, DeepLabv3+ with ResNet, DRN, MobileNet, GlacierNet, Mobile-Unet, Res-UNet, FCDenseNet, R2UNet, GLNet, Channel Attention U-net, and ENVINet5, are DL models designed for image processing and segmen-

tation tasks. The difference lies in their architecture: CNNs leverage convolutional layers to automatically extract features from input images, whereas traditional ML classifiers use predefined features. Some works are considered hybrid models, like RF-CNN and ANN with U-Net, as they combine elements from both traditional ML and DL learning to leverage their respective strengths. Methods like Relief-F and Pearson correlation are feature selection techniques that can be used to preprocess data for either traditional ML classifiers or CNNs, enhancing the performance by selecting the most relevant features.

### 3.2. AI for Monitoring of Glacier Evolution

Monitoring of glacier evolution becomes crucial for understanding the environment as glaciers worldwide respond to the effects of global climate change. AI offers tools for continuously tracking glacier dynamics, providing insights into changes in glacier extent, volume, and behavior over time. By leveraging AI algorithms in conjunction with satellite imagery and remote sensing data, researchers analyze trends, detect patterns, and forecast future glacier evolution with sufficient accuracy and efficiency. In this section, we delve into the innovative applications of AI in monitoring glacier evolution.

Bolibar et al. [56] simulated the annual glacier-wide surface mass balance (SMB) using a novel algorithm based on deep ANN. This was integrated into an open-source model for mapping selected regional glaciers. They evaluated the nonlinear deep learning SMB model and compared it with standard linear statistical methods using data obtained from French Alpine glaciers. ALPGM is an open-source Python glacier model mainly structured into: (i) a glacier-wide SMB simulation and (ii) an update module for glacier geometry. The SMB simulation component utilizes ML algorithms for predictive modeling, while the geometry update module produces glacier-dependent functions for annual geometry adjustments. The workflow (shown in Figure 22) execution is configurable via the model interface, where users are allowed to deploy or skip specific steps, including preprocessing meteorological forcings, training SMB models, evaluating model performances, and updating glacier geometries.

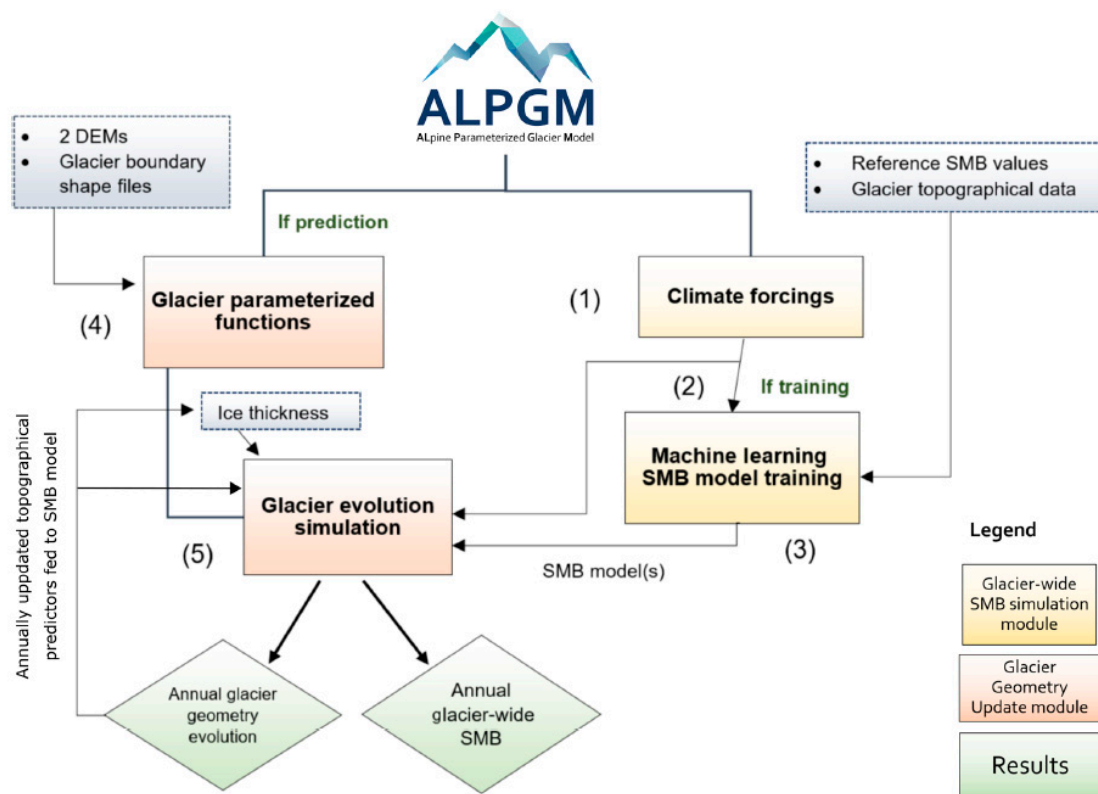


Figure 22. Structure and workflow of the ALPGM by Bolibar et al. [57].



The machine learning SMB model production workflow involves selecting relevant topographical and climatic predictors based on literature reviews and sensitivity analyses. To generate the SMB model, algorithms such as OLS, Lasso, and deep ANN may be selected, with ALPGM employing popular Python libraries like stats models, scikit-learn, and Keras with a TensorFlow backend. The presented approach showcases the potential of DL for the simulation of SMB, capturing nonlinearities not only in spatial, but also in temporal dimensions. The developed method showed explained variations of 64% for spatial and 108% for temporal, and accuracy values of 47% and 58% for spatial and temporal, respectively. This resulted in an  $r^2$  value of about 0.7 and an RMSE (root-mean-square error) of 0.5 m of water equivalent.

Ambinakudige and Intsiful [58] assessed the accuracy of three ML algorithms (SVM, RF, and MLC) for area classification and estimated the glacier volume change of Columbia Icefields from 1985 to 2020. All three algorithms classified images with over 99% accuracy and kappa coefficients of over 0.993, with SVM performing slightly better in identifying debris. The authors found that 10.4% of the ice/snow area was lost over the study period, which is consistent with other studies in the same region.

Utilizing Landsat satellite imagery from various years, the study revealed a significant decline in glacier area and volume in the Columbia Icefield between 1985 and 2020. SVM classification consistently showcased over 99% accuracy in classifying glacier features across different years, enabling accurate estimation of glacier changes over time. The observed trends align with broader global patterns of glacier retreat and volume loss attributed to climate change-induced warming. Moreover, the study underscores the importance of continued research leveraging ML methodologies, particularly in assessing glacier changes on a global scale. The findings not only reiterate the efficacy of ML techniques for glacier classification, but also emphasize the urgent need for comprehensive studies in order to understand the impacts of climate change on glacier dynamics. As glaciers continue to retreat worldwide, the integration of advanced ML approaches with remote sensing data holds promise for developing reliable records of glacier changes, which are essential for informing climate mitigation and adaptation strategies.

The study by Rajat et al. [59] applied U-Net to identify and map glacier evolution in the Himachal Pradesh province of India, leveraging Indian Remote Sensing (IRS) and Landsat satellite data spanning from 1994 to 2021. The results demonstrated a high identification accuracy of 95%, with a significantly reduced processing time compared to traditional methods. The findings revealed a concerning trend of glacial retreat in the region, with the glaciated area decreasing at a rate of approximately 67.84 km<sup>2</sup> per annum over the past three decades.

Utilizing Landsat satellite imagery from different years, the study evaluated changes in glacier area and volume, highlighting a substantial loss of approximately 1822 km<sup>2</sup> in glacier area from 1994 to 2021. This decline in glacial coverage underscores the urgency of understanding and mitigating the impacts of climate change on Himalayan glaciers, which are crucial water sources for the region.

The U-Net network model employed in the study effectively learns glacier characteristics and enhances feature extraction, leading to improved accuracy in glacier identification. By integrating deep learning with remote sensing data, the study offers a valuable tool for monitoring and assessing glacial changes, essential for water resource management and hydropower planning in the region. Furthermore, the paper suggests avenues for future research, including exploring the integration of additional variables such as thermal bands and precipitation data to enhance the machine learning model's accuracy. Incorporating in situ observations and debris glacier data could provide valuable insights into the relationship between glacier changes and climate change, facilitating more precise predictions of future glacier dynamics.

Yang et al. [60] conducted a study on glacier changes using remote sensing (RS) data and applied a DL technique to assess the risk of glacier debris flow in the region of the great bend of the Brahmaputra River in the Tibet Plateau, focusing particularly on the

Zelongnong ravine. Thus, they evaluated the glacier regions in the Zelongnong ravine using an automated semantic segmentation method trained using remote sensing data and the DL technique. They proceeded by computing variations in glacier elevation and volume between 2000 and 2016, examining the nature of changes within the research site.

Subsequently, they partitioned the Zelongnong ravine into five sub-basins, applied the glacier correction coefficient to enhance the initial geomorphic information entropy theory, and assessed the susceptibility of glacier debris flow in the Zelongnong ravine. Furthermore, glacier ablation is influenced by various factors, including slope, aspect, elevation, and climatic conditions such as sunlight exposure. These factors play crucial roles in determining the rate of glacier ablation. Therefore, the assessment of the susceptibility of debris flow can be obtained from the indicator—the ablation volume of the glaciers. Thus, by categorizing susceptibility grades based on the ablation volume, accurate predictions regarding glacier debris flow susceptibility can be made. The overall workflow and schematics of the developed method are shown in Figures 23 and 24.

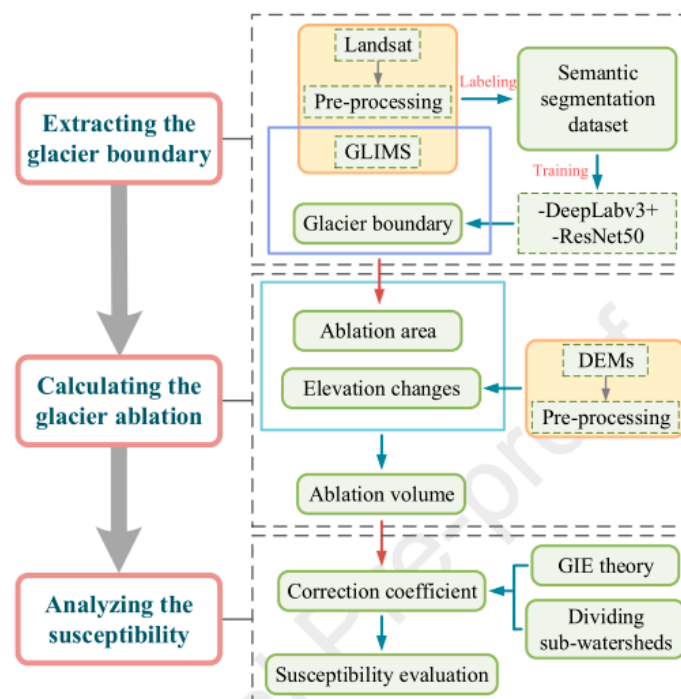


Figure 23. Workflow of this study by Yang et al. [60].

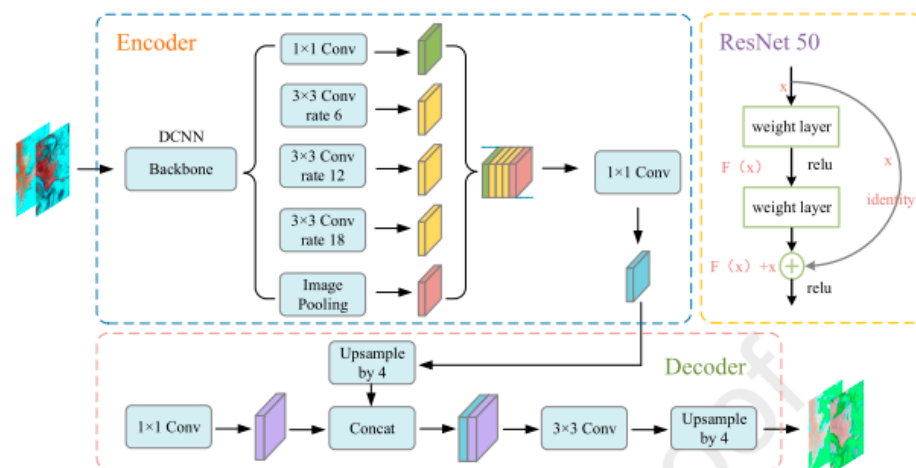


Figure 24. DeepLabv3+ semantic segmentation model and ResNet-50 residual unit [60].

Thus, the monitoring of glacier evolution using AI methods is advancing. It is more complex compared to mapping and inventory studies due to the inclusion of temporal changes in glaciers. Therefore, the development and testing of such methods require more time and effort. Nevertheless, it can be considered one of the main areas for future research in glacier studies using AI.

### 3.3. AI for Snow/Ice Differentiation

Another opportunity for AI applications arises in the area of snow and ice discrimination, which represents an innovative solution for optimizing the accuracy and optimization of remote sensing analysis. Through extensive training on a variety of datasets including satellite imagery and ground-based observations, AI models can quickly learn to discern the subtle spectral and textural nuances characteristic of snow and ice, overcoming the limitations of traditional manual interpretation or spectral analysis methods. This capability not only speeds up the processing of extensive remote sensing data, but also facilitates rigorous quantification of the extent of snow and ice, which is fundamental for climate research, hydrologic modeling, and environmental monitoring initiatives.

In their study, Prieur et al. [61] created an automated procedure that allows snow lines on glaciers to be identified from remote sensing images. It was tested on temperate glaciers located in the Alps of Europe. A feed-forward NN, SVM with Gaussian and linear kernels, and RF were selected as ML methods, and they used data from Landsat 8, especially data that considered the glacier inventory of the Alps in 2015 and the Copernicus DEM (Figure 25). The algorithms were designed to systematically categorize each glacier within the research region, employing a step-by-step binary classification approach. This process involves identifying and removing shadowed areas and eliminating leftover ice or snow pixels to eventually create a map that delineates ice and snow coverage on the glacier. The resulting map may be presented as either a binary map or a probability map, depending on the chosen method of map extraction. Since glaciers often have ice- and snow-covered areas devoid of clouds, the developed procedure suggests two techniques to identify the snow lines on the glaciers. If these methods fail, the mapping of the glacier is stopped. The initial method involves a modified version of automatic snow mapping on glaciers (ASMAG) bin decomposition detection process. This approach utilizes the snow line produced by ASMAG's procedure as an initialization vector for the detection of active contours. The alternative approach involves calculating the gradient of the snow cover map and then applying a threshold to this gradient based on elevation. This is intended to eliminate the gradient caused by patches of snow in the ablation region of the glacier. Both approaches provided good accuracy in identifying the lines between snow and glaciers, but discontinuous snow lines and steep sections of glaciers led to the failure of the methods.

### 3.4. AI for Ice Dynamics Modeling

AI also has the potential to transform the efficiency and accuracy of calculations in modeling ice dynamics, presenting another prospective application in this research domain. By leveraging vast amounts of observational data, satellite imagery, and remote sensing datasets, AI-based models can capture the nuanced interactions that include ice flow, mass balance, and calving dynamics. This capability not only speeds up the modeling time, but also allows researchers to gain a deeper understanding of the multifaceted drivers of glacier dynamics and their responses to environmental changes.

With this purpose, Jouvét et al. [62] introduced a glacier model (IGM), a novel approach to simulating ice dynamics, mass balance, and their combination, to estimate the evolution of glaciers and icefields. Central to the novelty of the model was its utilization of a convolutional neural network (CNN) to model ice flow, optimized using the data developed by means of a hybrid Shallow Ice Approximation (SIA) + Shallow Shelf Approximation (SSA) or Stokes ice flow model. This substitution of the computationally intensive ice flow component with a cost-effective emulator enabled IGM to model mountain glaciers up to 1000 times faster than traditional Stokes models on central processing units (CPUs), with

accuracy levels surpassing 90% in terms of ice flow solutions and nearly identical transient thickness evolution. Leveraging graphics processing units (GPUs) further enhanced speed-ups, especially for emulating Stokes dynamics or modeling at high spatial resolutions. IGM is an open-source Python code designed for 2D gridded input and output data, facilitating effective and user-friendly glacier and icefield simulations.

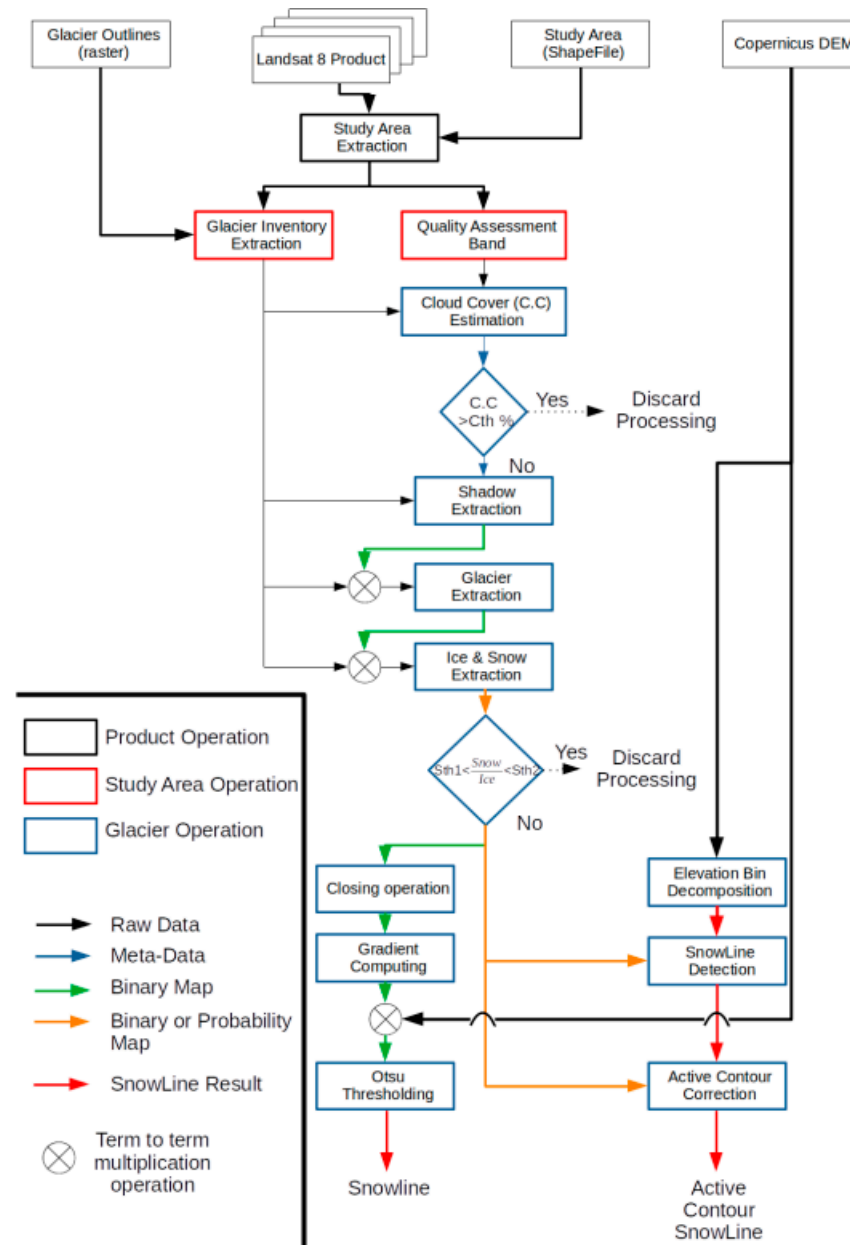


**Figure 25.** General flowchart of the proposed method [61].

The approach applies DL to ice flow modeling, employing CNN to predict ice flow using topographic properties as well as basal sliding parametrization in a generic manner. Unlike previous methods that emulated specific glacier dynamics from small-sized ensemble parameters, the neural network emulator in this study is trained from a large dataset generated from ice flow simulations obtained from state-of-the-art models—PISM and CfsFlow—equipped with hybrid SIA/SSA and Stokes mechanics at varying spatial resolutions. Integration of surface mass balance (SMB) and the conservation approach with the ice flow simulator yields the IGM, facilitating highly efficient and mechanically advanced ice flow simulations (Figure 26).



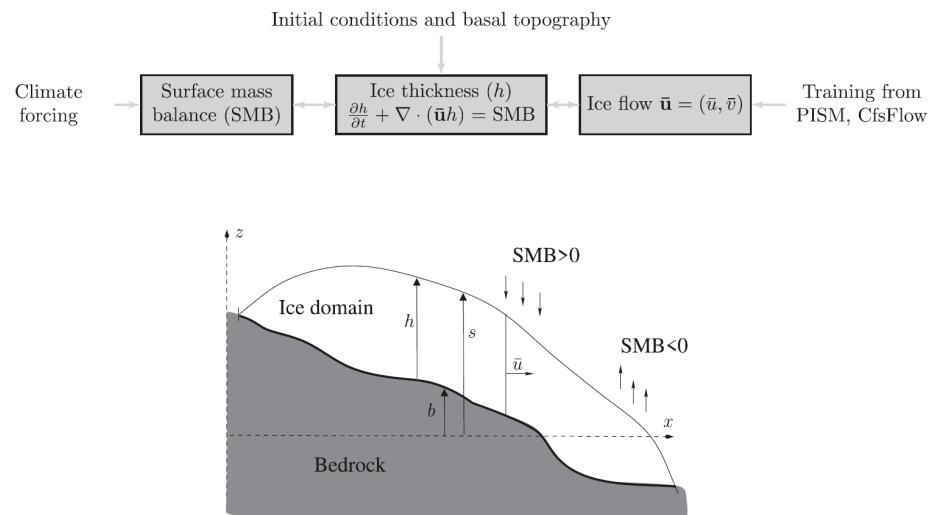


**Figure 26.** Connections between the model elements and the input data of IGM by Jouvét et al. [62].

However, IGM's limitations include dependency on the training dataset's representativeness, assumptions of isothermal ice, limitations in boundary conditions, and compatibility only with regular gridded data. Despite these limitations, IGM's computational efficiency opens new opportunities in paleo ice flow modeling, with applications in reconstructing glacial cycles, studying landscape evolution, inferring paleo climatic patterns, and improving global glacier modeling by reducing uncertainties associated with simplified models. Overall, IGM presents a promising advancement in glacier modeling, with potential applications in both paleo and modern ice sheet simulations.

The latest two areas of research, snow/ice differentiation and ice dynamics modeling, are relatively new and have not matured yet compared to the first two classified research areas. However, researchers have already begun working in these directions, and they are expected to become areas of greater interest in the near future.

#### 4. Discussion

The most common type of AI-based glacier study consists of mapping and glacier inventory. In fact, mapping and glacier inventory are crucial for evaluating glacier sizes and keeping track of them, providing essential data for understanding climate change impacts and predicting future water resources. These activities help scientists assess glacier health, contributing to global efforts in managing ecosystems and mitigating natural hazards. Thus, as can be noticed in the main section above, the earliest methods were classification methods such as random forest (RF), K-nearest neighbor (KNN), support vector machines (SVMs), decision trees (DTs), and gradient boosting (GB). In their work, Zhang et al. [40] selected the number of trees in RF as 100, but there was not any information on how the number of trees affected the accuracy of the RF in mapping glaciers, nor in testing or training sample sizes. Alifu et al. [45] compared these classification methods among each other and showed that RF was the best-performing and most robust ML method by carrying out hyperparameter analysis optimization. Khan et al. [43] also confirmed that RF performed better than the neural network method (i.e., ANN) when tested and compared using 26,688,723 pixels (391,907 labeled as debris-covered glacier, 1,354,622 as glacier, and 942,194 as non-glacier areas). The authors also mentioned that the computational complexity to train ANN is relatively higher. During the model parameter selection, only the learning rate and momentum were optimized, with fixed settings for other parameters (1000 iterations, sigmoid activation, and 200 hidden neurons), resulting in optimal accuracy with a learning rate of 0.1 and momentum of 0.8. Although tuning additional parameters such as the number of hidden layers, units per layer, batch size, and regularization techniques (e.g., dropout, weight decay) could have led to a better performance of ANN, it was not explored in this study.

The earliest studies of glaciers using CNN were conducted in 2019. Mohajerani et al. [41] and Baumhoer et al. [42] developed modified U-net models. The U-Net architecture by Mohajerani et al. [41] consists of 29 layers with three downsampling steps, increasing feature channels from 32 to 256, and uses custom sample weights to address class imbalance. In contrast, Baumhoer's [42] modified U-Net processes larger  $780 \times 780$ -pixel tiles with four input channels, includes four downsampling and upsampling units, and features 7.8 million trainable parameters. Both architectures use  $3 \times 3$  convolutions, ReLU activations,  $2 \times 2$  max pooling, and dropout layers, but differ in the number of layers, input size, and approach to handling class imbalance. Neither works performed thorough hyperparameter optimization to fine-tune parameters such as the learning rate, batch size, number of layers, and dropout rate, which could be used to evaluate the robustness of the models and potentially enhance their performance.

In other works [47–53], the authors proposed the combination of two methods into a hybrid AI approach to map glaciers, hoping for better accuracy compared to non-hybrid methods. For example, Lu et al. [47] combined RF with CNN and showed that the hybrid approach performs better than RF-only and CNN-only approaches in terms of user accuracy. However, in terms of producer accuracy, RF showed a better accuracy. Thus, the author clearly stated that due to the limited size of the glacier dataset in their experiment, the advantages of hybrid RF-CNN over traditional ML methods (i.e., RF and CNN) were not evident. In fact, the accuracy of the models depends on the testing data. For example, Kaushik et al. [17], in their study, showed that their developed GLNet method performed with an accuracy of 0.99 for site 1, while for site 2, this was reduced to 0.80, which is significantly low. They described this reduction in accuracy as being due to the presence of frozen and partly frozen lakes in the testing data, which was not accounted for during the training of GLNet.

The development of CNN-based models for glacier studies further continued and was actively studied by the authors, Xie, Asari, and Haritashya [48,49]. They initially developed the so-called GlacierNet and CNN segmentation model, and performed comparative analyses of their model with Mobile-UNet, Res-UNet, FCDenseNet, R2UNet, and DeepLabV3+. Based on their comparative analysis, DeepLabV3+ was the most effective for regional and large-scale glacier mapping due to its high intersection over union (IOU) and overall performance. During their study, they explored that the challenge lies in estimating the glacier terminus, which requires additional studies on the network's architecture, implementation of automated post-processing techniques, and incorporating additional terminus data. Peng et al. [14] also confirmed that DeepLabV3+ performed with higher accuracy; however, their proposed model with the LGT encoder and multiple LGCB layers was able to map both the complete glacier area and clear edges, making it potentially suitable for glaciers with accurate terminus mapping. Collectively, these studies illustrate the evolving landscape of AI techniques in glacier mapping, where various models are combined to improve the accuracy and address diverse challenges.

Another area of glacier studies where AI models have started to be actively applied is the monitoring of glacier evolution. Compared to glacier mapping, which focuses on spatial changes, monitoring glacier evolution also considers temporal variations, making it more complex than mapping studies. Bolibar et al. [56,57] studied the evolution of glaciers in the French Alps in the 21st century. Their comparative study showed that nonlinear DL models outperformed linear models by 94% to 108% in variance and 32% to 58% in accuracy, indicating that DL maintains a consistent performance across spatial and temporal dimensions, whereas linear methods struggle with the increased complexity of temporal SMB variations. Similarly, Ambinakudige and Intsiful [58] studied the glacier volume changes of Columbia Icefields from 1985 to 2020, but they used classification models such as SVM and RF. The latter models provided about 99% accuracy in classifying glacier features in 1985–2020. Furthermore, Rajat et al. [59] used U-Net to identify and map glacier evolution in the Himachal Pradesh province of India, but their timeline was from 1994 to 2021, and the accuracy of the model was around 95%. Yang et al. [60] clearly

outlined and acknowledged limitations in their approach in their study, including the assumption that all melted glacier ice converts to water, which overlooks the potential formation of new ice bodies and does not fully address variability or errors in glacier changes. Thus, because of the complexity of modeling dynamic glacier changes over time and space, AI models face notable challenges, highlighting the need for more advanced approaches. This presents an intriguing opportunity for exploring new AI techniques in order to better address these challenges. Moreover, the availability and time-frequency of data are crucial for the accuracy of AI models. Given that glacier monitoring spans several decades, consistent data throughout the measured and evaluated periods are essential for training AI models effectively.

Some other studies have pioneered new areas of study, such as snow/ice differentiation and ice dynamic modeling. In fact, snow/ice differentiation is indeed very important, because identifying the boundaries between snow and ice allows the size and volume of glaciers to be estimated. Prieur et al. [61] applied ML methods and showed good accuracy. However, their pre-processing algorithm (CFMask) might have compatibility problems with other multi-spectral products like Sentinel. They also mentioned another limitation, which was the need to retrain classifiers for new multi-spectral products, because different imaging systems offer varying spectral information. Therefore, training AI models for snow/ice differentiation using different types of images with varying spectral information is crucial. This is especially true for all image-based glacier studies using AI, particularly when developing advanced AI tools that can be applied to any glacier location once trained. In terms of ice dynamics modeling, Jouvet et al. [62] developed the instructed glacier model (IGM). In fact, ice has been modeled as a viscous, non-Newtonian fluid as described by computationally expensive Stokes equations. The authors explained that their IGM provides near-Stokes accuracy with high computational efficiency; operates on 2-D regular grids, simplifying data management; and requires only basic topographic inputs without the need for catchment or flowline identification. However, IGM's applicability is limited by its training dataset; it cannot model ice flow beyond the training data's scope; assumes isothermal ice; and only supports regular gridded data, excluding unstructured meshes.

## 5. Conclusions

Understanding changes in glaciers, evaluating their current conditions, inventorying, and predicting future scenarios based on climate change effects are highly crucial endeavors. Glaciers serve as vital sources of drinkable water, agricultural irrigation, and energy generation. Therefore, monitoring their status and forecasting their future behavior are important tasks in the face of ongoing environmental transformations.

As methods requiring less human interaction to deliver computational results evolve, the possibility of their application towards monitoring and forecasting glacier layers becomes feasible. Compared to conventional methods based on remote sensing, such methods, which mostly rely on artificial intelligence (AI) techniques, are highly accurate, cost-effective, and reliable once they are trained with accurate and sufficient datasets. With the rise of AI, the number of works dedicated to the application of ML and DL methods on glacier mapping and evaluation has notably increased. Therefore, within the scope of the current state-of-the-art review work, the available research works in AI-based glacier studies are studied and classified, and relative data are collected and tabulated for comparative purposes.

Thus, from the collected number of research papers, the following conclusions are obtained:

- All the reviewed works are classified by the purpose of their research. Among them, glacier mapping is the most studied area, followed by glacier evolution, ice/snow differentiation, and ice dynamic modeling.
- For AI-based glacier evolution studies, the availability of glacier data in terms of time-frequency and overall measured duration is highly important to accurately capture the temporal evolution of glaciers.

- Ice/snow differentiation and ice dynamic modeling are in their early stages regarding AI-based studies. However, the methods developed so far show promising accuracy and require further advancements.
- Methods such as random forest (RF), K-nearest neighbors (KNN), support vector machines (SVMs), and decision trees (DTs) have been foundational. Among them, RF often outperforms other traditional methods in accuracy and robustness, especially for glacier mapping studies.
- Recent studies in glacier mapping have developed CNN-based models, notably U-net and DeepLabV3+, which showed enhanced accuracy in glacier mapping. However, the robustness of these models needs to be tested with appropriate methods, such as hyperparameter optimization, to fine-tune parameters like the learning rate, batch size, number of layers, and dropout rate.
- Hybrid methods that combine two ML and/or DL methods generally show better performance compared to single methods. However, the compatibility and integrability of different methods in hybrid solutions have not been thoroughly studied yet, and comparative studies among hybrid methods are lacking.
- Overall, AI-based glacier research has notably been gaining the attention of scientists and requires more detailed studies. The consistency of AI-based methods needs to be further evaluated, particularly when training on one glacier dataset and testing on a different dataset. Additionally, the impact of training and testing dataset sizes, as well as the remote sensing technologies used to obtain these datasets, should be assessed.
- More generalized AI-based glacier assessment tools, particularly for worldwide glacier mapping and inventory, appear to be a promising direction for future research.

Overall, the integration of AI technologies holds enormous promise for improving glacier mapping and analysis, offering new insights into the complex dynamics of these vital components of the Earth's cryosphere. As researchers continue to explore and improve artificial intelligence methodologies, the potential for greater understanding and better management of glaciers in the context of climate change is becoming increasingly accessible.

The importance of the current state-of-the-art review is significant because it will serve as a guideline for future research works in AI-based glacier studies. As the first review paper in this area, the authors are confident that its results will provide notable value in this research field.

**Author Contributions:** Conceptualization, S.N. and Z.B.; software, A.M.; formal analysis, A.M. and N.S.; investigation, S.N. and A.M.; resources, N.S.; writing—original draft preparation, S.N. and N.S.; writing—review and editing, S.N., Z.B., A.M. and B.A.; visualization, A.M. and B.A.; supervision, S.N. and Z.B.; project administration, S.N. and N.S.; funding acquisition, S.N. All authors have read and agreed to the published version of the manuscript.

**Funding:** This research has been funded by the Science Committee of the Ministry of Science and Higher Education of the Republic of Kazakhstan within the framework of the projects AP14872134 and BR21882365. The APC was funded by the projects budget. This research was implemented with a focus on the partial requirements of PhD Candidate—Serik Nurakynov's doctoral dissertation on the "Assessment of the state of mountain cryosphere components using satellite technologies" at Department of Surveying and Geodesy, Satbayev University, Almaty, Kazakhstan.

**Data Availability Statement:** Data are contained within the article.

**Acknowledgments:** We are grateful to all the authors of the articles that were discussed in this review. Thanks are due to Ding Xiao-li, Department of Land Surveying and Geo-Informatics, The Hong Kong Polytechnic University for his scientific consult and encouragement.

**Conflicts of Interest:** The authors declare no conflicts of interest.



## References

1. Zemp, M.; Huss, M.; Thibert, E.; Eckert, N.; McNabb, R.; Huber, J.; Barandun, M.; Machguth, H.; Nussbaumer, S.U.; Gärtner-Roer, I.; et al. Global Glacier Mass Changes and Their Contributions to Sea-Level Rise from 1961 to 2016. *Nature* **2019**, *568*, 382–386. [CrossRef] [PubMed]
2. Wang, S. Opportunities and Threats of Cryosphere Change to the Achievement of UN 2030 SDGs. *Humanit. Soc. Sci. Commun.* **2024**, *11*, 44. [CrossRef]
3. Rasol, G.; Molden, D. The Global Social and Economic Consequences of Mountain Cryospheric Change. *Front. Environ. Sci.* **2019**, *7*, 91. [CrossRef]
4. Imdieke, A.; Pearson, P. Accelerated Glacier Retreat in the Himalayas Jeopardizes South Asian Agriculture—ICCI—International Cryosphere Climate Initiative. Available online: <https://iccinet.org/accelerated-glacier-retreat-in-the-himalayas-jeopardizes-south-asian-agriculture/> (accessed on 13 March 2024).
5. Puspitarini, H.D.; François, B.; Zaramella, M.; Brown, C.; Borga, M. The Impact of Glacier Shrinkage on Energy Production from Hydropower-Solar Complementarity in Alpine River Basins. *Sci. Total Environ.* **2020**, 719. [CrossRef]
6. Losapio, G.; Cerabolini, B.E.L.; Maffioletti, C.; Tampucci, D.; Gobbi, M.; Caccianiga, M. The Consequences of Glacier Retreat Are Uneven Between Plant Species. *Front. Ecol. Evol.* **2021**, *8*. [CrossRef]
7. Milner, A.M.; Khamis, K.; Battin, T.J.; Brittain, J.E.; Barrand, N.E.; Füreder, L.; Cauvy-Fraunié, S.; Gíslason, G.M.; Jacobsen, D.; Hannah, D.M.; et al. Glacier Shrinkage Driving Global Changes in Downstream Systems. *Proc. Natl. Acad. Sci. USA* **2017**, *114*, 9770–9778. [CrossRef] [PubMed]
8. WGMS, and National Snow and Ice Data Center (comps.). 1999, Updated 2012. World Glacier Inventory, Version 1. Boulder, Colorado USA. NSIDC: National Snow and Ice Data Center. Available online: <https://nsidc.org/data/g01130/versions/1> (accessed on 5 August 2024).
9. NSIDC. National Snow and Ice Data Center RGI 7.0 Consortium. *Randolph Glacier Inventory—A Dataset of Global Glacier Outlines, Version 7.0*; NSIDC: Boulder, CO, USA, 2023.
10. Friedl, P.; Weiser, F.; Fluhner, A.; Braun, M.H. Remote Sensing of Glacier and Ice Sheet Grounding Lines: A Review. *Earth-Sci. Rev.* **2020**, *201*. [CrossRef]
11. Winsvold, S.H.; Kääb, A.; Nuth, C. Regional Glacier Mapping Using Optical Satellite Data Time Series. *IEEE J. Sel. Top. Appl. Earth Obs. Remote Sens.* **2016**, *9*. [CrossRef]
12. Chouksey, A.; Thakur, P.K.; Sahni, G.; Swain, A.K.; Aggarwal, S.P.; Kumar, A.S. Mapping and Identification of Ice-Sheet and Glacier Features Using Optical and SAR Data in Parts of Central Dronning Maud Land (cDML), East Antarctica. *Polar Sci.* **2021**, *30*. [CrossRef]
13. Lu, Y.; Zhang, Z.; Kong, Y.; Hu, K. Integration of Optical, SAR and DEM Data for Automated Detection of Debris-Covered Glaciers over the Western Nyainqentanglha Using a Random Forest Classifier. *Cold Reg. Sci. Technol.* **2022**, 193. [CrossRef]
14. Peng, Y.; He, J.; Yuan, Q.; Wang, S.; Chu, X.; Zhang, L. Automated Glacier Extraction Using a Transformer Based Deep Learning Approach from Multi-Sensor Remote Sensing Imagery. *ISPRS J. Photogramm. Remote Sens.* **2023**, *202*, 303–313. [CrossRef]
15. Malenovsky, Z.; Rott, H.; Cihlar, J.; Schaepman, M.E.; García-Santos, G.; Fernandes, R.; Berger, M. Sentinels for Science: Potential of Sentinel-1, -2, and -3 Missions for Scientific Observations of Ocean, Cryosphere, and Land. *Remote Sens. Environ.* **2012**, *120*, 91–101. [CrossRef]
16. Rott, H.; Mätzler, C. Possibilities and Limits of Synthetic Aperture Radar for Snow and Glacier Surveying. *Ann. Glaciol.* **1987**, *9*, 195–199. [CrossRef]
17. Kaushik, S.; Singh, T.; Joshi, P.K.; Dietz, A.J. Automated Mapping of Glacial Lakes Using Multisource Remote Sensing Data and Deep Convolutional Neural Network. *Int. J. Appl. Earth Obs. Geoinf.* **2022**, *115*, 103085. [CrossRef]
18. Rastner, P.; Strozzi, T.; Paul, F. Fusion of Multi-Source Satellite Data and DEMs to Create a New Glacier Inventory for Novaya Zemlya. *Remote Sens.* **2017**, *9*, 1122. [CrossRef]
19. Zhang, L.; Zhang, Q.; Du, B.; Huang, X.; Tang, Y.Y.; Tao, D. Simultaneous Spectral-Spatial Feature Selection and Extraction for Hyperspectral Images. *IEEE Trans. Cybern.* **2018**, *48*, 16–28. [CrossRef] [PubMed]
20. Zhang, L.; Zhang, L.; Du, B. Deep Learning for Remote Sensing Data: A Technical Tutorial on the State of the Art. *IEEE Geosci. Remote Sens. Mag.* **2016**, *4*, 22–40. [CrossRef]
21. Jamil, A.; Bayram, B. Tree Species Extraction and Land Use/Cover Classification from High-Resolution Digital Orthophoto Maps. *IEEE J. Sel. Top. Appl. Earth Obs. Remote Sens.* **2018**, *11*, 89–94. [CrossRef]
22. Qian, Y.; Zhou, W.; Yan, J.; Li, W.; Han, L. Comparing Machine Learning Classifiers for Object-Based Land Cover Classification Using Very High Resolution Imagery. *Remote Sens.* **2015**, *7*, 153–168. [CrossRef]
23. Zarea, A.; Mohammadzadeh, A. A Novel Building and Tree Detection Method from LiDAR Data and Aerial Images. *IEEE J. Sel. Top. Appl. Earth Obs. Remote Sens.* **2016**, *9*, 1864–1875. [CrossRef]
24. Zhang, L.; You, J. A Spectral Clustering Based Method for Hyperspectral Urban Image. In Proceedings of the 2017 Joint Urban Remote Sensing Event, JURSE 2017, Dubai, United Arab Emirates, 6–8 March 2017.
25. Wu, Y.; Jiang, B.; Wang, Y. Incipient Winding Fault Detection and Diagnosis for Squirrel-Cage Induction Motors Equipped on CRH Trains. *ISA Trans.* **2020**, *99*, 488–495. [CrossRef]
26. Amin, A.A.; Sajid Iqbal, M.; Hamza Shahbaz, M. Development of Intelligent Fault-Tolerant Control Systems with Machine Learning, Deep Learning, and Transfer Learning Algorithms: A Review. *Expert Syst. Appl.* **2024**, *238*, 121956. [CrossRef]

27. Pal, N.R.; Pal, S.K. A Review on Image Segmentation Techniques. *Pattern Recognit.* **1993**, *26*, 1277–1294. [\[CrossRef\]](#)
28. Paul, F.; Huggel, C.; Kääb, A. Combining Satellite Multispectral Image Data and a Digital Elevation Model for Mapping Debris-Covered Glaciers. *Remote Sens. Environ.* **2004**, *89*, 510–518. [\[CrossRef\]](#)
29. Bibi, L.; Khan, A.A.; Khan, G.; Ali, K.; Hassan, S.N.U.; Qureshi, J.; Jan, I.U. Snow Cover Trend Analysis Using Modis Snow Products: A Case of Shayok River Basin in Northern Pakistan. *J. Himal. Earth Sci.* **2019**, *52*, 145–160.
30. Nijhawan, R.; Garg, P.; Thakur, P. A Comparison of Classification Techniques for Glacier Change Detection Using Multispectral Images. *Perspect. Sci.* **2016**, *8*, 377–380. [\[CrossRef\]](#)
31. Alifu, H.; Tateishi, R.; Johnson, B. A New Band Ratio Technique for Mapping Debris-Covered Glaciers Using Landsat Imagery and a Digital Elevation Model. *Int. J. Remote Sens.* **2015**, *36*, 2063–2075. [\[CrossRef\]](#)
32. Gindraux, S.; Boesch, R.; Farinotti, D. Accuracy Assessment of Digital Surface Models from Unmanned Aerial Vehicles' Imagery on Glaciers. *Remote Sens.* **2017**, *9*, 186. [\[CrossRef\]](#)
33. Han, W.; Zhang, X.; Wang, Y.; Wang, L.; Huang, X.; Li, J.; Wang, S.; Chen, W.; Li, X.; Feng, R.; et al. A Survey of Machine Learning and Deep Learning in Remote Sensing of Geological Environment: Challenges, Advances, and Opportunities. *ISPRS J. Photogramm. Remote Sens.* **2023**, *202*, 87–113. [\[CrossRef\]](#)
34. Barillaro, L. Deep Learning Platforms: PyTorch. In *Reference Module in Life Sciences*; Elsevier: Amsterdam, The Netherlands, 2024. [\[CrossRef\]](#)
35. Janardhanan, P.S. Project Repositories for Machine Learning with TensorFlow. *Procedia Comput. Sci.* **2020**, *171*, 188–196. [\[CrossRef\]](#)
36. Barillaro, L. Deep Learning Platforms: Keras. In *Reference Module in Life Sciences*; Elsevier: Amsterdam, The Netherlands, 2024. [\[CrossRef\]](#)
37. Zhang, H.K.; Qiu, S.; Suh, J.W.; Luo, D.; Zhu, Z. *Machine Learning and Deep Learning in Remote Sensing Data Analysis. Reference Module in Earth Systems and Environmental Sciences*; Elsevier: Amsterdam, The Netherlands, 2024. [\[CrossRef\]](#)
38. Intergovernmental Panel on Climate Change (IPCC). *Climate Change 2013: The Physical Science Basis; Contribution of Working Group I to the Fifth Assessment Report of the Intergovernmental Panel on Climate Change*; Stocker, T.F., Qin, D., Plattner, G.-K., Tignor, M., Allen, S.K., Boschung, J., Nauels, A., Xia, Y., Bex, V., Eds.; Cambridge University Press: Cambridge, UK; New York, NY, USA, 2013; 1535p.
39. Fenza, G.; Gallo, M.; Loia, V.; Orciuoli, F.; Herrera-Viedma, E. Data Set Quality in Machine Learning: Consistency Measure Based on Group Decision Making. *Appl. Soft Comput.* **2021**, *106*, 107366. [\[CrossRef\]](#)
40. Zhang, J.; Jia, L.; Menenti, M.; Hu, G. Glacier Facies Mapping Using a Machine-Learning Algorithm: The Parlung Zangbo Basin Case Study. *Remote Sens.* **2019**, *11*, 452. [\[CrossRef\]](#)
41. Mohajerani, Y.; Wood, M.; Velicogna, I.; Rignot, E. Detection of Glacier Calving Margins with Convolutional Neural Networks: A Case Study. *Remote Sens.* **2019**, *11*, 74. [\[CrossRef\]](#)
42. Baumhoer, C.A.; Dietz, A.J.; Kneisel, C.; Kuenzer, C. Automated Extraction of Antarctic Glacier and Ice Shelf Fronts from Sentinel-1 Imagery Using Deep Learning. *Remote Sens.* **2019**, *11*, 2529. [\[CrossRef\]](#)
43. Khan, A.A.; Jamil, A.; Hussain, D.; Taj, M.; Jabeen, G.; Malik, M.K. Machine-Learning Algorithms for Mapping Debris-Covered Glaciers: The Hunza Basin Case Study. *IEEE Access* **2020**, *8*, 12725–12734. [\[CrossRef\]](#)
44. Zhang, E.; Liu, L.; Huang, L.; Ng, K.S. An Automated, Generalized, Deep-Learning-Based Method for Delineating the Calving Fronts of Greenland Glaciers from Multi-Sensor Remote Sensing Imagery. *Remote Sens. Environ.* **2021**, *254*, 112265. [\[CrossRef\]](#)
45. Alifu, H.; Vuillaume, J.F.; Johnson, B.A.; Hirabayashi, Y. Machine-Learning Classification of Debris-Covered Glaciers Using a Combination of Sentinel-1/-2 (SAR/Optical), Landsat 8 (Thermal) and Digital Elevation Data. *Geomorphology* **2020**, *369*, 107365. [\[CrossRef\]](#)
46. Robson, B.A.; Bolch, T.; MacDonell, S.; Hölbling, D.; Rastner, P.; Schaffer, N. Automated Detection of Rock Glaciers Using Deep Learning and Object-Based Image Analysis. *Remote Sens. Environ.* **2020**, *250*, 112033. [\[CrossRef\]](#)
47. Lu, Y.; Zhang, Z.; Shangguan, D.; Yang, J. Novel Machine Learning Method Integrating Ensemble Learning and Deep Learning for Mapping Debris-Covered Glaciers. *Remote Sens.* **2021**, *13*, 2595. [\[CrossRef\]](#)
48. Xie, Z.; Asari, V.K.; Haritashya, U.K. Evaluating Deep-Learning Models for Debris-Covered Glacier Mapping. *Appl. Comput. Geosci.* **2021**, *12*, 100071. [\[CrossRef\]](#)
49. Xie, Z.; Haritashya, U.K.; Asari, V.K.; Bishop, M.P.; Kargel, J.S.; Aspiras, T.H. GlacierNet2: A Hybrid Multi-Model Learning Architecture for Alpine Glacier Mapping. *Int. J. Appl. Earth Obs. Geoinf.* **2022**, *112*, 102921. [\[CrossRef\]](#)
50. Erharder, G.H.; Wagner, T.; Winkler, G.; Marcher, T. Machine Learning—An Approach for Consistent Rock Glacier Mapping and Inventorying – Example of Austria. *Appl. Comput. Geosci.* **2022**, *16*, 100093. [\[CrossRef\]](#)
51. Tian, S.; Dong, Y.; Feng, R.; Liang, D.; Wang, L. Mapping Mountain Glaciers Using an Improved U-Net Model with cSE. *Int. J. Digit. Earth* **2022**, *15*, 463–477. [\[CrossRef\]](#)
52. Sood, V.; Tiwari, R.K.; Singh, S.; Kaur, R.; Parida, B.R. Glacier Boundary Mapping Using Deep Learning Classification over Bara Shigri Glacier in Western Himalayas. *Sustainability* **2022**, *14*, 13485. [\[CrossRef\]](#)
53. Sharda, S.; Srivastava, M.; Gusain, H.S.; Sharma, N.K.; Bhatia, K.S.; Bajaj, M.; Kaur, H.; Zawbaa, H.M.; Kamel, S. A Hybrid Machine Learning Technique for Feature Optimization in Object-Based Classification of Debris-Covered Glaciers. *Ain Shams Eng. J.* **2022**, *13*, 101809. [\[CrossRef\]](#)
54. Thomas, D.J.; Robson, B.A.; Racoviteanu, A. An Integrated Deep Learning and Object-Based Image Analysis Approach for Mapping Debris-Covered Glaciers. *Front. Remote Sens.* **2023**, *4*. [\[CrossRef\]](#)

55. Hu, Y.; Liu, L.; Huang, L.; Zhao, L.; Wu, T.; Wang, X.; Cai, J. Mapping and Characterizing Rock Glaciers in the Arid Western Kunlun Mountains Supported by InSAR and Deep Learning. *J. Geophys. Res. Earth Surf.* **2023**, *128*, e2023JF007206. [[CrossRef](#)]
56. Bolibar, J.; Rabatel, A.; Gouttevin, I.; Zekollari, H.; Galiez, C. Nonlinear Sensitivity of Glacier Mass Balance to Future Climate Change Unveiled by Deep Learning. *Nat. Commun.* **2022**, *13*, 409. [[CrossRef](#)]
57. Bolibar, J.; Rabatel, A.; Gouttevin, I.; Galiez, C.; Condom, T.; Sauquet, E. Deep Learning Applied to Glacier Evolution Modelling. *Cryosphere* **2020**, *14*, 565–584. [[CrossRef](#)]
58. Ambinakudige, S.; Intsiful, A. Estimation of Area and Volume Change in the Glaciers of the Columbia Icefield, Canada Using Machine Learning Algorithms and Landsat Images. *Remote Sens. Appl. Soc. Environ.* **2022**, *26*, 100732. [[CrossRef](#)]
59. Rajat, S.; Rajeshwar Singh, B.; Prakash, C.; Anita, S. Glacier Retreat in Himachal from 1994 to 2021 Using Deep Learning. *Remote Sens. Appl. Soc. Environ.* **2022**, *28*, 100870. [[CrossRef](#)]
60. Yang, S.; Mei, G.; Zhang, Y. Susceptibility Analysis of Glacier Debris Flow by Investigating Glacier Changes Based on Remote Sensing Imagery and Deep Learning: A Case Study. *Nat. Hazards Res.* **2023**; *in press*. [[CrossRef](#)]
61. Prieur, C.; Rabatel, A.; Thomas, J.B.; Farup, I.; Chanussot, J. Machine Learning Approaches to Automatically Detect Glacier Snow Lines on Multi-Spectral Satellite Images. *Remote Sens.* **2022**, *14*, 3868. [[CrossRef](#)]
62. Juvet, G.; Cordonnier, G.; Kim, B.; Lüthi, M.; Vieli, A.; Aschwanden, A. Deep Learning Speeds up Ice Flow Modelling by Several Orders of Magnitude. *J. Glaciol.* **2022**, *68*, 651–664. [[CrossRef](#)]

**Disclaimer/Publisher's Note:** The statements, opinions and data contained in all publications are solely those of the individual author(s) and contributor(s) and not of MDPI and/or the editor(s). MDPI and/or the editor(s) disclaim responsibility for any injury to people or property resulting from any ideas, methods, instructions or products referred to in the content.